International Ocean Discovery Program Expedition 382 Scientific Prospectus

Iceberg Alley and South Falkland Slope Ice and Ocean Dynamics

Michael E. Weber
Co-Chief Scientist
Steinmann-Institute
University of Bonn
Germany

Maureen E. Raymo
Co-Chief Scientist
Lamont-Doherty Earth Observatory
Palisades NY
USA

Victoria L. Peck
Lead proponent, South Falkland Slope sites
British Antarctic Survey
Cambridge
UK

Trevor Williams
Expedition Project Manager/Staff Scientist
International Ocean Discovery Program
Texas A&M University
USA

IODP
INTERNATIONAL OCEAN DISCOVERY PROGRAM

Publisher's notes

This publication was prepared by the *JOIDES Resolution* Science Operator (JRSO) at Texas A&M University (TAMU) as an account of work performed under the International Ocean Discovery Program (IODP). Funding for IODP is provided by the following international partners:

National Science Foundation (NSF), United States
Ministry of Education, Culture, Sports, Science and Technology (MEXT), Japan
European Consortium for Ocean Research Drilling (ECORD)
Ministry of Science and Technology (MOST), People's Republic of China
Korea Institute of Geoscience and Mineral Resources (KIGAM)
Australia-New Zealand IODP Consortium (ANZIC)
Ministry of Earth Sciences (MoES), India
Coordination for Improvement of Higher Education Personnel (CAPES), Brazil

Portions of this work may have been published in whole or in part in other IODP documents or publications.

This IODP *Scientific Prospectus* is based on precruise *JOIDES Resolution* Facility advisory panel discussions and scientific input from the designated Co-Chief Scientists on behalf of the drilling proponents. During the course of the cruise, actual site operations may indicate to the Co-Chief Scientists, the Staff Scientist/Expedition Project Manager, and the Operations Superintendent that it would be scientifically or operationally advantageous to amend the plan detailed in this prospectus. It should be understood that any proposed changes to the science deliverables outlined in the plan presented here are contingent upon the approval of the IODP JRSO Director.

Disclaimer

Any opinions, findings, and conclusions or recommendations expressed in this publication are those of the author(s) and do not necessarily reflect the views of the participating agencies, TAMU, or Texas A&M Research Foundation.

Copyright

Citation

Weber, M.E., Raymo, M.E., Peck, V.L., and Williams, T., 2018. *Expedition 382 Scientific Prospectus: Iceberg Alley and South Falkland Slope Ice and Ocean Dynamics.* International Ocean Discovery Program. https://doi.org/10.14379/iodp.sp.382.2018

ISSN
World Wide Web: 2332-1385

Abstract

International Ocean Discovery Program Expedition 382, Iceberg Alley and South Falkland Slope Ice and Ocean Dynamics, will investigate the long-term climate history of Antarctica, seeking to understand how polar ice sheets responded to changes in atmospheric CO_2 in the past and how ice sheet evolution influenced global sea level. We will drill six sites in the Scotia Sea, east of the Antarctic Peninsula, providing the first deep drilling in this region of the Southern Ocean. We expect to recover >600 m of late Neogene sediment that will be used to reconstruct the past history and variability in Antarctic Ice Sheet (AIS) mass loss and associated changes in oceanic and atmospheric circulation.

Expedition 382 expects to deliver the first spatially and temporally integrated record of iceberg flux from "Iceberg Alley," the main pathway by which icebergs are calved from the margin of the AIS and travel equatorward into warmer waters of the Antarctic Circumpolar Current (ACC). In particular, we will characterize the magnitude of iceberg flux during key times of AIS evolution:

- The middle Miocene glacial intensification of the East Antarctic Ice Sheet,
- The mid-Pliocene warm interval,
- The late Pliocene glacial expansion of the West Antarctic Ice Sheet,
- The mid-Pleistocene transition, and
- The "warm interglacials" and glacial terminations of the last 800 ky.

We will use the geochemical provenance of iceberg-rafted detritus and other glacially eroded material to determine regional sources of AIS mass loss in this region, address interhemispheric phasing of ice sheet growth and decay, study the distribution and history of land-based versus marine-based ice sheets around the continent over time, and explore the links between AIS variability and global sea level.

By comparing north–south variations across the Scotia Sea, Expedition 382 will also deliver critical information on how climate changes in the Southern Ocean affect ocean circulation through the Drake Passage, meridional overturning in the region, water-mass production, CO_2 transfer by wind-induced upwelling, sea ice variability, bottom water outflow from the Weddell Sea, Antarctic weathering inputs, and changes in oceanic and atmospheric fronts in the vicinity of the ACC.

Comparing changes in dust proxy records between the Scotia Sea and Antarctic ice cores will also provide a detailed reconstruction of changes in the Southern Hemisphere westerlies on millennial and orbital timescales for the last 800 ky. Extending the ocean dust record beyond the last 800 ky will help to evaluate climate-dust couplings since the Pliocene, the potential role of dust in iron fertilization and atmospheric CO_2 drawdown during glacials, and whether dust input to Antarctica played a role in the mid-Pleistocene transition.

The principal scientific objective of the South Falkland Slope sites to the north is to reconstruct and understand how ocean circulation and intermediate water formation responds to changes in climate with a special focus on the connectivity between the Atlantic and Pacific basins. The South Falkland Slope Drift, a contourite drift on the Falkland margin deposited between 400 and 2000 m water depth, is ideally situated to monitor millennial- to orbital-scale variability in the export of Antarctic Intermediate Water beneath the Subantarctic Front over at least the last 2 My. We anticipate that these sites will yield a wide array of paleoceanographic records that can be used to interpret past changes in the density structure of the Atlantic sector of the Southern Ocean and track the migration of the Subantarctic Front. We expect the cored sediments to capture the following significant climate episodes:

- The most recent warm interglacials of the late Pleistocene;
- The mid-Pleistocene transition, when $\delta^{18}O$ records shifted from dominantly 41 to 100 ky periodicity; and possibly
- Mid-Pliocene warm intervals, often invoked as the best analog for possible future climate change.

Schedule for Expedition 382

International Ocean Discovery Program (IODP) Expedition 382 is based on IODP drilling Proposals 902-Full, 902-Add, 902-Add2, APL 846, and APL846-Add (**https://iodp.tamu.edu/scienceops/expeditions/iceberg_alley_paleoceanography.html**).

Following evaluation by the IODP Science Evaluation Panel, the expedition was scheduled for the R/V *JOIDES Resolution*, operating under contract with the *JOIDES Resolution* Science Operator (JRSO). At the time of publication of this *Scientific Prospectus*, the expedition is scheduled to start in Punta Arenas, Chile, on 20 March 2019 and to end in Punta Arenas on 20 May 2019. A total of 56 days will be available for the transit, drilling, coring, and downhole measurements described in this report (for the current detailed schedule, see **http://iodp.tamu.edu/scienceops**). Further details about the facilities aboard the *JOIDES Resolution* can be found at **http://iodp.tamu.edu/publicinfo/drillship.html**.

Introduction

Several decades of research on the paleoceanography and paleoclimatology of the Scotia Sea using short cores and remote-sensing data have revealed a wealth of information on late Pleistocene ice sheet-ocean-climate interactions. However, deep drilling is required to understand the evolution and sensitivity of these interactions over much longer timescales, in particular during periods of Earth's history that were significantly warmer than today. Drilling deep sites in Pirie Basin and Dove Basin will allow us to decipher the geological history of the Antarctic region back to the Miocene and to test competing hypotheses in this important yet undersampled region. In particular, recovery of long records will improve our understanding of how the coupled Antarctic ice-ocean-atmosphere system evolved to the present state and how it behaved across major climate transitions and during warmer-than-present times. We will test whether seismic Reflectors a–d, which divide five regional units, relate to key changes in Antarctic Ice Sheet (AIS) and/or climate evolution. These changes could include the middle Miocene glacial intensification of the East Antarctic Ice Sheet (EAIS), the mid-Pliocene warm interval, the late Pliocene glacial enhancement of the West Antarctic Ice Sheet (WAIS), the Mid-Pleistocene Transition (MPT), or more recent glacial–interglacial changes. Using a variety of proxies and modeling approaches, the sediments recovered during Expedition 382 will be used to address key topics discussed in the following sections in order of importance.

Past AIS behavior

The Scotia Sea sites are strategically located in two areas of Iceberg Alley, the major Antarctic gateway to lower latitudes where Antarctic icebergs generally exit to the Southern Ocean (Figure **F1**).

Weber et al. (2014) revealed that times of enhanced iceberg-rafted debris (IBRD) indicate times of AIS instability. Accordingly, we should be able to generate the first spatially integrated and long-term reconstruction of AIS variability and its relation to sea level and climate change. A recent proof-of-concept study revealed that, at least for the late Pleistocene, sedimentation rates at these sites are high enough to record climate and ice sheet changes on decadal-to-centennial timescales. The discovery that massive episodes of iceberg discharge begin abruptly, within decades (Weber et al., 2014), has fundamental implications for projections of future AIS behavior in a warming world. Also, expanded sea ice could enhance thermal isolation and AIS expansion and vice versa. In addition, IBRD provenance is able to discriminate circum-Antarctic from regional AIS events, and sea level, ice sheet, and iceberg modeling will be used to improve our understanding of AIS dynamics, especially during warmer-than-present periods and glacial terminations.

Regional atmospheric circulation and dust transport

Our two drilling areas in the Scotia Sea are located to monitor the history of prevailing Southern Hemisphere westerlies (SHW), located between Patagonian dust sources to the north and Antarctic ice-core dust records to the south (e.g., European Project for Ice Coring in Antarctica [EPICA] Community Members, 2006) (Figure **F1**). With our cores, we will reconstruct dust transport history with attendant implications for the SHW in more northerly (proximal) and southerly (distal) positions relative to the dust source. We will also investigate whether marine and ice-core dust proxies were coupled for the last 800 ky and whether and how dust variability covaried with orbital variability prior to the late Pleistocene.

Drake Passage throughflow and deep-water history

The Scotia Sea sites, complemented by the South Falkland Slope sites, are located to reconstruct the strength of Drake Passage throughflow immediately east of this major geographic bottleneck constraining the flow of the Antarctic Circumpolar Current (ACC) (McCave et al., 2014). Using proxy records from these core sites, we should be able to identify times of stronger ACC influence (higher proportions of Circumpolar Deep Water [CDW]) from times of stronger Weddell Sea influence (higher proportions of Weddell Sea Bottom Water [WSBW]). Finally, because the sites stretch across major latitudinal ocean and atmosphere fronts, we should be able to reconstruct past changes in ocean productivity, sea ice extent, and regional wind patterns for the key periods described above, including late Quaternary glacial–interglacial and millennial-scale cycles.

Background

Geological setting

The age of basement in the Scotia Sea has not yet been determined because of the lack of deep drilling but could be Eocene (Eagles et al., 2006) or younger (Maldonado et al., 2006). For Dove Basin, Galindo-Zaldívar et al. (2014) provide estimated ages of 21–24 Ma (late Oligocene to early Miocene) constrained by combined magnetic anomaly and $^{40}Ar/^{39}Ar$ data. For Pirie Basin, estimated ages range from 25 Ma (Barker et al., 2013) to 14 Ma (Galindo-Zaldívar et al., 2006).

Five seismic units bounded by high-amplitude reflectors characterize the Scotia/Antarctic plate boundary above acoustic basement (Maldonado et al., 2006). Seismic Units IV and V indicate deposition after initial rifting and seafloor spreading (Reflector d; tentatively ~14.5 Ma; Figure **F2**). The overlying contourite Units I–III were likely deposited from the interplay between the northeastward flowing WSBW and the westward flowing ACC.

A basin-wide unconformity (Reflector c at the base of Unit III) is also identified in the Weddell Sea and shows a northward progradational pattern. Tectonic movements during the middle Miocene (tentatively ~12.5 Ma) opened the South Scotia Ridge gateway through Jane Basin (Maldonado et al., 2006) and uplifted the Shackleton Fracture Zone. These tectonic events likely forced the ACC to shift north, thereby contributing to the thermal isolation of Antarctica (Martos et al., 2013). These changes could also be the cause of EAIS expansion and establishment of full-glacial conditions in the Weddell Sea (Lindeque et al., 2013).

Seismic Unit II with basal Reflector b (tentatively late Miocene; ~6.5 Ma) represents sheeted deposits possibly related to enhanced erosion caused by WSBW (Martos et al., 2013) and expansion of the WAIS. Unit I, a contourite drift with basal Reflector a (tentatively Pliocene; ~3.5 Ma), represents the youngest regional sedimentary unit and was possibly deposited in concert with the intensification of Northern Hemisphere glaciation or/and postulated WAIS expansion (McKay et al., 2012).

Recent seismic interpretations for Dove Basin (Pérez et al., 2015) and Pirie Basin (Pérez et al., 2014) add Reflector a? (tentatively 2.6 Ma at the Pliocene/Pleistocene boundary) in Unit I. These preliminary ages (Figure **F2**) rely mainly on Maldonado et al. (2003). For all depth conversions reported here, 1.6 km/s seismic velocities were used, relying on core measurements of 1.5 km/s near the top of acoustic basement (Weber et al., 2012) and on processing values of up to ~1.65 km/s above it. Under this assumption, Units I–V are 100–300 m thick (Figures **F3**, **F4**), and the acoustic basement is generally observed at ~1 km subbottom depth.

The proposed sites are located in two small basins (Pirie and Dove Basins) of the Scotia Sea (Figures **F3**, **F5**). For Dove Basin, three seismic lines indicate a basin-like structure with several small-scale ridges and continuous reflectors in the central part (Figures **F3**, **F4**). Primary Site SCO-14 is located along seismic Line 03/04 in a basinal position. Primary Site SCO-13 is located to the north along Line 10/04, also over the deepest part of the basin. Both sites provide the best compromise between relatively thick and least disturbed strata for Dove Basin. Alternate Site SCO-15 is located at the crossing of Lines 10/04 and 03/04 in a more marginal position. Alternate Site SCO-18 is located in the north of Dove Basin along Line 07/04. Available groundtruth data for Dove Basin comes from shallow sediment Core MD07-3134 (Weber et al., 2012) for the upper 59 meters below seafloor (mbsf).

In Pirie Basin, east–west running seismic Lines 13/13 and 11/08 indicate a north–south oriented basin (Figures **F5**, **F6**). Drilling in Pirie Basin should retrieve structurally intact and thick Plio–Pleistocene deposits. Accordingly, proposed Sites SCO-17 and SCO-11, both with relatively thick and planar strata of seismic Units I and II in the center of the small basin, were chosen as primary sites. Alternate Site SCO-01 (MD07-3133) is located west of Site SCO-11. Alternate Site SCO-19 is even farther west at the margin of the basin, at the crossing of Lines 13/13 and 11/13. North–south running Line 11/13 crosses the basin at the western perimeter with alternate Site SCO-12 to the south, near Site SCO-16.

Expedition 382 will also drill two sites on the South Falklands Slope: Sites SFSD-02 and SFSD-03. The sediments targeted are part of a regional contourite drift largely composed of clay with silty

horizons and deposited beneath the Subantarctic Front along the southern flank of the Falkland Plateau. The South Falkland Slope Drift comprises four sediment packages that exhibit a parallel to subparallel stratigraphy with internal unconformities and overlie a prominent unconformity representing the base of the drift. Koenitz et al. (2008) suggest that these four units were likely deposited under different oceanographic and climatic boundary conditions that occurred since the deep opening of Drake Passage and consequential onset of deep ACC flow in the early Miocene.

Site survey data

Seismic and bathymetric surveys have been conducted by a number of Spanish cruises since 1992 (the Scotia Antarctica [SCAN] expeditions). For Dove Basin, data was used from Expeditions SCAN 2001, SCAN 2004, and SCAN 2008 (Figures **F3**, **F4**); for Pirie Basin, data was used from Expeditions SCAN 2001, SCAN 2008, and SCAN 2013 (Figures **F5**, **F7**); and for Jane Basin, data was used from Expedition SCAN and legacy seismic Line BRA790 was reprocessed and used. The track lines and shot points for each seismic line are indicated in Figures **F3** and **F5**.

Multichannel seismic data was acquired by the R/V *Hesperides* for seismic Lines SM06, 03/04, 07/04, 10/04, and 11/08 (Sites SCO-13 through SCO-18 and SCO-21). The survey was carried out with a tuned array of six Bolt air guns with a total volume of 15.26 L, a 96-channel streamer with an active length of 2.4 km, and a shot interval of 50 m. Multichannel seismic data were recorded with a DFS V digital system and sampling record intervals of 2 ms and 10 s. The seismic data fold was 24. The seismic signals were acquired in SEGY format with the Delph Seismic Plus software. Data were processed with a standard protocol using ProMax 2D software, version 2003.3.2, including velocity analyses, stacking, deconvolution, filtering, migrating, and plotting. Seisee software was used for better display of the seismic data.

For seismic Lines 11/13 and 13/13 (Sites SCO-01, SCO-11, SCO-12, and SCO-19), seismic profiles were collected in 2013 with a high-resolution system composed of a seismic source, a streamer, and an acquisition system. A cluster of two air guns (255 + 265 ci) was used, with the guns separated by 1 m and deployed at 4–5 m water depth. Shot interval was 30 m. Two Hamworthy compressors provided 314 m^3/h of air at 140 bar. The streamer had three active sections of 50 m each, with forty hydrophones in each active section. The seismic signals were acquired in SEGY format with the Delph Seismic Plus software. Postprocessing was executed by using RadExPro and HotShot software and applying the following sequence: reading of raw data, trace georeferencing by considering the acquisition geometry, three-channel stacking and generation of preprocessed SEGY files, notch filter (50 Hz) and bandpass filtering, time-variant gain, water column muting, trace resampling, and generation of reprocessed SEGY. Seisee software was also used for postprocessing and better display of the seismic data.

The multibeam system Simrad EM 120 was used to the collect bathymetric data. The system works at a frequency of 12 kHz, can operate in 20–11,000 m water depth, and has a vertical resolution of 10–40 cm. The sampling frequency is 2 kHz, and the maximum emission rate is 5 Hz. The system uses 191 beams at an opening angle of the swath system of 120°–50°, resulting in a 3.5–5× coverage of the water depth.

The bathymetric data was processed with the Caris Hydrographic Information Processing System, taking into account ship geometry and moving characteristics (pitch, roll, and yaw) and calibration of sound velocity in the water column profile by deploying a number of expendable bathythermographs. For the bathymetric maps in this proposal, we used Geosoft software to create grids with a 50 m resolution.

For the Falklands Plateau Sites SFSD-02 and SFSD-03Y, high-quality seismic reflection profiles were acquired by Geco-Prakla (now WesternGeco) in 1993. These profiles demonstrate the simple structural setting of this contourite deposit (Figure **F8**). The South Falkland Slope Drift comprises four sediment units (1A, 1B, 2A, and 2B; oldest to youngest) slightly offset from each other (Koenitz et al., 2008) (Figure **F9**). Both primary sites (SFSD-02A and SFSD-03A) are located along seismic Line SGF193_107, which runs east–west through the South Falkland Slope Drift. Site SFSD-02 (830 m water depth) is close to the intersection of Line SGF193_166 and targets the most expanded section of sediment Unit 2A. Site SFSD-03 (780 m water depth), ~4 nmi to the west, targets the most expanded sections of Units 2B and 1B. Depending on refusal depth, this site may also recover the uppermost section of Unit 1A.

The supporting site survey data for Expedition 382 are archived at the IODP Site Survey Data Bank (**https://ssdb.iodp.org/SSDBquery/SSDBquery.php**; select P902 for proposal number).

Scientific objectives

Reconstructing history of AIS growth and decay

Marine IBRD records provide a nearly continuous history of variability in ice sheet mass loss. The majority of large icebergs (>5 km long) that calve from the AIS margin (Stuart and Long, 2011) are routed through Iceberg Alley after traveling counterclockwise around Antarctica in the ACC (Figure **F1**). Melt rates increase when icebergs reach the warmer ACC in our study area (Silva et al., 2006). Because icebergs currently account for ~50% of the total AIS mass loss (Gladstone et al., 2001), the Scotia Sea IBRD record will, for the first time, capture a spatially integrated signal that is representative of variability in the flux of icebergs released by the AIS over million-year timescales.

IBRD records of the last deglaciation demonstrate the outstanding opportunity for developing well-dated, long records of AIS discharge history. Based on X-radiograph counts, Weber et al. (2014) identified eight events of increased AIS discharge (AID1–AID8; Figure **F10**) that occurred between 19 and 9 ka. These records provide the first robust evidence for centennial- to millennial-scale variability in deglacial mass loss from the AIS. Specifically, AID6 (~15–13.9 ka) has the largest IBRD flux, peaking at 14.76–14.4 ka, synchronous with the timing (14.65–14.31 ka) and duration (340 y) of Meltwater Pulse 1A (MWP-1A) (Deschamps et al., 2012), providing the first direct evidence for an Antarctic contribution to MWP-1A.

This interpretation is supported by novel modeling and ice-core studies (Fogwill et al., 2017; Golledge et al., 2014) but is in marked contrast to reconstructions arguing for a minor and later (after ~14 ka) AIS retreat (e.g., Bentley et al., 2010; Conway et al., 1999; Mackintosh et al., 2011, 2014; Peltier, 2004). However, those studies rely on temporally and geographically restricted terrestrial and shallow-marine near-field sequences (Anderson et al., 2014; Heroy and Anderson, 2007; Hillenbrand et al., 2013).

The contribution of the AIS to past sea level change remains poorly constrained, yet it is important for assessing the sensitivity of the AIS to climate change and its contribution to future sea level rise (Church et al., 2013). Thus, large uncertainties remain in our understanding of the interactions between the AIS, Southern and Northern Hemisphere climate, and global sea level. Studying the in-

tegrated variability in AIS volume through critical periods of Earth's history has the potential to substantially advance our knowledge on several fronts. Even for the mid-to-late Holocene, a time of relative AIS stability, the IBRD record from Iceberg Alley reveals substantial decadal- to centennial-scale variations in ice mass loss that have far-field effects and significant implications on the future AIS development (Bakker et al., 2016).

In this context, can we confirm a mid-Miocene EAIS glacial intensification? This change could be associated with Reflector c, the widespread discontinuity believed to mark the onset of WSBW in the Scotia Sea (Pérez et al., 2015) and the transition to full glacial conditions in the Weddell Sea (Lindeque et al., 2013) (Figure **F2**). Can we confirm AIS expansion and cooling during the late Pliocene as reconstructed for the WAIS (McKay et al., 2012)? This event could be associated with Reflector a. Can we identify significant WAIS volume changes during mid-Pliocene warm intervals (Naish et al., 2009)? What does the iceberg flux tell us about the size of the AIS during warm periods (e.g., the mid-Miocene climate optimum and the mid-Pliocene warming)? Also, there are still no firm constraints on the AIS contribution to sea level high stands during previous warm periods (Masson-Delmotte et al., 2013). Is the AIS involved in the MPT, and if so, will we observe abrupt or gradual changes in IBRD flux? How similar are previous glacial terminations to the last deglaciation? Does the more northerly Pirie Basin contain a higher percentage of WAIS icebergs that escaped the generally clockwise circulation around Antarctica and instead were routed through Drake Passage? Can we link the delivery of icebergs to Milankovitch orbital cycles, and how do these patterns evolve with time?

IBRD records will be produced from both grain-size measurements and X-radiography to identify periods of enhanced AIS mass loss throughout the record. To simulate dynamics and changes in volume associated with circum-AIS instabilities, we will use the Potsdam Parallel Ice Sheet Model, which accounts for stress boundary conditions and mass transport parameterization at the ice margin by enabling calving-front movement (Levermann et al., 2012; Winkelmann et al., 2012).

Chronology and climate-dust couplings

We will follow the approach of Cody et al. (2008) to establish a coherent low-resolution chronology by combining diatom biostratigraphy, magnetostratigraphy, and tephrostratigraphy. Also, oxygen isotopes ($\delta^{18}O$) on biogenic silica (Collins et al., 2012) should help constrain the timing and related changes in global ice volume and deep-ocean circulation. Sediment physical and optical properties and X-ray fluorescence (XRF) scanner data will be used for orbital tuning and identification of tephra layers, followed by microscopic identification and $^{40}Ar/^{39}Ar$ dating. Prominent sources of ash layers are located to the west (e.g., Deception Island; Moreton and Smellie, 1998).

In addition to measuring the magnetic reversal history (Stoner et al., 2003, 2002), relative paleointensity offers the potential for suborbital magnetic stratigraphy between polarity boundaries (Channell et al., 2009; Stoner et al., 2000; Valet, 2003; Valet et al., 2005; Ziegler et al., 2011). We will test the dust chronology hypothesis in the younger sections, and calibration of paleointensity with the dust/ice-core chronology could potentially be exported to the sedimentary record beyond the Southern Ocean (Channell et al., 2016). A better understanding of magnetic susceptibility should be derived through particle-size specific (magnetic) measurements (Hatfield and Stoner, 2013; Hatfield et al., 2013).

Correlating dust proxies such as magnetic susceptibility, Ca, and Fe to the Antarctic ice-core dust flux (Weber et al., 2012) should provide high-resolution chronological control at least for the Pleistocene and allow us to reconstruct atmospheric circulation (Figure **F11**). The correlation of marine dust records to well-dated ice-core dust records has been a major step forward in developing Southern Ocean chronologies for the Subantarctic Pacific (Lamy et al., 2014), the Subantarctic Atlantic (Martínez-Garcia et al., 2011, 2014; Anderson et al. 2004), and the Scotia Sea (Weber et al., 2012) because dust deposition is thought to be coherent and synchronous across much of the Southern Ocean and the AIS. Age models developed for Cores MD07-3133 and MD07-3134 follow this strategy by synchronizing marine dust proxies (magnetic susceptibility and XRF-based counts of Ca and Fe) to ice-core dust proxies (e.g., non–sea salt Ca fluxes) (McCave et al., 2014; Pugh et al., 2009; Weber et al., 2012) (Figure **F11**), revealing high sedimentation rates (0.2–2 m/ky).

We will use this strategy for the past 800 ky (length of ice-core records) and evaluate the robustness of the strategy used by Martínez-Garcia et al. (2011), who correlated ocean dust proxies to the LR04 stack (Lisiecki and Raymo, 2005) (Figure **F11**) back to the base of the Pleistocene. Biostratigraphy, magnetostratigraphy, and tephrostratigraphy will all be used.

Martínez-Garcia et al. (2011) suggested that dust plays a major role in intensification of Northern Hemisphere glaciation since the mid-Pliocene, with a distinct and abrupt increase at the start of the MPT at 1.25 Ma. They posited an important role for dust in the subsequent intensification of glaciations (see also Rodríguez-Sanza et al., 2012). In contrast, Elderfield et al. (2012) inferred an abrupt increase in AIS volume at ~900 ka attributed to the onset of the MPT. Finally, Raymo et al. (2006) proposed that the MPT was associated with the establishment of largely marine based ice margins around Antarctica. In any of these scenarios, drilling the Scotia Sea sites will provide a unique opportunity to address iceberg-dust-climate interactions and their possible role in AIS behavior, as well as help evaluate the role of dust in the evolution of Plio–Pleistocene glacial cycles and iron fertilization with glacial CO_2 drawdown (Martínez-Garcia et al., 2011, 2014).

Relative paleointensity and magnetic reversal determinations will be used in tandem to obtain further age control for the younger sections. Paleointensity has proven to work in the Southern Hemisphere (Channell et al., 2000; Mazaud et al., 2002; Stoner et al., 2003, 2002) and on the Antarctic margin (Guyodo et al., 2001; Sagnotti et al., 2001). The paleointensity record is dated by correlation to the LR04 stack for at least the last 2.2 My (NARPI-2200, Channell et al., 2016; PISO-1500, Channell et al., 2009; SINT-2000, Valet et al., 2005; PDAM2M, Ziegler et al., 2011) and to 3 Ma (EPAPIS, Yamazaki and Oda, 2005), based on tuning of rock magnetic variables to LR04 and other $\delta^{18}O$ records (e.g., Tian et al., 2002).

AIS mass loss and regional-to-global sea level change

Sea level changes originating from the AIS show a complex spatial variability that is sensitive to the geometry and timescale of mass loss. For example, a rapid mass loss causes local sea level fall adjacent to the former ice source, a fall that can be an order of magnitude greater than the associated globally averaged (eustatic) sea level rise. At progressively greater distances from the region of mass

loss, the amplitude of sea level rise increases, peaking at ~30% above eustatic in the far field. Thus, any rapid AIS mass loss would drive a local, large-amplitude sea level fall that may stabilize the ice sheet to further retreat (Gomez et al., 2010, 2013). In contrast, rapid mass loss from Northern Hemisphere ice sheets will lead to a sea level rise adjacent to the AIS, with a strong geographic gradient and maximum amplitudes in the Atlantic sector (Figure **F12C, F12D**). This far-field sea level rise will impact AIS stability, and the gradient will make the Atlantic sector particularly susceptible to collapse (Clark et al., 2002; Weber et al., 2011).

The peak IBRD flux of AID6 corresponds to the time of MWP-1A (Figure **F10**), with a six-fold increase in flux relative to the Holocene steady state average. This peak flux suggests that the IBRD record of Iceberg Alley may provide a proxy for the relative amount of mass released by the AIS and its associated contribution to global sea level rise for other times in the late Neogene. Through development of long IBRD records from Iceberg Alley, we will evaluate whether meltwater pulses occurred and use sea level calculations to assess their possible contribution to global sea level and the possible role of regional sea level in modulating AIS mass loss.

For past warm periods (e.g., marine isotopic Stages [MIS] 5.5, 11, and 31) it would be of specific interest to identify the source and relative timing of AIS lost mass. For instance, was there a late sea level highstand during MIS 5.5 (O'Leary et al., 2013)? Is there physical evidence for an AIS trigger? Investigations will be accompanied by deglacial simulations for iceberg transport around Antarctica, focusing on the last two deglaciations (e.g., Siddall et al., 2006) and warmer-than-present periods (e.g., MIS 31, 11.3, 9.3, and 5.5) to better understand high-latitude climate processes and AIS dynamics and their impact on sea level.

To explore the impact of ice-mass changes on sea level in the near and far field, we will adopt a state-of-the-art sea level model that incorporates all deformational, gravitational, and rotational effects of glacial isostatic adjustment (Kendall et al., 2005). This model also takes account of shoreline migration associated with local onlap/offlap of water and changes in the extent of grounded, marine-based ice. Sensitivity studies will be performed using Maxwell viscoelastic Earth models in which Earth's structure varies with depth through the lithosphere. We will also perform calculations incorporating lateral variations in viscosity structure using a finite element numerical model (Latychev et al., 2005). This model may be particularly important given seismic inferences of large differences in mantle structure below the WAIS and EAIS (Danesi and Morelli, 2001) and its impact on dynamic topography (Austermann et al., 2015).

Water mass changes and ocean thermal forcing

The Southern Ocean plays an important role in the Atlantic Meridional Overturning Circulation (AMOC) because it controls, through upwelling, the rate of heat and carbon exchange with the surface (Marshall and Speer, 2012), which is a major driver of climate change. This interhemispheric teleconnection shows that a reduction in the AMOC and attendant decrease in northward heat transport leads to warming of the Southern Hemisphere and to changes in the relative contributions of North Atlantic Deep Water (NADW) to Antarctic Bottom Water (AABW) and WSBW, as well as the amount of CDW that is formed through mixing. Our goal is to study the changes in water mass properties that lead to atmospheric and oceanic reorganizations and associated changes in wind fields, sea ice, marine productivity, atmospheric CO_2, surface ocean and atmosphere temperatures, and AIS mass loss.

The radiogenic isotope composition of authigenic neodymium (ε_{Nd}) provides important information on past changes in deep-water mixing (e.g., Rutberg et al., 2000; Goldstein and Hemming, 2003; Gutjahr et al., 2008; Piotrowski et al., 2004, 2005, 2008; Scher and Martin, 2006; van de Flierdt et al., 2006a; Pena and Goldstein, 2014). The isotopic signal of seawater-derived ε_{Nd} will be separated from other sedimentary components following the method of Gutjahr et al. (2007), using the method of Roberts et al. (2010 and 2012) if we have carbonates, and, where possible, from fish teeth (e.g., Martin and Scher, 2004) or discrete ferromanganese nodules or carbonate constituents to ensure seawater origin. Recent water-column measurements resolved the modern spatial ε_{Nd} variability in the Drake Passage (Stichel et al., 2012).

Based on van de Flierdt et al. (2006b) and Robinson and van de Flierdt (2009), CDW was very likely much more radiogenic (higher ε_{Nd}) during glacials because of lower admixing of NADW relative to CDW (Piotrowski et al., 2004, 2005, 2008). In combination with modeling efforts, we will (1) assess past changes in water mass composition using authigenic neodymium isotopes to test the ocean thermal forcing hypothesis for previous terminations (Böhm et al., 2015) and (2) test whether changes in NADW, CDW, and WSBW (Pérez et al., 2015) are associated with the formation of Reflectors a, b, and c.

Given the importance of ocean thermal forcing to the dynamics of AIS marine margins and grounding lines, we will also evaluate the relationship between sea-surface temperature (SST) and IBRD flux. Because the alkenone unsaturation index ($U^{k'}_{37}$) is likely not applicable (Shevenell et al., 2011), we will extract isoprenoid and branched glycerol diether glycerol tetraether (GDGT) lipids to measure the TEX_{86} ratio (Schouten et al., 2002) and convert it to SST using published calibrations (e.g., Kim et al., 2008).

Provenance studies

Identifying the regional sources of individual IBRD events is crucial to assess past AIS evolution. In particular, does the IBRD signal at any given time reflect an ice sheet wide contribution, or were different iceberg discharges associated with specific sectors of the AIS? The diverse geology of the Weddell embayment and East Antarctica provides distinct isotope geochemical sources that will be distinguished in IBRD and the fine sediment fraction. For example, the $^{40}Ar/^{39}Ar$ age of a single hornblende (or mica) IBRD grain allows it to be traced to a source on the continent with a similar $^{40}Ar/^{39}Ar$ age, and a population of ~30 hornblende grains should show which sources are most actively exporting debris in icebergs, which is information critical to reconstructing the past history of the AIS (e.g., Roy et al., 2007; Williams et al., 2010; Pierce et al., 2011, 2014). Similarly, Pb-Pb and $^{40}Ar/^{39}Ar$ in feldspars (e.g., Hemming and Rasbury, 2000; Flowerdew et al., 2013), U-Pb in zircons (e.g., Pierce et al., 2014), and other thermochronometers (e.g., reviewed in Licht and Hemming, 2017) can distinguish input from different source areas. Combining these mineral tracers should lead to more accurate identification of provenance and hence the spatial history of AIS glaciation.

The provenance of glacially eroded fine sediment will also be assessed using radiogenic isotope systems. For example, Sm-Nd isotopes, which reflect the "crustal extraction" bedrock age (e.g., Goldstein et al. 1984) have been widely used for AIS provenance studies (e.g., Basile et al., 1997; Roy et al., 2007; Hemming et al., 2007; Pierce et al., 2011; Cook et al., 2013; Farmer et al., 2006). Recent studies on the Wilkes Land margin (Cook et al., 2013), for instance, indicate extensive EAIS retreat that might have contributed

to the mid-Pliocene sea level high stand. Overall, East and West Antarctic bedrock have distinctly different Nd isotopic compositions, so Sm-Nd isotope results should be able to gauge the balance of sediment input between East and West Antarctica. Although there is some overlap between the radiogenic isotopes from East and West Antarctica (Farmer et al., 2006; Roy et al., 2007; van de Flierdt et al., 2007; Hemming et al., 2007), broadly there is considerably older crust (and thus lower ε_{Nd} and ε_{Hf} and higher $^{87}Sr/^{86}Sr$ from East Antarctic sources). In some cases, the provenance information from the sand fraction and the fine fraction can provide contrasting evidence (e.g., Cook et al., 2017; Pierce et al., 2017; Licht and Hemming, 2017), so it is important to examine both. Other geochemical tracers, especially radiogenic isotopes systems such Rb-Sr, U-Th-Pb, Lu-Hf, and K-Ar are likely to provide greater clarity in the assessment of mixing from difference sources.

Finally, provenance studies may help to resolve a longstanding issue by constraining the source of the high sea level during MIS 5, which was 5–9 m higher than today (Dutton and Lambeck, 2012; Kopp et al., 2009; O'Leary et al., 2013). Greenland contributed from 1 to 4 m (Colville et al., 2011; NEEM Community Members, 2013), implying an additional contribution from the AIS (Masson-Delmotte et al., 2013). Although the WAIS is commonly invoked as the most likely source, no data support this assumption, and additional sources from the EAIS should also be considered, particularly with the growing recognition that it also has substantial areas of marine-based ice (Cook et al., 2013; Vaughan et al., 2013) that may play an increasing role in future AIS mass loss and global sea level scenarios (Mengel and Levermann, 2014).

Glacial–interglacial sea ice shifts and the carbon cycle

Changes in sea ice extent influences the flux of heat and carbon between the deep ocean and the atmosphere (Schmitt et al., 2012) and the degree of primary production (Anderson et al., 2009). Sea ice is recognized as an important amplifier of high-latitude climate anomalies, and of particular interest is the role of sea ice variability on glacial–interglacial climate. Expanded Antarctic sea ice during glacials increases export of AABW/WSBW and limits mixing and ventilation of the deep ocean, possibly causing ~20% to ~60% of the glacial–interglacial CO_2 change according to carbon cycle models (Ferrari et al., 2014; Sigman et al., 2010; Stephens and Keeling, 2000). However, there are few proxy constraints to test these models, and large uncertainties remain. Little is known about the areal extent and duration of summer and winter sea ice during previous glacials and interglacials. Similarly, the primary controls on changing sea ice distribution and associated feedbacks are also poorly constrained. In combination with modeling efforts, seasonal sea ice changes will be investigated over multiple glacial cycles to help shed light on the processes that cause changes in ocean circulation, ventilation, and CO_2 sequestration.

We hypothesize that changes in Antarctic winter and summer sea ice extent are driven by migration of the SHW and fluxes of glacial meltwater to the surface ocean. The sea salt Na^+ flux record of the EPICA Dronning Maud Land (EDML) ice core suggests that sea ice extent underwent large fluctuations during the last deglaciation (Wolff et al., 2006) (Figure **F10E**), which have been simulated by modeling studies (Menviel et al., 2011). Similarly, models suggest that ocean thermal forcing during the last deglaciation induced increased freshwater at the onset of MWP-1A (Figure **F12**), causing consecutive sea ice expansion during the Antarctic Cold Reversal and retreat thereafter at the begin of the Younger Dryas (Fogwill et al., submitted; Weber et al., 2014). Based on findings for the last glacial (Allen et al., 2011; Collins et al., 2013), we hypothesize that previous glacial expansions of summer and winter sea ice in the Scotia Sea will reach their maximum extents at ~59° and ~55°S, respectively.

Fogwill et al. (2014) modeled a 9° poleward shift of the SHW and a 0.2°–0.9°C warming in the upper 500 m of the subpolar gyres that persisted for millennia during deglaciation. Associated AIS drawdown might also have induced large-scale sea ice expansion and IBRD increase (Fogwill et al., 2017). Reconstructing these Antarctic sea ice conditions and dust-climate couplings will provide much needed empirical data to assess whether changes in sea ice cover are driven by the position of the southern SHW and/or flux of glacial meltwater.

The Scotia Sea sites are ideally located to record past variations in both summer and winter sea ice boundaries (Figures **F1**, **F13B**). We will use diatom assemblages (Allen et al., 2011) and a new biomarker-based method that uses highly branched isoprenoids (HBI) (Collins et al., 2013). For sea ice, biomarker IP_{25}, a monounsaturated HBI biomarker derived from sea ice diatoms, has been successfully used to reconstruct sea ice conditions in Arctic regions for Quaternary to Pliocene timescales (Belt et al., 2007; Belt and Müller, 2013; Müller et al., 2009; Stein and Fahl, 2013). HBI has been used as a corresponding proxy for seasonal sea ice in the Southern Ocean (Massé et al., 2011). Importantly, the source organism of HBI, *Berkeleya adeliensis*, has now been identified (Belt et al., 2016). *B. adeliensis* is endemic to Antarctic sea ice only and has been named $IPSO_{25}$. Because *B. adeliensis* flourishes in platelet ice, its sedimentary abundance is sensitive to nearby glacial or ice-shelf settings, likely explaining its occurrence in glacial Scotia Sea sediment (Collins et al., 2013). Also, Belt et al. (2015) and Smik et al. (2016) demonstrated enhanced production of a different HBI biomarker in a retreating ice edge environment. Combined analysis of $IPSO_{25}$ with other HBIs should therefore provide insights into seasonal sea ice dynamics.

Analysis of sea ice diatoms (*Fragiliariopsis curta*, *Fragiliariopsis cylindrus*, and *Fragiliariopsis obliquecostata*) (Gersonde and Zielinski, 2000) has also been successfully used to reconstruct Pleistocene sea ice extent in the Southern Ocean (Allen et al., 2011; Gersonde et al., 2005), and the same approach will be implemented here to complement the HBI analysis.

Both methods were applied to piston cores along north–south transects, with the Scotia Sea sites in the center and the South Falkland Slope sites to the north (Figure **F13A**), to determine the presence/absence of permanent and/or seasonal sea ice, the position of the marginal ice zone, and associated wind mixing and ocean stratification for the last 60 ky (Figure **F13B**). We will apply these same methods to older intervals. To further strengthen our investigation of the silica inventory, we will also include $\delta^{30}Si$ and $\delta^{18}O$ studies on diatoms.

Reconstructions of sea ice and paleotemperature will be accompanied by transient climate model simulations (e.g., Timmermann et al., 2014). To study Southern Hemisphere climate changes throughout past glacial–interglacial cycles, the global Earth system model, LOVECLIM (Menviel et al., 2008, 2010; Timmermann et al., 2009), will be used, based on a dynamical atmosphere coupled to an ocean general circulation model and dynamic/thermodynamic sea ice and diagnostic vegetation models. This model has been used to simulate the transient evolution of the past four glacial–interglacial cycles (Timmermann et al., 2014). Numerical experiments are also underway with the Pennsylvania State University AIS model (Pol-

lard and De Conto, 2009), forced by the LOVECLIM transient model output of the past 408 ky, which will allow future investigations of climate–ice sheet interactions on orbital timescales and comparisons with paleoproxy data generated with Iceberg Alley drill cores. Climate–ice sheet interactions can also be studied with the Consortium for Small Scale Modeling (COSMOS) climate model, a state-of-the art comprehensive coupled general circulation model that has been extensively used to study past climate (Knorr et al., 2011; Wei et al., 2012; Zhang et al., 2013). The COSMOS model is now coupled to an ice sheet model that includes ice-shelf and grounding-line dynamics (Barbi et al., 2013; Thoma et al., 2014).

ACC flow speed reconstruction

The SHW are crucial for the Drake Passage throughflow (e.g., Marshall and Speer, 2012; Toggweiler and Samuels, 1995), atmospheric CO_2 release (Denton et al., 2010; Lamy et al., 2007; Sigman and Boyle, 2000), and paleoproductivity (Anderson et al., 2009; Lamy et al., 2014; Roberts et al., 2016; Sprenk et al., 2013). For the last glaciation, a northward shift or extension of SST gradients and oceanic fronts is suggested for the Southeast Pacific (Lamy et al., 2007; Moreno et al., 1999), the South Atlantic (e.g., Barker et al., 2009; Park and Latif, 2008), and the Southwest Pacific/Indian Ocean region (e.g., De Deckker et al., 2012; Lorrey et al., 2012). Modeling studies suggest a reduction of ACC transport volume during glacial stages and an increase during glacial terminations (Knorr and Lohmann, 2003, 2007), during which the ACC and associated fronts shifted south.

Based on grain size analyses on 12 cores from a north–south transect across the Scotia Sea (Figure **F13**), McCave et al. (2014) examined the frontal system of the ACC and concluded that during the Last Glacial Maximum (LGM), near-bottom current velocities were essentially the same as they are today, except for the sea ice zone south of ~56°S where they were slower (Figure **F13A**). Recent study found a glacial reduction and millennia-timescale variability in the ACC throughflow (Lamy et al., 2018). Our drill sites are located in the southern half of this transect (Figure **F1**). Using a similar methodology, we will reconstruct paleocurrents to evaluate the long-term evolution of current speeds in the ACC and whether changes in Drake Passage throughflow and shifts in frontal systems are associated with the seismic units and occurred on glacial–interglacial and/or millennial timescales. Analyses will be made in conjunction with modeling efforts and compared to other Southern Ocean regions.

Drilling in more southerly Dove Basin should also provide insights into the evolution of the WSBW overflow through the Orkney Passage. As a working hypothesis, this process could have started with Reflector c during the mid-Miocene and strengthened after Reflector a during the late Pliocene, according to Maldonado et al. (2006). Both Dove Basin and isolated basins in the South Scotia Ridge show complex contourite systems (Maldonado et al., 2003). Could this imply that Dove Basin was generally more dominated by WSBW, whereas Pirie Basin was under higher influence of CDW? Today, WSBW flows northwest at relatively high speed (≤0.6 m/s) at the southern limit of Dove Basin (Naveira Garabato et al., 2002).

Plio–Pleistocene ice age climate cycles and underlying causes

The global cooling trend (Figure **F11C**) observed over the last 3–5 My, with the initiation of Northern Hemisphere glaciation at ~2.6 Ma, has been attributed to the interplay of changes in orbital configuration (Lisiecki and Raymo, 2005), CO_2 decrease (Lunt et al., 2008; Raymo et al., 1988), tectonic development (Cane and Molnar, 2001; Raymo et al., 1988), intensification of Antarctic glaciation (McKay et al., 2012), and the emergence of the cold tongue in the Eastern Equatorial Pacific (Martínez-Garcia et al., 2010). Prevalent theories for subsequent glacial–interglacial changes propose that fluctuations in global ice volume are caused by variations in the amount of insolation received at critical latitudes and seasons due to variations in Earth's orbital parameters. In particular, it is widely agreed that variations in ice volume over the last 700,000 years at the precessional (~23 ky) and obliquity (41 ky) frequencies are directly forced by and coherent with Northern Hemisphere summer insolation, whereas the ~100 ky eccentricity component of the ice age cycle results from nonlinear amplification mechanisms (e.g., Abe-Ouchi et al., 2013; Imbrie et al., 1993, 1992). However, during the late Pliocene–early Pleistocene interval from ~3 to 1 Ma, only weak variance at 100 and 23 ky periods is observed in proxy ice-volume records such as benthic $\delta^{18}O$ (e.g., Raymo and Nisancioglu, 2003). Instead, the records are dominated by the 41 ky obliquity cycle (Figure **F11C**). So why is there no strong precessional signal as predicted by the Milankovitch model?

Hypotheses presented to explain this conundrum point to the Southern Hemisphere and its important role in contributing to the observed global climate signal (Huybers and Denton, 2008; Raymo et al., 2006; Raymo and Nisancioglu, 2003). However, there are only a few records from the Southern Ocean (e.g., Ocean Drilling Program [ODP] Site 1090; Martínez-Garcia et al., 2011), East Antarctica (e.g., IODP Site U1356 from Wilkes Land; Cook et al., 2013; Patterson et al., 2014) and West Antarctica (e.g., ANDRILLL AND-1B core; McKay et al., 2012) available to test these various hypotheses. For instance, McKay et al. (2012) suggested that the intensification of Antarctic cooling strengthened SHW, invigorated circulation in the Southern Ocean, reduced the AMOC, and thereby contributed to Northern Hemisphere glaciation. On the other hand, Raymo et al. (2006) proposed that the precession cycle should be obvious in Antarctic ice-volume variations prior to the MPT but is absent in globally integrated records such as $\delta^{18}O$ because precession is out of phase between the Northern and Southern Hemisphere ice sheets. Because our proposed sites are located in a key region to reconstruct the evolution of the Southern Ocean and AIS, the climate and ice sheet signals we find should help in solving this Neogene puzzle.

Scientific objectives for the South Falkland slope sites

Cores from the South Falkland Slope sites will allow us to extend reconstructions of Antarctic Intermediate Water history and the position of the Subantarctic Front (Figure **F14**) to at least 1 Ma. Existing short (~7 m) cores from the South Falkland Slope demonstrate the potential of these sediments to yield paleoceanographic records that document past changes in surface and intermediate waters (Figure **F15**). Deposited beneath the jet of the Subantarctic Front, the South Falkland Slope is sensitive to velocity changes associated with frontal migration. Roberts et al. (2017) compared sortable silt records from the South Falkland Slope with records from Drake Passage to infer a more northerly position of the Subantarctic Front during the last glacial. Grain size data also suggest that the Subantarctic Front shifted to its current position during the deglaciation, enhancing throughflow of Pacific-sourced intermediate wa-

ters into the South Atlantic. Stable isotope and elemental analyses of benthic foraminifers in these cores were also used to reconstruct the history of intermediate–deep density stratification in the Atlantic sector of the Southern Ocean since the LGM (Roberts et al., 2016).

Cores recovered from proposed Sites SFSD-02 and SFSD-03 will enable us to better understand the role of the "cold water route" on millennial, orbital, and longer timescales. Suitable calcareous benthic foraminifers persist in the South Falkland Slope Drift throughout the last glacial cycle, and tuning of benthic $\delta^{18}O$ to the LR04 stack provides a robust age model. Extending the $\delta^{18}O$ stratigraphy will provide an orbital-scale age model for the longer South Falkland slope records. Accurately resolving interhemispheric phasing will help identify interactions between the cold-water route and the AMOC (Barker et al., 2011). In addition, new records from the South Falkland Slope will complement the "warm route"/Agulhas leakage records of the Southeast Atlantic (e.g., Marino et al., 2013; Martínez-Méndez et al., 2010; Peeters et al., 2004), as well as the records generated from ODP Leg 177 (e.g., Caley et al., 2013; Martínez-Garcia et al., 2011) and emerging records from IODP Expedition 361.

Additional objectives include providing the first long-term marine perspective on the Pleistocene evolution of the Patagonian Ice Sheet and its interactions with the Southwest Atlantic and generating the first long-term SST records from the subantarctic Southwest Atlantic.

Broader implications

Drilling at our proposed sites will provide an outstanding opportunity to understand late Neogene AIS variability, to identify regional sources of ice mass loss, and to deliver an important historical context for future projections of AIS behavior in a warmer world. Recent novel findings (Bakker et al., 2016; Fogwill et al., 2017; Weber et al., 2014) and the hypotheses developed for this proposal address AIS stability and its relation to climate change. In particular, they challenge scenarios in which the AIS made only a relatively small contribution to the LGM sea level lowstand (e.g., Whitehouse et al., 2012) and made virtually no contribution to MWP-1A (e.g., Bentley et al., 2010, 2014; Mackintosh et al., 2011; Mackintosh et al., 2014). A better understanding of the Antarctic sea level contribution is critical to understanding late Neogene changes and projecting sea level rise in a future warming world. Global mean sea level could rise ≥1 m by 2100, and large uncertainties remain in projecting AIS contributions to sea level rise beyond that time (Church et al., 2013). Recently appreciated mechanisms such as ice-cliff failure and hydrofracturing (DeConto and Pollard, 2016) may increase the possible contribution of the AIS to future sea level rise substantially, specifically on the multicentennial timescale. Understanding the role of ocean thermal forcing and the resulting changes in water masses and sea ice extent, as well as their influence on past AIS behavior will help constrain projections of future sea level rise.

Furthermore, by reconstructing past variability in sea ice, SSTs, water masses, dust-climate couplings, and deep-water current speeds in this major Antarctic gateway, back to the mid-Miocene, our expedition holds the potential to provide important new understanding of the relation between AIS volume changes, shifting SHWs, ocean fertilization, and associated changes in CO_2.

Operations plan/drilling strategy

Proposed drill sites

The proposed sites at the Falkland Slope and Pirie and Dove Basins, along with their alternates, align northwest–southeast along a piston core transect that has previously been investigated for LGM to recent times (Allen et al., 2011; Collins et al., 2013; McCave et al., 2014) (Figures **F1**, **F13**). All proposed sites for Expedition 382 are listed in Table **T1**.

Two primary sites will be drilled on the southern Falkland Slope to recover a complete sedimentary record since the mid-Pleistocene. The record is separated into four sedimentary units (1A, 1B, 2A, and 2B; from old to young). At deeper Site SFSD-03, Units 2B and 1B will be recovered, and Unit 1A will at least be penetrated. At shallower Site SFSD-02, an expanded section of Unit 2A will be recovered (Figure **F9**).

For both Pirie and Dove Basins, a complete and representative sediment record will be obtained for each basin. However, this objective probably cannot be achieved at a single site for three reasons. First, because of the hummocky terrain and the seismic reflection character, individual locations may exhibit discontinuities such as hiatuses and mass transport deposits; therefore, the combination of two sites may produce a more complete combined record. Second, the thicknesses of seismic Units I–V vary between the sites (Table **T2**), so we can obtain an expanded record using the thicker units from individual sites (Figure **F16**). Third, at least some of the deeper reflectors may be time transgressive and represent, for instance, the opal-CT boundary. To avoid for these potential shortcomings, two sites will be drilled in each basin.

In Dove Basin, the few available seismic lines indicate a basin-like structure with several small-scale ridges and continuous reflectors in the central part (Figures **F3**, **F4**). Given these preexisting constraints, primary Sites SCO-14 and SCO-13 promise the thickest sediment in the upper part (Table **T2**). Primary Site SCO-14 is located along seismic Line 03/04 at the eastern end of a small basin. Primary Site SCO-13 is located along Line 10/04 farther northeast. Alternate Site SCO-15 is located at the crossing of Lines 10/04 and 03/04. Alternate Site SCO-18 is located farther north along Line 07/04. The only existing site in Dove Basin with a highly resolved record of AIS variability (Weber et al., 2014) is Core MD07-3134 (3663 m water depth; 58.2 m long; 93 ka base age; 0.2–1.2 m/ky sedimentation rates) (Weber et al., 2012). Core MD07-3134 is also located in the same basin structure, although far west of Line 10/04 and not directly on an existing seismic line (Figure **F3**), which is why it could not be chosen as drill site.

Two primary sites will also be drilled to capture a representative record in Pirie Basin (Figure **F5**). Here, east–west seismic Lines 13/13 and 11/08 indicate a north–south oriented basin (Figures **F5**, **F6**, **F7**). Core MD07-3133 (alternate Site SCO-01) was retrieved in 2007 (Weber et al., 2012) and provides the only groundtruth data for Pirie Basin (3101 m water depth; 32.8 m long; 36 ka base age; 0.3–2 m/ky sedimentation rates). North–south Line 11/13 crosses the basin at the western perimeter. Accordingly, drilling at the two crossing lines (e.g., alternate Sites SCO-16 and SCO-19) should yield continuous deposition in that structural unit only for the upper ~100–200 m. Therefore, primary Sites SCO-17 and SCO-11 are located east into the center of that basin along Lines 11/08

and13/13, respectively, where thicker and more stratigraphically continuous sections are expected. Upper Unit I (0–2.6 Ma?) is ~256 m thick at Site SCO-17 compared to ~96 m thick at Site SCO-11, whereas lower Unit I (2.6–3.3 Ma?) is ~128 m thick at Site SCO-17 compared to ~304 m thick at Site SCO-11. Together, the two sites cover the last 3.3 My at high resolution. Also, alternate Site SCO-12 could recover a rather continuous sedimentary section of that basin.

Given the fact that very long MD cores (as long as 58 m) of fine-grained and soft sediment were retrieved (note that encapsulated IBRD is ≤2 mm and embedded in muddy matrix; i.e., not obstructing coring), we expect very good recovery, at least until the opal-CT transition depth is reached at ~400–600 mbsf. We also expect the core recovery and hole stability for downhole logging to be good.

Simple extrapolation of sedimentation rates obtained by piston cores (20–200 cm/ky; see below) implies young ages (≤5 Ma) for the base of the sediment sequence that overlies basement. These ages are younger than the interpreted ages of basement in Dove Basin (~23 Ma) and Pirie Basin (~14 Ma) (Figure **F2**), implying slower sedimentation rates with depth and/or hiatuses in the sequence. High accumulation may have only occurred in small troughs and therefore (1) seismic records may have overestimated ages for the upper three units and/or (2) sedimentation was interrupted by hiatuses of longer duration (e.g., Reflector b is thought to represent stronger erosion) (Pérez et al., 2015). Hiatuses in the sediment sequence may themselves provide valuable information of changing current regimes in the study area. If the upper units are young, drilling will be extended as far as possible; if they are old (Miocene or older), drilling at multiple sites will concentrate on younger sections.

The depths to target seismic reflectors are based on an estimated seismic velocity of 1.6 km/s. The actual velocity will likely be <1.6 km/s in the upper part, so the depth to reflectors may be slightly shallower than expected. Velocity may increase to >1.6 km/s in the lower part of the sequence, so the depth to target reflectors may be deeper than expected.

Operations plan

Expedition 382 will depart from and return to Punta Arenas. The operations plan is detailed in Table **T3** and Figure **F16**. If no hazards occur, operations will be as follows. Transit time to the South Falkland Slope will be 1.8 days. Here, coring operations will commence by first drilling Site SFSD-03A to refusal (~300 mbsf; note that all sites will be triple cored), and then Site SFSD-02A will be drilled to 120 mbsf. Coring operations at the Falkland Slope are expected to take 4.6 days. After the transit to Pirie Basin (2.3 days), Site SCO-11 will be drilled to Reflector c (620 mbsf), which should take 9.3 days. Transit to Dove Basin will take 0.6 days, where Site SCO-13 will be drilled to basement (806 mbsf pending Environmental Protection and Safety Panel [EPSP] approval of this depth extension), requiring 11.1 days. Then Site SCO-14 will be drilled to Reflector c (592 mbsf) in 9.9 days. After transiting back to Pirie Basin (0.5 days), Site SCO-17 will be drilled to 732 mbsf, which should take 10.2 days. Transit back to Punta Arenas will take 4.0 days.

If sea ice conditions are forecast to be severe (e.g., new sea ice grows from the south to cover the Dove Basin sites early in the expedition; see Figure **F17**), drilling operations shall commence in the southernmost study area and then continue north. If drilling is not possible at the Falkland Slope sites as planned at the beginning of the expedition (because of adverse weather or sea conditions), we will return to those sites later in the expedition. If drilling is prohibited at the primary sites in Dove and Pirie Basins because of hazards or technical problems, the alternate sites should offer almost equally good core quality and recovery. If drilling is prohibited in the central and southern Scotia Sea, the contingency plan, drilling Site SCO-21B to the south at the location of ODP Site 697, should be executed.

Downhole measurement strategy

Temperature measurements are planned to reconstruct the thermal gradient and heat flow at each site. Typically, ~3–5 measurements will be made in one hole per site using the advanced piston corer temperature tool (APCT-3), potentially supplemented by the Sediment Temperature Tool (SET) where sediments are more consolidated.

Wireline logging is planned with two tool strings for all the Scotia Sea sites. The triple combination (triple combo) tool string provides formation resistivity, density, porosity, natural (spectral) gamma radiation, and borehole diameter data. The Formation MicroScanner (FMS)-sonic tool string will provide an oriented 360° resistivity image of the borehole wall, as well as formation acoustic velocity, natural gamma radiation, and borehole diameter data. These data will provide in situ formation characterization and are the only data obtained where core recovery is incomplete, allowing interpretation of stratigraphy across core gaps. For example, alternations between microfossil-rich and microfossil-poor layers may be seen, and larger IBRD clasts will be apparent in the FMS resistivity images. Porosity, gamma ray, sonic, and density logs together will provide additional constraints on the depositional history. Velocity logs together with core velocity data will provide a means to tie the borehole stratigraphy to the reflectors in the seismic profile and thus extend the knowledge gained from the cores over a much broader area. A combination of sonic velocity and density data will be used to generate a synthetic seismic profile at each site to refine the borehole-seismic ties. At the moment, we do not plan on running check shot surveys, but we will have this capability on board in case we need further in situ velocity information for core-log-seismic integration. Details of the logging tools are available at **http://iodp.ldeo.columbia.edu/TOOLS_LABS/tools.html**.

Risks and contingency

The area of operation (central and southern Scotia Sea) has a number of risks involved. Potential hazards may arise from sea ice, icebergs, wind speed, wave heights, or technical problems. Hence, flexibility will be required, and drilling operations will need to move forward as dictated by the drilled material and the potential hazards. Drilling operations could shift between primary and alternate sites in a given region or between Pirie Basin and Dove Basin.

Alternate Site SCO-21 in Jane Basin (ODP Leg 113 Site 697; Figure **F1**) is our contingency plan if drilling will not or will only partially be possible in the central Scotia Sea. This alternate site is not far to the south at a similar water depth, with good magnetostratigraphy and early Pliocene material at depths suitable for advanced piston corer (APC) drilling (Pudsey, 1990). The site was single-cored in 1987 with moderate recovery, which we plan on extending to 468 mbsf (the current EPSP limit) with improved recovery with current APC/half-length APC (HLAPC) technology and triple coring.

Sea ice

Daily data of Antarctic sea ice conditions from the Advanced Microwave Scanning Radiometer-EOS (AMSR-E and its successor, AMSR-2) (Spreen et al., 2008) show a fairly consistent pattern of annual sea ice development for the last 15 y (daily images available at **http://iup.physik.uni-bremen.de:8084/amsr**).

The seasonal sea ice cycle shows a rapid decrease in sea ice extent from circum-Antarctic coverage to near-coastal regions for November to December, when sea ice is mainly in the western Weddell Sea. Sea ice usually remains south of 65°S from January to April. From May to June, progressive north and east sea ice expansion into the Scotia Sea can extend beyond 60°N. This expansion could affect the southern site for the austral winter period, although the Scotia Sea sites are usually north of the average position of maximum (winter) sea ice extent. Biweekly displays over the last 5 y (Figure **F17**) that record the seasonal conditions during Expedition 382 (March–May) show the seasonal progression of sea ice to the north but also some interannual variability. One or more ice observers will sail with the expedition, and we will monitor the sea ice conditions and forecasts continuously (e.g., at **https://www7320.nrlssc.navy.mil/GLBhycomcice1-12/antarc.html**)

Icebergs

Icebergs pose an additional threat to drilling operations, and the *JOIDES Resolution* will have to move off site if an iceberg approaches too close to a site location. In these instances, we will have a free-fall funnel (FFF) ready to deploy that would allow for hole reentry after the iceberg passes. Icebergs will be monitored visually by radar and where possible by satellite images.

Available information on iceberg drift is less specific to region and season (**http://www.scp.byu.edu/data/iceberg/database1.html**). Stuart and Long (2011; fig. 8) described an annual pattern for large tabular icebergs (≥18 km in length for 2002–2009) with lowest counts in the early austral summer ablation period in January, followed by an increase in March to June, and generally highest numbers during austral winter. This pattern basically follows the sea ice configuration, although iceberg counts during the austral summer ice-melt season underestimate the true number of icebergs, most of which are too small to be observed by satellite. Smaller icebergs (1–2.8 km in length for 2002–2010) (Tournadre et al., 2012; figs. 4 and 5) are most abundant during the austral summer but exhibit significant interannual variability.

Wind speeds and wave heights

The Scotia Sea is windy with intermediate wave heights throughout the year (**http://apdrc.soest.hawaii.edu/las/v6/dataset?catitem=2893**). Average wind speeds were 2–7 m/s and wave heights were 2.5–3.5 m for 1957–2002. Current velocities were rather low (0–30 cm/s) for 1999–2009 (**http://apdrc.soest.hawaii.edu/las/v6/data set?catitem=1445**) and varied seasonally (minor peaks during austral winter). Current speeds were slightly higher in the north.

Data for the month of April, provided to IODP by Wilkens Weather, suggest that wind speeds are >22 kt about 43% of the time and wave heights are >12 ft 31% of the time. It is likely that some operations time during the expedition will be lost while we wait out bad weather conditions.

Coring and operational risks

Reentry options (FFFs) will be used for each site if we require the ability to reoccupy a hole because of iceberg or other hazards.

Sampling and data sharing strategy

Shipboard and shore-based researchers should refer to the IODP Sample, Data, and Obligations policy (**http://www.iodp.org/top-resources/program-documents/policies-and-guidelines**). This document outlines the policy for distributing IODP samples and data to research scientists, curators, and educators. The document also defines the obligations that sample and data recipients incur.

The Sample Allocation Committee (SAC) must approve all requests for core samples and data. The SAC is composed of the Co-Chief Scientists, Expedition Project Manager, and IODP Curator on shore or curatorial representative on board the ship. For the South Falkland Slope sites, the lead proponent of those sites will be part of the SAC. The SAC will work with the entire scientific party to formulate a formal expedition-specific sampling plan for shipboard and postexpedition sampling.

Scientists are expected to submit sample and data requests using the Sample and Data Request Database (**http://iodp.tamu.edu/sdrm**) several months before the beginning of the expedition. Based on shipboard and shore-based research plans submitted by this deadline, the SAC will prepare a tentative sampling plan that will be revised on the ship as dictated by recovery and expedition objectives. The sampling plan will be subject to modification depending upon the actual material recovered and collaborations that may evolve between scientists during the expedition. Modification of sample and data requests during the expedition must be approved by the SAC.

The minimum permanent archive will be the standard archive half of each core. All sample frequencies and sizes must be justified on a scientific basis and will depend on core recovery, the full spectrum of other requests, and the expedition objectives. Some redundancy of measurement is unavoidable, but minimizing the duplication of measurements among the shipboard party and identified shore-based collaborators will be a factor in evaluating sample requests.

If some critical intervals are recovered, there may be considerable demand for samples from a limited amount of cored material. These intervals may require special handling, a higher sampling density, reduced sample size, or continuous core sampling for the highest priority research objectives.

Following Expedition 382, cores will be delivered to the Core Repository in Bremen (Germany), where the postexpedition sample party will take place. All collected data and samples will be protected by a 1 y moratorium period following the completion of the postexpedition sampling meeting, during which time data and samples will be available only to the Expedition 382 science party and approved shore-based participants.

Postexpedition analytical work will include magneto-, bio-, and tephrostratigraphy combined with dust tuning, stable isotopes, and relative paleointensity to establish the chronology; production of seawater-derived radiogenic isotope records, IBRD, physical properties, XRF scanning, and provenance studies to constrain ice dynamics; geochemistry, sortable silt, stable isotopes, and biomarkers;

and diatom assemblages to reconstruct ocean temperature, current strength, productivity, and sea ice extent. Models will help investigate possible physical mechanisms that cause changes in ice sheet dynamics, ocean-atmosphere interactions, and sea level changes.

Expedition scientists and scientific participants

The current list of participants for Expedition 382 can be found at **https://iodp.tamu.edu/scienceops/expeditions/iceberg_alley_paleoceanography.html**.

References

Abe-Ouchi, A., Saito, F., Kawamura, K., Raymo, M.E., Okuno, J., Takahashi, K., and Blatter, H., 2013. Insolation-driven 100,000-year glacial cycles and hysteresis of ice-sheet volume. *Nature,* 500(7461):190–193. **https://doi.org/10.1038/nature12374**

Allen, C.S., Pike, J., and Pudsey, C.J., 2011. Last glacial–interglacial sea-ice cover in the SW Atlantic and its potential role in global deglaciation. *Quaternary Science Reviews,* 30(19–20):2446–2458. **https://doi.org/10.1016/j.quascirev.2011.04.002**

Anderson, J.B., and Andrews, J.T., 1999. Radiocarbon constraints on ice sheet advance and retreat in the Weddell Sea, Antarctica. *Geology,* 27(2):179–182. **https://doi.org/10.1130/0091-7613(1999)027<0179:RCOISA>2.3.CO;2**

Anderson, J.B., Conway, H., Bart, P.J., Witus, A.E., Greenwood, S.L., McKay, R.M., Hall, B.L., et al., 2014. Ross Sea paleo-ice sheet drainage and deglacial history during and since the LGM. *Quaternary Science Reviews,* 100:31–54. **https://doi.org/10.1016/j.quascirev.2013.08.020**

Anderson, R.F., Barker, S., Fleisher, M., Gersonde, R., Goldstein, S.L., Kuhn, G., Mortyn, P.G., Pahnke, K., and Sachs, J.P., 2014. Biological response to millennial variability of dust and nutrient supply in the Subantarctic South Atlantic Ocean. *Philosophical Transactions of the Royal Society A: Mathematical, Physical and Engineering Sciences,* 372(219):20130054. **https://doi.org/10.1098/rsta.2013.0054**

Anderson, R.F., Ali, S., Bradtmiller, L.I., Nielsen, S.H.H., Fleisher, M.Q., Anderson, B.E., and Burckle, L.H., 2009. Wind-driven upwelling in the Southern Ocean and the deglacial rise in atmospheric CO_2. *Science,* 323(5920):1443–1448. **https://doi.org/10.1126/science.1167441**

Arhan, M., Heywood, K.J., and King, B.A., 1999. The deep waters from the Southern Ocean at the entry to the Argentine Basin. *Deep Sea Research, Part II: Topical Studies in Oceanography,* 46(1–2):475–499. **https://doi.org/10.1016/S0967-0645(98)00110-6**

Austermann, J., Pollard, D., Mitrovica, J.X., Moucha, R., Forte, A.M., DeConto, R.M., Rowley, D.B., and Raymo, M.E., 2015. The impact of dynamic topography change on Antarctic ice sheet stability during the mid-Pliocene warm period. *Geology,* 43(10):927–930. **https://doi.org/10.1130/G36988.1**

Bakker, P., Clark, P.U., Golledge, N.R., Schmittner, A., and Weber, M.E., 2016. Centennial-scale Holocene climate variations amplified by Antarctic Ice Sheet discharge. *Nature,* 541(7635):72–76. **https://doi.org/10.1038/nature20582**

Barbi, D., Lohmann, G., Grosfeld, K., and Thoma, M., 2013. Ice sheet dynamics within an Earth system model: coupling and first results on ice stability and ocean circulation. *Geoscientific Model Development Discussions,* 6(1):1–35. **https://doi.org/10.5194/gmdd-6-1-2013**

Barker, P.F., Lawver, L.A., and Larter, R.D., 2013. Heat-flow determinations of basement age in small oceanic basins of the southern central Scotia Sea. *Geological Society Special Publications,* 381(1):139–150. **https://doi.org/10.1144/SP381.3**

Barker, S., Diz, P., Vautravers, M.J., Pike, J., Knorr, G., Hall, I.R., and Broecker, W.S., 2009. Interhemispheric Atlantic seesaw response during the last deglaciation. *Nature,* 457(7233):1097–1102. **https://doi.org/10.1038/nature07770**

Barker, S., Knorr, G., Edwards, R.L., Parrenin, F., Putnam, A.E., Skinner, L.C., Wolff, E., and Ziegler, M., 2011. 800,000 years of abrupt climate variability. *Science,* 334(6054):347–351. **https://doi.org/10.1126/science.1203580**

Basile, I., Grousset, F.E., Revel, M., Petit, J.R., Biscaye, P.E., and Barkov, N.I., 1997. Patagonian origin of glacial dust deposited in East Antarctica (Vostok and Dome C) during glacial Stages 2, 4 and 6. *Earth and Planetary Science Letters,* 146(3–4):573–589. **https://doi.org/10.1016/S0012-821X(96)00255-5**

Belt, S.T., Cabedo-Sanz, P., Smik, L., Navarro-Rodriguez, A., Berben, S.M.P., Knies, J., and Husum, K., 2015. Identification of paleo Arctic winter sea ice limits and the marginal ice zone: optimised biomarker-based reconstructions of late Quaternary Arctic sea ice. *Earth and Planetary Science Letters,* 431:127–139. **https://doi.org/10.1016/j.epsl.2015.09.020**

Belt, S.T., Massé, G., Rowland, S.J., Poulin, M., Michel, C., and LeBlanc, B., 2007. A novel chemical fossil of palaeo sea ice: IP_{25}. *Organic Geochemistry,* 38(1):16–27. **https://doi.org/10.1016/j.orggeochem.2006.09.013**

Belt, S.T., and Müller, J., 2013. The Arctic sea ice biomarker IP_{25}: a review of current understanding, recommendations for future research and applications in palaeo sea ice reconstructions. *Quaternary Science Reviews,* 79:9–25. **https://doi.org/10.1016/j.quascirev.2012.12.001**

Belt, S.T., Smik, L., Brown, T.A., Kim, J.-H., Rowland, S.J., Allen, C.S., Gal, J.-K., Shin, K.-H., Lee, J.I., and Taylor, K.W.R., 2016. Source identification and distribution reveals the potential of the geochemical Antarctic sea ice proxy $IPSO_{25}$. *Nature Communications,* 7:12655. **https://doi.org/10.1038/ncomms12655**

Bentley, M.J., Fogwill, C.J., Le Brocq, A.M., Hubbard, A.L., Sugden, D.E., Dunai, T.J., and Freeman, S.P.H.T., 2010. Deglacial history of the West Antarctic Ice Sheet in the Weddell Sea embayment: constraints on past ice volume change. *Geology,* 38(5):411–414. **https://doi.org/10.1130/G30754.1**

Bentley, M.J., Ó Cofaigh, C., Anderson, J.B., Conway, H., Davies, B., Graham, A.G.C., Hillenbrand, C.-D., et al., 2014. A community-based geological reconstruction of Antarctic Ice Sheet deglaciation since the Last Glacial Maximum. *Quaternary Science Reviews,* 100:1–9. **https://doi.org/10.1016/j.quascirev.2014.06.025**

Böhm, E., Lippold, J., Gutjahr, M., Frank, M., Blaser, P., Antz, B., Fohlmeister, J., Frank, N., Andersen, M.B., and Deininger, M., 2015. Strong and deep Atlantic meridional overturning circulation during the last glacial cycle. *Nature,* 517(7532):73–76. **https://doi.org/10.1038/nature14059**

Caley, T., Zaragosi, S., Bourget, J., Martinez, P., Malaizé, B., Eynaud, F., Rossignol, L., Garlan, T., and Ellouz-Zimmermann, N., 2013. Southern Hemisphere imprint for Indo-Asian summer monsoons during the last glacial period as revealed by Arabian Sea productivity records. *Biogeosciences,* 10(11):7347–7359. **https://doi.org/10.5194/bg-10-7347-2013**

Cane, M.A., and Molnar, P., 2001. Closing of the Indonesian Seaway as a precursor to East African aridification around 3–4 million years ago. *Nature,* 411(6834):157–162. **https://doi.org/10.1038/35075500**

Channell, J.E.T., Hodell, D.A., and Curtis, J.H., 2016. Relative paleointensity (RPI) and oxygen isotope stratigraphy at IODP Site U1308: North Atlantic RPI stack for 1.2–2.2 Ma (NARPI-2200) and age of the Olduvai Subchron. *Quaternary Science Reviews,* 131(A):1–19. **https://doi.org/10.1016/j.quascirev.2015.10.011**

Channell, J.E.T., Stoner, J.S., Hodell, D.A., and Charles, C.D., 2000. Geomagnetic paleointensity for the last 100 kyr from the sub-antarctic South Atlantic: a tool for inter-hemispheric correlation. *Earth and Planetary Science Letters,* 175(1–2):145–160. **https://doi.org/10.1016/S0012-821X(99)00285-X**

Channell, J.E.T., Xuan, C., and Hodell, D.A., 2009. Stacking paleointensity and oxygen isotope data for the last 1.5 Myr (PISO-1500). *Earth and Planetary Science Letters,* 283(1–4):14–23. **https://doi.org/10.1016/j.epsl.2009.03.012**

Church, J.A., Clark, P.U., Cazenave, A., Gregory, J.M., Jevrejeva, S., Levermann, A., Merrifield, M.A., et al., 2013. Sea level change. *In* Stocker, T.F., Qin, D., Plattner, G.-K., Tignor, M., Allen, S.K., Boschung, J., Nauels, A., Xia, Y., Bex, V., Midgley, P.M. (Eds.), *Climate Change 2013: The Physical Science Basis. Contribution of Working Group I to the Fifth Assessment*

Report of the Intergovernmental Panel on Climate Change: Cambridge, United Kingdom (Cambridge University Press), 1137–1216. **http://www.climatechange2013.org/images/report/WG1AR5_Chapter13_FINAL.pdf**

Clark, P.U., Mitrovica, J.X., Milne, G.A., and Tamisiea, M.E., 2002. Sea-level fingerprinting as a direct test for the source of global meltwater Pulse 1A. *Science,* 295(5564):2438–2441. **https://doi.org/10.1126/science.1068797**

Cody, R.D., Levy, R.H., Harwood, D.M., and Sadler, P.M., 2008. Thinking outside the zone: high-resolution quantitative diatom biochronology for the Antarctic Neogene. *Palaeogeography, Palaeoclimatology, Palaeoecology,* 260(1–2):92–121. **https://doi.org/10.1016/j.palaeo.2007.08.020**

Collins, L.G., Allen, C.S., Pike, J., Hodgson, D.A., Weckström, K., and Massé, G., 2013. Evaluating highly branched isoprenoid (HBI) biomarkers as a novel Antarctic sea-ice proxy in deep ocean glacial age sediments. *Quaternary Science Reviews,* 79:87–98. **https://doi.org/10.1016/j.quascirev.2013.02.004**

Collins, L.G., Hounslow, M.W., Allen, C.S., Hodgson, D.A., Pike, J., and Karloukovski, V.V., 2012. Palaeomagnetic and biostratigraphic dating of marine sediments from the Scotia Sea, Antarctica: first identification of the Laschamp excursion in the Southern Ocean. *Quaternary Geochronology,* 7:67–75. **https://doi.org/10.1016/j.quageo.2011.10.002**

Colville, E.J., Carlson, A.E., Beard, B.L., Hatfield, R.G., Stoner, J.S., Reyes, A.V., and Ullman, D.J., 2011. Sr-Nd-Pb isotope evidence for ice-sheet presence on southern Greenland during the last interglacial. *Science,* 333(6042):620–623. **https://doi.org/10.1126/science.1204673**

Conway, H., Hall, B.L., Denton, G.H., Gades, A.M., and Waddington, E.D., 1999. Past and future grounding-line retreat of the West Antarctic Ice Sheet. *Science,* 286(5438):280–283. **https://doi.org/10.1126/science.286.5438.280**

Cook, C.P., Hemming, S.R., van de Flierdt, T., Pierce Davis, E.L, Williams, T., Lopez Galindo, A., Jiménez-Espejo, F.J., and Escutia, C., 2017. Glacial erosion of East Antarctica in the Pliocene: a comparative study of multiple marine sediment provenance tracers. *Chemical Geology,* 466:199–218. **https://doi.org/10.1016/j.chemgeo.2017.06.011**

Cook, C.P., van de Flierdt, T., Williams, T., Hemming, S.R., Iwai, M., Kobayashi, M., Jimenez-Espejo, F.J., et al., 2013. Dynamic behaviour of the East Antarctic Ice Sheet during Pliocene warmth. *Nature Geoscience,* 6(9):765–769. **https://doi.org/10.1038/ngeo1889**

Danesi, S., and Morelli, A., 2001. Structure of the upper mantle under the Antarctic plate from surface wave tomography. *Geophysical Research Letters,* 28(23):4395–4398. **https://doi.org/10.1029/2001GL013431**

De Deckker, P., Moros, M., Perner, K., and Jansen, E., 2012. Influence of the tropics and southern westerlies on glacial interhemispheric asymmetry. *Nature Geoscience,* 5(4):266–269. **https://doi.org/10.1038/ngeo1431**

DeConto, R.M., Galeotti, S., Pagani, M., Tracy, D., Schafer, K., Zhang, T., Pollard, D., and Beerling, D.J., 2012. Past extreme warming events linked to massive carbon release from thawing permafrost. *Nature,* 484(7392):87–91. **https://doi.org/10.1038/nature10929**

DeConto, R.M., and Pollard, D., 2016. Contribution of Antarctica to past and future sea-level rise. *Nature,* 531(7596):591–597. **https://doi.org/10.1038/nature17145**

Denton, G.H., Anderson, R.F., Toggweiler, J.R., Edwards, R.L., Shaefer, J.M., and Putnam, A.E., 2010. The last glacial termination. *Science,* 328(5986):1652–1656. **https://doi.org/10.1126/science.1184119**

Deschamps, P., Durand, N., Bard, E., Hamelin, B., Camoin, G., Thomas, A.L., Henderson, G.M., Okuno, J., and Yokoyama, Y., 2012. Ice-sheet collapse and sea-level rise at the Bølling warming 14,600 years ago. *Nature,* 483(7391):559–564. **https://doi.org/10.1038/nature10902**

Diekmann, B., Kuhn, G., Rachold, V., Abelmann, A., Brathauer, U., Fütterer, D.K., Gersonde, R., and Grobe, H., 2000. Terrigenous sediment supply in the Scotia Sea (Southern Ocean): response to late Quaternary ice dynamics in Patagonia and on the Antarctic Peninsula. *Palaeogeography, Palaeoclimatology, Palaeoecology,* 162(3–4):357–387. **https://doi.org/10.1016/S0031-0182(00)00138-3**

Dutton, A., and Lambeck, K., 2012. Ice volume and sea level during the last interglacial. *Science,* 337(6091):216–219. **https://doi.org/10.1126/science.1205749**

Eagles, G., Livermore, R., and Morris, P., 2006. Small basins in the Scotia Sea: the Eocene Drake Passage gateway. *Earth and Planetary Science Letters,* 242(3–4):343–353. **https://doi.org/10.1016/j.epsl.2005.11.060**

Elderfield, H., Ferretti, P., Greaves, M., Crowhurst, S., McCave, I.N., Hodell, D., and Piotrowski, A.M., 2012. Evolution of ocean temperature and ice volume through the mid-Pleistocene Climate Transition. *Science,* 337(6095):704–709. **https://doi.org/10.1126/science.1221294**

EPICA Community Members, 2006. One-to-one coupling of glacial climate variability in Greenland and Antarctica. *Nature,* 444(7116):195–198. **https://doi.org/10.1038/nature05301**

Farmer, L.G., Licht, K., Swope, R.J., and Andrews, J., 2006. Isotopic constraints on the provenance of fine-grained sediment in LGM tills from the Ross Embayment, Antarctica. *Earth and Planetary Science Letters,* 249(1–2):90–107. **https://doi.org/10.1016/j.epsl.2006.06.044**

Ferrari, R., Jansen, M.F., Adkins, J.F., Burke, A., Stewart, A.L., and Thompson, A.F., 2014. Antarctic sea ice control on ocean circulation in present and glacial climates. *Proceedings of the National Academy of Sciences,* 111(24):8753–8758. **https://doi.org/10.1073/pnas.1323922111**

Fischer, H., Fundel, F., Ruth, U., Twarloh, B., Wegner, A., Udisti, R., Becagli, S., et al., 2007. Reconstruction of millennial changes in dust emission, transport and regional sea ice coverage using the deep EPICA ice cores from the Atlantic and Indian Ocean sector of Antarctica. *Earth and Planetary Science Letters,* 260(1–2):340–354. **https://doi.org/10.1016/j.epsl.2007.06.014**

Flowerdew, M.J., Tyrrell, S., and Peck, V.L., 2013. Inferring sites of subglacial erosion using the Pb isotopic composition of ice-rafted feldspar: examples from the Weddell Sea, Antarctica. *Geology,* 41(2):147–150. **https://doi.org/10.1130/G33644.1**

Fogwill, C.J., Turney, C.S.M., Golledge, N.R., Etheridge, D.M., Rubino, M., Thornton, D.P., Baker, A., et al., 2017. Antarctic ice sheet discharge driven by atmosphere-ocean feedbacks at the Last Glacial Termination. *Scientific Reports,* 7:39979. **https://doi.org/10.1038/srep39979**

Fogwill, C.J., Turney, C.S.M., Meissner, K.J., Golledge, N.R., Spence, P., Roberts, J.L., England, M.H., Jones, R.T., and Carter, L., 2014. Testing the sensitivity of the East Antarctic Ice Sheet to Southern Ocean dynamics: past changes and future implications. *Journal of Quaternary Science,* 29(1):91–98. **https://doi.org/10.1002/jqs.2683**

Fogwill, C.J., Turney, C.S.M., Menviel, L., Baker, A., Weber, M.E., Ellis, B., Thomas, Z.A., et al., submitted. Seasonal sea-ice variability enhanced the Southern Ocean carbon sink during the Antarctic Cold Reversal. *Nature Communications.*

Galindo-Zaldívar, J., Bohoyo, F., Maldonado, A., Schreider, A., Suriñach, E., and Vázquez, J.T., 2006. Propagating rift during the opening of a small oceanic basin: the Protector Basin (Scotia Arc, Antarctica). *Earth and Planetary Science Letters,* 241(3–4):398–412. **https://doi.org/10.1016/j.epsl.2005.11.056**

Galindo-Zaldívar, J., Puga, E., Bohoyo, F., González, F.J., Maldonado, A., Martos, Y.M., Pérez, L.F., et al., 2014. Magmatism, structure and age of Dove Basin (Antarctica): a key to understanding South Scotia Arc development. *Global and Planetary Change,* 122:50–69. **https://doi.org/10.1016/j.gloplacha.2014.07.021**

Gersonde, R., Crosta, X., Abelmann, A., and Armand, L., 2005. Sea-surface temperature and sea ice distribution of the Southern Ocean at the EPILOG Last Glacial Maximum—a circum-Antarctic view based on siliceous microfossil records. *Quaternary Science Reviews,* 24(7–9):869–896. **https://doi.org/10.1016/j.quascirev.2004.07.015**

Gersonde, R., and Zielinski, U., 2000. The reconstruction of late Quaternary Antarctic sea-ice distribution—the use of diatoms as a proxy for sea ice. *Palaeogeography, Palaeoclimatology, Palaeoecology,* 162(3–4):263–286. **https://doi.org/10.1016/S0031-0182(00)00131-0**

Gladstone, R.M., Bigg, G.R., and Nicholls, K.W., 2001. Iceberg trajectory modeling and meltwater injection in the Southern Ocean. *Journal of Geophys-*

ical Research: Oceans, 106(C9):19903–19915. **https://doi.org/10.1029/2000JC000347**

Goldstein, S.L., and Hemming, S.R., 2003. Long-lived isotopic tracers in oceanography, paleoceanography and ice sheet dynamics. In Elderfield, H. (Ed.), Treatise on Geochemistry (Volume 6): The Oceans and Marine Geochemistry. Holland, H.D., and Turekian, K.K. (Series Eds.): New York (Elsevier), 453–489. **https://doi.org/10.1016/B0-08-043751-6/06179-X**

Goldstein, S.L., O'Nions, R.K., and Hamilton, P.J., 1984. A Sm-Nd isotopic study of atmospheric dusts and particulates from major river systems. *Earth and Planetary Science Letters,* 70(2):221–236. **https://doi.org/10.1016/0012-821X(84)90007-4**

Golledge, N.R., Menviel, L., Carter, L., Fogwill, C.J., England, M.H., Cortese, G., and Levy, R.H., 2014. Antarctic contribution to meltwater Pulse 1A from reduced Southern Ocean overturning. *Nature Communications,* 5:5107. **https://doi.org/10.1038/ncomms6107**

Gomez, N., Mitrovica, J.X., Huybers, P., and Clark, P.U., 2010. Sea level as a stabilizing factor for marine-ice-sheet grounding lines. *Nature Geoscience,* 3(12):850–853. **https://doi.org/10.1038/ngeo1012**

Gomez, N., Pollard, D., and Mitrovica, J.X., 2013. A 3-D coupled ice sheet—sea level model applied to Antarctica through the last 40 ky. *Earth and Planetary Science Letters,* 384:88–99. **https://doi.org/10.1016/j.epsl.2013.09.042**

Gutjahr, M., Frank, M., Stirling, C.H., Keigwin, L.D., and Halliday, A.N., 2008. Tracing the Nd isotope evolution of North Atlantic Deep and Intermediate Waters in the western North Atlantic since the Last Glacial Maximum from Blake Ridge sediments. *Earth and Planetary Science Letters,* 266(1–2):61–77. **https://doi.org/10.1016/j.epsl.2007.10.037**

Gutjahr, M., Frank, M., Stirling, C.H., Klemm, V., van de Flierdt, T., and Halliday, A.N., 2007. Reliable extraction of a deepwater trace metal isotope signal from Fe-Mn oxyhydroxide coatings of marine sediments. *Chemical Geology,* 242(3–4):351–370. **https://doi.org/10.1016/j.chemgeo.2007.03.021**

Guyodo, Y., Acton, G.D., Brachfeld, S., and Channell, J.E.T., 2001. A sedimentary paleomagnetic record of the Matuyama Chron from the Western Antarctic margin (ODP Site 1101). *Earth and Planetary Science Letters,* 191(1–2):61–74. **https://doi.org/10.1016/S0012-821X(01)00402-2**

Hatfield, R.G., and Stoner, J.S., 2013. Paleoceanography, physical and chemical proxies: magnetic proxies and susceptibility. *In* Elias, S.A., and Mock, C.J. (Eds.), *Encyclopedia of Quaternary Science* (2nd edition): Amsterdam (Elsevier), 884–898.

Hatfield, R.G., Stoner, J.S., Carlson, A.E., Reyes, A.V., and Housen, B.A., 2013. Source as a controlling factor on the quality and interpretation of sediment magnetic records from the northern North Atlantic. *Earth and Planetary Science Letters,* 368:69–77. **https://doi.org/10.1016/j.epsl.2013.03.001**

Hein, A.S., Hulton, N.R.J., Dunai, T.J., Sugden, D.E., Kaplan, M.R., and Xu, S., 2010. The chronology of the Last Glacial Maximum and deglacial events in central Argentine Patagonia. *Quarternary Science Reviews,* 29(9–10):1212–1227. **https://doi.org/10.1016/j.quascirev.2010.01.020**

Hemming, S.R., and Rasbury, E.T., 2000. Pb isotope measurements of sanidine monitor standards: implications for provenance analysis and tephrochronology. *Chemical Geology,* 165(3–4):331–337. **https://doi.org/10.1016/S0009-2541(99)00174-6**

Hemming, S.R., van de Flierdt, T., Goldstein, S.L., Franzese, A.M., Roy, M., Gastineau, G., and Landrot, G., 2007. Strontium isotope tracing of terrigenous sediment dispersal in the Antarctic Circumpolar Current: implications for constraining frontal positions. *Geochemistry, Geophysics, Geosystems,* 8(6):Q06N13. **https://doi.org/10.1029/2006GC001441**

Heroy, D.C., and Anderson, J.B., 2007. Radiocarbon constraints on Antarctic Peninsula Ice Sheet retreat following the Last Glacial Maximum (LGM). *Quaternary Science Reviews,* 26(25–28):3286–3292. **https://doi.org/10.1016/j.quascirev.2007.07.012**

Hillenbrand, C.-D., Kuhn, G., Smith, J.A., Gohl, K., Graham, A.G.C., Larter, R.D., Klages, J.P., Downey, R., Moreton, S.G., Forwick, M., and Vaughan, D.G., 2013. Grounding-line retreat of the West Antarctic Ice Sheet from inner Pine Island Bay. *Geology,* 41(1):35–38. **https://doi.org/10.1130/G33469.1**

Huybers, P., and Denton, G., 2008. Antarctic temperature at orbital timescales controlled by local summer duration. *Nature Geoscience,* 1(11):787–792. **https://doi.org/10.1038/ngeo311**

Imbrie, J., Berger, A., Boyle, E., Clemens, S., Duffy, A., Howard, W., Kukla, G., et al., 1993. On the structure and origin of major glaciation cycles, 2. The 100,000-year cycle. *Paleoceanography,* 8(6):699–735. **https://doi.org/10.1029/93PA02751**

Imbrie, J., Boyle, E.A., Clemens, S.C., Duffy, A., Howard, W.R., Kukla, G., Kutzbach, J., et al., 1992. On the structure and origin of major glaciation cycles, 1. Linear responses to Milankovitch forcing. *Paleoceanography,* 7(6):701–738. **https://doi.org/10.1029/92PA02253**

Iriondo, M., 2000. Patagonian dust in Antarctica. *Quaternary International,* 68–67:83–86. **https://doi.org/10.1016/S1040-6182(00)00035-5**

Kendall, R.A., Mitrovica, J.X., Milne, G.A., 2005. On post-glacial sea level—II. Numerical formulation and comparative results on spherically symmetric models. *Geophysical Journal International,* 161(3):679–706. **https://doi.org/10.1111/j.1365-246X.2005.02553.x**

Kim, J.-H., Schouten, S., Hopmans, E.C., Donner, B., and Sinninghe Damsté, J.S., 2008. Global sediment core-top calibration of the TEX_{86} paleothermometer in the ocean. *Geochimica et Cosmochimica Acta,* 72(4):1154–1173. **https://doi.org/10.1016/j.gca.2007.12.010**

Knorr, G., Butzin, M., Micheels, A., and Lohmann, G., 2011. A warm Miocene climate at low atmospheric CO_2 levels. *Geophysical Research Letters,* 38(20):L20701. **https://doi.org/10.1029/2011GL048873**

Knorr, G., and Lohmann, G., 2003. Southern Ocean origin for the resumption of Atlantic thermohaline circulation during deglaciation. *Nature,* 424(6948):532–536. **https://doi.org/10.1038/nature01855**

Knorr, G., and Lohmann, G., 2007. Rapid transitions in the Atlantic thermohaline circulation triggered by global warming and meltwater during the last deglaciation. *Geochemistry, Geophysics, Geosystems,* 8(12):Q12006. **https://doi.org/10.1029/2007GC001604**

Koenitz, D., White, N., McCave, I.N., and Hobbs, R., 2008. Internal structure of a contourite drift generated by the Antarctic Circumpolar Current. *Geochemistry, Geophysics, Geosystems,* 9(6):Q06012. **https://doi.org/10.1029/2007GC001799**

Kopp, R.E., Simons, F.J., Mitrovica, J.X., Maloof, A.C., and Oppenheimer, M., 2009. Probabilistic assessment of sea level during the last interglacial stage. *Nature,* 462(7275):863–867. **https://doi.org/10.1038/nature08686**

Lamy, F., Gersonde, R., Winckler, G., Esper, O., Jaeschke, A., Kuhn, G., Ullermann, J., Martinez-Garcia, A., Lambert, F., and Kilian, R., 2014. Increased dust deposition in the Pacific Southern Ocean during glacial periods. *Science,* 343(6169):403–407. **https://doi.org/10.1126/science.1245424**

Lamy, F., Kaiser, J., Arz, H.W., Hebbeln, D., Ninnemann, U., Timm, O., Timmermann, A., and Toggweiler, J.R., 2007. Modulation of the bipolar seesaw in the southeast Pacific during Termination 1. *Earth and Planetary Science Letters,* 259(3–4):400–413. **https://doi.org/10.1016/j.epsl.2007.04.040**

Lamy, F., Arz, H.W., Kilian, R., Lange, C.B., Lembke-Jene, L., Wengler, M., Kaiser, J., et al., 2018. Glacial reduction and millennial-scale variations in Drake Passage throughflow. *Proceedings of the National Academy of Sciences of the United States of America,* 112(44):13496–13501. **https://doi.org/10.1073/pnas.1509203112**

Latychev, K., Mitrovica, J.X., Tromp, J., Tamisiea, M.E., Komatitsch, D., and Christara, C.C., 2005. Glacial isostatic adjustment on 3-D Earth models: a finite-volume formulation. *Geophysical Journal International,* 161(2):421–444. **https://doi.org/10.1111/j.1365-246X.2005.02536.x**

Levermann, A., Albrecht, T., Winkelmann, R., Martin, M.A., Haseloff, M., and Joughin, I., 2012. Kinematic first-order calving law implies potential for abrupt ice-shelf retreat. *The Cryosphere,* 6(2):273–286. **https://doi.org/10.5194/tc-6-273-2012**

Licht, K.J., and Hemming, S.R., 2017. Analysis of Antarctic glacigenic sediment provenance through geochemical and petrologic applications. *Quaternary Science Reviews,* 164:1–24. **https://doi.org/10.1016/j.quascirev.2017.03.009**

Lindeque, A., Martos, Y.M., Gohl, K., and Maldonado, A., 2013. Deep-sea preglacial to glacial sedimentation in the Weddell Sea and southern Scotia

Sea from a cross-basin seismic transect. *Marine Geology,* 336;61–83. **https://doi.org/10.1016/j.margeo.2012.11.004**

Lisiecki, L.E., and Raymo, M.E., 2005. A Pliocene–Pleistocene stack of 57 globally distributed benthic δ^{230}O records. *Paleoceanography,* 20(1):PA1003. **https://doi.org/10.1029/2004PA001071**

Lorrey, A.M., Vandergoes, M., Almond, P., Renwick, J., Stephens, T., Bostock, H., Mackintosh, A., et al., 2012. Palaeocirculation across New Zealand during the Last Glacial Maximum at ~21 ka. *Quaternary Science Reviews,* 36:189–213. **https://doi.org/10.1016/j.quascirev.2011.09.025**

Lunt, D.J., Foster, G.L., Haywood, A.M., and Stone, E.J., 2008. Late Pliocene Greenland glaciation controlled by a decline in atmospheric CO_2 levels. *Nature,* 454(7208):1102–1105. **https://dx.doi.org/10.1038/nature07223**

Mackintosh, A., Golledge, N., Domack, E., Dunbar, R., Leventer, A., White, D., Pollard, D., et al., 2011. Retreat of the East Antarctic Ice Sheet during the Last Glacial Termination. *Nature Geoscience,* 4(3):195–202. **https://doi.org/10.1038/ngeo1061**

Mackintosh, A.N., Verleyen, E., O'Brien, P.E., White, D.A., Jones, R.S., McKay, R., Dunbar, R., et al., 2014. Retreat history of the East Antarctic Ice Sheet since the Last Glacial Maximum. *Quaternary Science Reviews,* 100:10–13. **https://doi.org/10.1016/j.quascirev.2013.07.024**

Maldonado, A., Barnolas, A., Bohoyoa, F., Galindo-Zaldívar, J., Hernández-Molina, J., Lobo, F., Rodríguez-Fernández, J., Somoza, L., and Vázquez, J.T., 2003. Contourite deposits in the central Scotia Sea: the importance of the Antarctic Circumpolar Current and the Weddell Gyre flows. *Palaeogeography, Palaeoclimatology, Palaeoecology,* 198(1–2):187–221. **https://doi.org/10.1016/S0031-0182(03)00401-2**

Maldonado, A., Bohoyo, F., Bozzano, G., Casas, D., Elizondo, M.E., Esteban, F.D., Galindo-Zaldívar, J., et al., 2013. Scientific report of SCAN 2013 cruise. 91.

Maldonado, A., Bohoyo, F., Carvalho, A.L., Hernández-Molina, F.J., Galindo-Zaldívar, J., Lodolo, E., Medialdea, T., et al., 2008. Scientific report of SCAN 2008 cruise. 92.

Maldonado, A., Bohoyo, F., Drehmer, L.H., Galindo-Zaldívar, J., Gulmezova, E.L., Hernández-Molina, F.J., Jabaloy, A., et al., 2004. Scientific report of SCAN 2004 cruise. 66.

Maldonado, A., Bohoyo, F., Galindo-Zaldívar, J., Hernández-Molina, J., Jabaloy, A., Lobo, F.J., Rodríguez-Fernández, J., Suriñach, E., and Vázquez, J.T., 2006. Ocean basins near the Scotia–Antarctic plate boundary: influence of tectonics and paleoceanography on the Cenozoic deposits. *Marine Geophysical Researches,* 27(2):83–107. **https://doi.org/10.1007/s11001-006-9003-4**

Marino, G., Zahn, R., Ziegler, M., Purcell, C., Knorr, G., Hall, I.R., Ziveri, P., and Elderfield, H., 2013. Agulhas salt-leakage oscillations during abrupt climate changes of the Late Pleistocene. *Paleoceanography,* 28(3):599–606. **https://doi.org/10.1002/palo.20038**

Marshall, J., and Speer, K., 2012. Closure of the meridional overturning circulation through Southern Ocean upwelling. *Nature Geoscience,* 5(3):171–180. **https://doi.org/10.1038/ngeo1391**

Martin, E.E., and Scher, H.D., 2004. Preservation of seawater Sr and Nd isotopes in fossil fish teeth: bad news and good news. *Earth and Planetary Science Letters,* 220(1–2):25–39. **https://doi.org/10.1016/S0012-821X(04)00030-5**

Martínez-Garcia, A., Rosell-Melé, A., Jaccard, S.L., Geibert, W., Sigman, D.M., and Haug, G.H., 2011. Southern Ocean dust–climate coupling over the past four million years. *Nature,* 476(7360):312–315. **https://doi.org/10.1038/nature10310**

Martínez-Garcia, A., Rosell-Melé, A., McClymont, E.L., Gersonde, R., and Haug, G.H., 2010. Subpolar link to the emergence of the modern equatorial Pacific cold tongue. *Science,* 328(5985):1550–1553. **https://doi.org/10.1126/science.1184480**

Martínez-Garcia, A., Sigman, D.M., Ren, H., Anderson, R.F., Straub, M., Hodell, D.A., Jaccard, S.L., Eglinton, T.I., and Haug, G.H., 2014. Iron fertilization of the Subantarctic Ocean during the Last Ice Age. *Science,* 343(6177):1347–1350. **https://doi.org/10.1126/science.1246848**

Martínez-Méndez, G., Zahn, R., Hall, I.R., Peeters, F.J.C., Pena, L.D., Cacho, I., and Negre, C., 2010. Contrasting multiproxy reconstructions of surface ocean hydrography in the Agulhas Corridor and implications for the Agulhas leakage during the last 345,000 years. *Paleoceanography,* 25(4):PA4227. **https://doi.org/10.1029/2009PA001879**

Martos, Y.M., Maldonado, A., Lobo, F.J., Hernández-Molina, F.J., and Pérez, L.F., 2013. Tectonics and palaeoceanographic evolution recorded by contourite features in southern Drake Passage (Antarctica). *Marine Geology,* 343:76–91. **https://doi.org/10.1016/j.margeo.2013.06.015**

Massé, G., Belt, S.T., Crosta, X., Schmidt, S., Snape, I., Thomas, D.N., and Rowland, S.J., 2011. Highly branched isoprenoids as proxies for variable sea ice conditions in the Southern Ocean. *Antarctic Science,* 23(05)487–498. **https://doi.org/10.1017/S0954102011000381**

Masson-Delmotte, V., Schulz, M., Abe-Ouchi, A., Beer, J., Ganopolski, A., González Rouco, J.F., Jansen, E., Lambeck, K., Luterbacher, J., Naish, T., Osborn, T., Otto-Bliesner, B., Quinn, T., Ramesh, R., Rojas, M., Shao, X., and Timmerman, A., 2013. Information from paleoclimate archives. *In* Stocker, T.F., Qin, D., Plattner, G.-K., Tignor, M., Allen, S.K., Boschung, J., Nauels, A., Xia, Y., Bex, V., and Midgley, P.M. (Eds.), *Climate Change 2013: The Physical Science Basis. Contribution of Working Group I to the Fifth Assessment Report of the Intergovernmental Panel on Climate Change:* Cambridge, United Kingdom (Cambridge University Press), 383–464. **http://www.climatechange2013.org/images/report/WG1AR5_Chapter05_FINAL.pdf**

Mazaud, A., Sicre, M.A., Ezat, U., Pichon, J.J., Duprat, J., Laj, C., Kissel, C., Beaufort, L., Michel, E., and Turon, J.L., 2002. Geomagnetic-assisted stratigraphy and sea surface temperature changes in core MD94-103 (Southern Indian Ocean): possible implications for north–south climatic relationships around H4. *Earth and Planetary Science Letters,* 201(1):159–170. **https://doi.org/10.1016/S0012-821X(02)00662-3**

McCave, I.N., Crowhurst, S.J., Kuhn, G., Hillenbrand, C.D., and Meredith, M.P., 2014. Minimal change in Antarctic Circumpolar Current flow speed between the last glacial and Holocene. *Nature Geoscience,* 7(2):113–116. **https://doi.org/10.1038/ngeo2037**

McCulloch, R.D., Bentley, M.J., Purves, R.S., Hulton, N.R.J., Sugden, D.E., and Clapperton, C.M., 2000. Climatic inferences from glacial and palaeoecological evidence at the Last Glacial Termination, southern South America. *Journal of Quaternary Science,* 15(4):409–417. **https://doi.org/10.1002/1099-1417(200005)15:4<409::AID-JQS539>3.0.CO;2-#**

McKay, R., Naish, T., Carter, L., Riesselman, C., Dunbar, R., Sjunneskog, C., Winter, D., et al., 2012. Antarctic and Southern Ocean influences on late Pliocene global cooling. *Proceedings of the National Academy of Sciences of the United States of America,* 109(17):6423–6428. **https://doi.org/10.1073/pnas.1112248109**

Mengel, M., and Levermann, A., 2014. Ice plug prevents irreversible discharge from East Antarctica. *Nature Climate Change,* 4(6):451–455. **https://doi.org/10.1038/nclimate2226**

Menviel, L., Timmermann, A., Mouchet, A., and Timm, O., 2008. Climate and marine carbon cycle response to changes in the strength of the Southern Hemispheric westerlies. *Paleoceanography,* 23(4):PA4201. **https://doi.org/10.1029/2008PA001604**

Menviel, L., Timmermann, A., Timm, O.E., and Mouchet, A., 2010. Climate and biogeochemical response to a rapid melting of the West Antarctic Ice Sheet during interglacials and implications for future climate. *Paleoceanography,* 25(4):PA4231. **https://doi.org/10.1029/2009PA001892**

Menviel, L., Timmermann, A., Timm, O.E., and Mouchet, A., 2011. Deconstructing the Last Glacial Termination: the role of millennial and orbital-scale forcings. *Quaternary Science Reviews,* 30(9–10):1155–1172. **https://doi.org/10.1016/j.quascirev.2011.02.005**

Moreno, P.I., Lowell, T.V., Jacobson Jr, G.L., and Denton, G.H., 1999. Abrupt vegetation and climate changes during the Last Glacial Maximum and Last Termination in the Chilean lake district: a case study from Canal De La Puntilla (41°S). *Geografiska Annaler, Series A: Physical Geography,* 81(2):285–311. **https://doi.org/10.1111/1468-0459.00059**

Moreton, S.G., and Smellie, J.L., 1998. Identification and correlation of distal tephra layers in deep-sea sediment cores, Scotia Sea, Antarctica. *Annals of Glaciology,* 27:285–289. **https://doi.org/10.3189/1998AoG27-1-285-289**

Müller, J., Masse, G., Stein, R., and Belt, S.T., 2009. Variability of sea-ice conditions in the Fram Strait over the past 30,000 years. *Nature Geoscience,* 2(11):772–776. **https://doi.org/10.1038/ngeo665**

Naish, T.R., Powell, R., Levy, R., Wilson, G., Scherer, R., Talarico, F., Krissek, L., et al., 2009. Obliquity-paced Pliocene West Antarctic Ice Sheet oscillations. *Nature,* 458(7236):322–329. **https://doi.org/10.1038/nature07867**

Naveira Garabato, A.C., McDonagh, E.L., Stevens, D.P., Heywood, K.J., and Sanders, R.J., 2002. On the export of Antarctic Bottom Water from the Weddell Sea. *Deep Sea Research, Part II: Topical Studies in Oceanography,* 49(21):4715–4742. **https://doi.org/10.1016/S0967-0645(02)00156-X**

NEEM Community Members, 2013. Eemian interglacial reconstructed from a Greenland folded ice core. *Nature,* 493(7433):489–494. **https://doi.org/10.1038/nature11789**

NGRIP Members, 2004. High-resolution record of Northern Hemisphere climate extending into the last interglacial period. *Nature,* 431(7005):147–151. **https://doi.org/10.1038/nature02805**

O'Leary, M.J., Hearty, P.J., Thompson, W.G., Raymo, M.E., Mitrovica, J.X., and Webster, J.M., 2013. Ice sheet collapse following a prolonged period of stable sea level during the last interglacial. *Nature Geoscience,* 6(9):796–800. **https://doi.org/10.1038/ngeo1890**

Orsi, A.H., Whitworth III, T., and Nowlin, W.D., Jr., 1995. On the meridional extent and fronts of the Antarctic Circumpolar Current. *Deep-Sea Research, Part I,* 42(5):641–673. **https://doi.org/10.1016/0967-0637(95)00021-W**

Park, W., and Latif, M., 2008. Multidecadal and multicentennial variability of the meridional overturning circulation. *Geophysical Research Letters,* 35(22):L22703. **https://doi.org/10.1029/2008GL035779**

Peeters, F.J.C., Acheson, R., Brummer, G.-J.A., de Ruijter, W.P.M., Schneider, R.R., Ganssen, G.M., Ufkes, E., and Kroon, D., 2004. Vigorous exchange between the Indian and Atlantic Oceans at the end of the past five glacial periods. *Nature,* 430(7000):661–665. **https://doi.org/10.1038/nature02785**

Peltier, W.R., 2004. Global glacial isostasy and the surface of the ice-age Earth: the ICE-5G (VM2) model and GRACE. *Annual Review of Earth and Planetary Sciences,* 32(1):111–149. **https://doi.org/10.1146/annurev.earth.32.082503.144359**

Pérez, L.F., Maldonado, A., Bohoyo, F., Hernández-Molina, F.J., Vázquez, J.T., Lobo, F.J., and Martos, Y.M., 2014. Depositional processes and growth patterns of isolated oceanic basins: the Protector and Pirie basins of the Southern Scotia Sea (Antarctica). *Marine Geology,* 357:163–181. **https://doi.org/10.1016/j.margeo.2014.08.001**

Pérez, L.F., Maldonado, A., Hernández-Molina, F.J., Lodolo, E., Bohoyo, F., and Galindo-Zaldívar, J., 2015. Tectonic and oceanographic control of sedimentary patterns in a small oceanic basin: Dove Basin (Scotia Sea, Antarctica). *Basin Research,* 29(S1):255–276. **https://doi.org/10.1111/bre.12148**

Pierce, E.L., Hemming, S.R., Williams, T., van de Flierdt, T., Thomson, S.N., Reiners, P.W., Gehrels, G.E., Brachfeld, S.A., and Goldstein, S.L., 2014. A comparison of detrital U–Pb zircon, $^{40}Ar/^{39}Ar$ hornblende, $^{40}Ar/^{39}Ar$ biotite ages in marine sediments off East Antarctica: implications for the geology of subglacial terrains and provenance studies. *Earth-Science Reviews,* 138:156–178. **https://doi.org/10.1016/j.earscirev.2014.08.010**

Pierce, E.L., van de Flierdt, T., Williams, T., Hemming, S.R., Cook, C., and Passchier, S., 2017. Evidence for a dynamic East Antarctic ice sheet during the mid-Miocene climate transition. *Earth and Planetary Science Letters,* 478:1–13. **https://doi.org/10.1016/j.epsl.2017.08.011**

Pierce, E.L., Williams, T., van de Flierdt, T., Hemming, S.R., Goldstein, S.L., and Brachfeld, S.A, 2011. Characterizing the sediment provenance of East Antarctica's weak underbelly: the Aurora and Wilkes sub-glacial basins. *Paleoceanography,* 26(4):PA4217. **https://doi.org/10.1029/2011PA002127**

Piotrowski, A.M., Goldstein, S.L., Hemming, S.R., and Fairbanks, R.G., 2004. Intensification and variability of ocean thermohaline circulation through the last deglaciation. *Earth and Planetary Science Letters,* 225(1–2):205–220. **https://doi.org/10.1016/j.epsl.2004.06.002**

Piotrowski, A.M., Goldstein, S.L., Hemming, S.R., Fairbanks, R.G., and Zylberberg, D.R., 2008. Oscillating glacial northern and southern deep water formation from combined neodymium and carbon isotopes. *Earth and Planetary Science Letters,* 272(1–2):394–405. **https://doi.org/10.1016/j.epsl.2008.05.011**

Pollard, D., and DeConto, R.M, 2009. Modelling West Antarctic Ice Sheet growth and collapse through the past five million years. *Nature,* 458(7236):329–332. **https://doi.org/10.1038/nature07809**

Pudsey, C.J., 1990. Grain size and diatom content of hemipelagic sediments at Site 697, ODP Leg 113: a record of Pliocene–Pleistocene climate. *In* Barker, P.F., Kennett, J.P., et al., *Proceedings of the Ocean Drilling Program, Scientific Results,* 113: College Station, TX (Ocean Drilling Program), 111–120. **http://dx.doi.org/10.2973/odp.proc.sr.113.147.1990**

Pugh, R.S., McCave, I.N., Hillenbrand, C.D., and Kuhn, G., 2009. Circum-Antarctic age modelling of Quaternary marine cores under the Antarctic Circumpolar Current: ice-core dust–magnetic correlation. *Earth and Planetary Science Letters,* 284(1–2):113–123. **https://doi.org/10.1016/j.epsl.2009.04.016**

Raymo, M.E., Lisiecki, L.E., and Nisancioglu, K.H., 2006. Plio–Pleistocene ice volume, Antarctic climate, and the global $\delta^{18}O$ record. *Science,* 313(5786):492–495. **https://doi.org/10.1126/science.1123296**

Raymo, M.E., and Nisancioglu, K., 2003. The 41 kyr world: Milankovitch's other unsolved mystery. *Paleoceanography,* 18(1):1011. **https://doi.org/10.1029/2002PA000791**

Raymo, M.E., Ruddiman, W.F., and Froelich, P.N., 1988. Influence of late Cenozoic mountain building on ocean geochemical cycles. *Geology,* 16(7):649–653. **http://dx.doi.org/10.1130/0091-7613(1988)016<0649:IOLCMB>2.3.CO;2**

Roberts, J., Gottschalk, J., Skinner, L.C., Peck, V.L., Kender, S., Elderfield, H., Waelbroeck, C., Vázquez Riveiros, N., and Hodell, D.A., 2016. Evolution of South Atlantic density and chemical stratification across the last deglaciation. *Proceedings of the National Academy of Sciences,* 113(3):514–519. **https://doi.org/10.1073/pnas.1511252113**

Roberts, J., McCave, I.N., McClymont, E.L., Kender, S., Hillenbrand, C.D., Matano, R., Hodell, D.A., and Peck, V.L., 2017. Deglacial changes in flow and frontal structure through the Drake Passage. *Earth and Planetary Science Letters,* 474:397–408. **https://doi.org/10.1016/j.epsl.2017.07.004**

Roberts, N.L., Piotrowski, A.M., Elderfield, H., Eglinton, T.I., and Lomas, M.W., 2012. Rare earth element association with foraminifera. *Geochimica et Cosmochimica Acta,* 94:57–71. **https://doi.org/10.1016/j.gca.2012.07.009**

Roberts, N.L., Piotrowski, A.M., McManus, J.F., and Keigwin, L.D., 2010. Synchronous deglacial overturning and water mass source changes. *Science,* 327(5961):75–78. **https://doi.org/10.1126/science.1178068**

Robinson, L.F., and van de Flierdt, T., 2009. Southern Ocean evidence for reduced export of North Atlantic Deep Water during Heinrich Event 1. *Geology,* 37(3):195–198. **https://doi.org/10.1130/G25363A.1**

Rodríguez-Sanza, L., Mortyn, P.G., Martínez-Garcia, A., Rosell-Melé, A., and Hall, I.R., 2012. Glacial Southern Ocean freshening at the onset of the middle Pleistocene climate transition. *Earth and Planetary Science Letters,* 345–348:194–202. **https://doi.org/10.1016/j.epsl.2012.06.016**

Rostami, K., Peltier, W.R., and Mangini, A., 2000. Quaternary marine terraces, sea-level changes and uplift history of Patagonia, Argentina: comparisons with predictions of the ICE-4G (VM2) model of the global process of glacial isostatic adjustment. *Quaternary Science Reviews,* 19(14–15):1495–1525. **https://doi.org/10.1016/S0277-3791(00)00075-5**

Roy, M., van de Flierdt, T., Hemming, S.R., and Goldstein, S.L., 2007. $^{40}Ar/^{39}Ar$ ages of hornblende grains and bulk Sm/Nd isotopes of circum-Antarctic glacio-marine sediments: implications for sediment provenance in the Southern Ocean. *Chemical Geology,* 244(3–4):507–519. **https://doi.org/10.1016/j.chemgeo.2007.07.017**

Rutberg, R.L., Hemming, S.R., and Goldstein, S.L., 2000. Reduced North Atlantic Deep Water flux to the glacial Southern Ocean inferred from neodymium isotope ratios. *Nature,* 405(6789):935–938. **https://doi.org/10.1038/35016049**

Sagnotti, L., Macrí, P., Camerlenghi, A., and Rebesco, M., 2001. Environmental magnetism of Antarctic late Pleistocene sediments and interhemispheric correlation of climatic events. *Earth and Planetary Science Letters,* 192(1):65–80. **https://doi.org/10.1016/S0012-821X(01)00438-1**

Scher, H.D., and Martin, E.E., 2006. Timing and climatic consequences of the opening of Drake Passage. *Science,* 312(5772):428–430. **https://doi.org/10.1126/science.1120044**

Schmitt, J., Schneider, R., Elsig, J., Leuenberger, D., Lourantou, A., Chappellaz, J., Köhler, P., et al., 2012. Carbon isotope constraints on the deglacial CO_2 rise from ice cores. *Science,* 336(6082):711–714. **https://doi.org/10.1126/science.1217161**

Schouten, S., Hopmans, E.C., Schefuß, E., and Sinninghe Damsté, J.S., 2002. Distributional variations in marine crenarchaeotal membrane lipids: a new tool for reconstructing ancient sea water temperatures? *Earth and Planetary Science Letters*, 204(1–2):265–274. **https://doi.org/10.1016/S0012-821X(02)00979-2**

Shevenell, A.E., Ingalls, A.E., Domack, E.W., and Kelly, C., 2011. Holocene Southern Ocean surface temperature variability west of the Antarctic Peninsula. *Nature,* 470(7333):250–254. **https://doi.org/10.1038/nature09751**

Siddall, M., Bard, E., Rohling, E.J., and Hemleben, C., 2006. Sea-level reversal during Termination II. *Geology,* 34(10):817–820. **https://doi.org/10.1130/G22705.1**

Sigman, D.M., and Boyle, E.A., 2000. Glacial/interglacial variations in atmospheric carbon dioxide. *Nature,* 407(6806):859–869. **https://doi.org/10.1038/35038000**

Sigman, D.M., Hain, M.P., and Haug, G.H., 2010. The polar ocean and glacial cycles in atmospheric CO_2 concentration. *Nature,* 466(7302)47–55. **https://doi.org/10.1038/nature09149**

Smik, L., Belt, S.T., Lieser, J.L., Armand, L.K., and Leventer, A., 2016. Distributions of highly branched isoprenoid alkenes and other algal lipids in surface waters from East Antarctica: further insights for biomarker-based paleo sea-ice reconstruction. *Organic Geochemistry,* 95:71–80. **https://doi.org/10.1016/j.orggeochem.2016.02.011**

Smith, W.H.F., and Sandwell, D.T., 1997. Global seafloor topography from satellite altimetry and ship depth soundings. *Science,* 277(5334):1956–1962. **https://doi.org/10.1126/science.277.5334.1956**

Spreen, G., Kaleschke, L., anc Heygster, G., 2008. Sea ice remote sensing using AMSR-E 89-GHz channels. *Journal of Geophysical Research: Oceans,* 113(C2):C02S03. **https://doi.org/10.1029/2005JC003384**

Sprenk, D., Weber, M.E., Kuhn, G., Rosén, P., Frank, M., Molina-Kescher, M., Liebetrau, V., and Röhling, H.-G., 2013. Southern Ocean bioproductivity during the last glacial cycle—new decadal-scale insight from the Scotia Sea. *Geological Society Special Publications,* 381(1):245–261. **https://doi.org/10.1144/SP381.17**

Stein, R., and Fahl, K., 2013. Biomarker proxy shows potential for studying the entire Quaternary Arctic sea ice history. *Organic Geochemistry,* 55:98–102. **https://doi.org/10.1016/j.orggeochem.2012.11.005**

Stephens, B.B., and Keeling, R.F., 2000. The influence of Antarctic sea ice on glacial-interglacial CO_2 variation. *Nature,* 404(6774):171–174. **https://doi.org/10.1038/35004556**

Stichel, T., Frank, M., Rickli, J., and Haley, B.A., 2012. The hafnium and neodymium isotope composition of seawater in the Atlantic sector of the Southern Ocean. *Earth and Planetary Science Letters,* 317–318:282–294. **https://doi.org/10.1016/j.epsl.2011.11.025**

Stoner, J.S., Channell, J.E.T., Hillaire-Marcel, C., and Kissel, C., 2000. Geomagnetic paleointensity and environmental record from Labrador Sea Core MD95-2024: global marine sediment and ice core chronostratigraphy for the last 110 kyr. *Earth and Planetary Science Letters,* 183(1–2):161–177. **http://dx.doi.org/10.1016/S0012-821X(00)00272-7**

Stoner, J.S., Channell, J.E.T., Hodell, D.A., and Charles, C.D., 2003. A ~580 kyr paleomagnetic record from the sub-Antarctic South Atlantic (Ocean Drilling Program Site 1089). *Journal of Geophysical Research: Solid Earth,* 108(B5):2244. **https://doi.org/10.1029/2001JB001390**

Stoner, J.S., Laj, C., Channell, J.E.T., and Kissel, C., 2002. South Atlantic and North Atlantic geomagnetic paleointensity stacks (0–80 ka): implications for inter-hemispheric correlation. *Quaternary Science Reviews,* 21(10):1141–1151. **https://doi.org/10.1016/S0277-3791(01)00136-6**

Stuart, K.M., and Long, D.G., 2011. Tracking large tabular icebergs using the SeaWinds Ku-band microwave scatterometer. *Deep Sea Research, Part II: Topical Studies in Oceanography,* 58(11–12):1285–1300. **https://doi.org/10.1016/j.dsr2.2010.11.004**

Thoma, M., Grosfeld, K., Barbi, D., Determann, J., Goeller, S., Mayer, C., and Pattyn, F., 2014. RIMBAY—a multiapproximation 3D ice-dynamics model for comprehensive applications: model description and examples. *Geoscientific Model Development,* 7(1):1–21. **https://doi.org/10.5194/gmd-7-1-2014**

Tian, J., Wang, P., Cheng, X., and Li, Q., 2002. Astronomically tuned Plio–Pleistocene benthic $\delta^{18}O$ record from South China Sea and Atlantic-Pacific comparison. *Earth and Planetary Science Letters,* 203(3–4):1015–1029. **https://doi.org/10.1016/S0012-821X(02)00923-8**

Timmermann, A., Friedrich, T., Timm, O.E., Chikamoto, M.O., Abe-Ouchi, A., and Ganopolski, A., 2014. Modeling obliquity and CO_2 effects on Southern Hemisphere climate during the past 408 ka. *Journal of Climate,* 27(5):1863–1875. **https://doi.org/10.1175/JCLI-D-13-00311.1**

Timmermann, A., Timm, O., Stott, L., and Menviel, L., 2009. The roles of CO_2 and orbital forcing in driving Southern Hemispheric temperature variations during the last 21 000 yr. *Journal of Climate,* 22(7):1626–1640. **https://doi.org/10.1175/2008JCLI2161.1**

Toggweiler, J.R., and Samuels, B., 1995. Effect of Drake Passage on the global thermohaline circulation. *Deep Sea Research, Part I,* 42(4):477–500. **https://doi.org/10.1016/0967-0637(95)00012-U**

Tournadre, J., Girard-Ardhuin, F., and Legrésy, B., 2012. Antarctic icebergs distributions, 2002–2010. *Journal of Geophysical Research: Oceans,* 117(C5):C05004. **https://doi.org/10.1029/2011JC007441**

Valet, J.-P., 2003. Time variations in geomagnetic intensity. *Reviews Of Geophysics,* 41:1004. **https://doi.org/10.1029/2001RG000104**

Valet, J.-P., Meynadier, L., and Guyodo, Y., 2005. Geomagnetic dipole strength and reversal rate over the past two million years. *Nature*, 435(7043):802–805. **https://doi.org/10.1038/nature03674**

van de Flierdt, T., Goldstein, S.L., Hemming, S.R., Roy, M., Frank, M., and Halliday, A.N., 2007. Global neodymium-hafnium systematics—revisited. *Earth and Planetary Science Letters,* 259(3–4):432–441. **https://doi.org/10.1016/j.epsl.2007.05.003**

van de Flierdt, T., Hemming, S.R., Goldstein, S.L., and Abouchami, W., 2006a. Radiogenic isotope fingerprint of Wilkes Land-Adélie Coast Bottom Water in the circum-Antarctic Ocean. *Geophysical Research Letters*, 33(12):L12606. **https://doi.org/10.1029/2006GL026020**

van de Flierdt, T., Robinson, L.F., Adkins, J.F., Hemming, S.R., and Goldstein, S.L., 2006b. Temporal stability of the neodymium isotope signature of the Holocene to glacial North Atlantic. *Paleoceanography,* 21(4):PA4102. **https://doi.org/10.1029/2006PA001294**

Vaughan, D.G., Comiso, J.C., Allison, I., Carrasco, J., Kaser, G., Kwok, R., Mote, P., et al., 2013. Observations: Cryosphere. *In* Stocker, T.F., Qin, D., Plattner, G.-K., Tignor, M., Allen, S.K., Boschung, J., Nauels, A., Xia, Y., Bex, V., Midgley, P.M. (Eds.), *Climate Change 2013: The Physical Science Basis. Contribution of Working Group I to the Fifth Assessment Report of the Intergovernmental Panel on Climate Change:* Cambridge, United Kingdom (Cambridge University Press), 317–382. **http://www.climatechange2013.org/images/report/WG1AR5_Chapter04_FINAL.pdf**

Weber, M.E., Clark, P.U., Kuhn, G., Timmermann, A., Sprenk, D., Gladstone, R., Zhang, X., et al., 2014. Millennial-scale variability in Antarctic ice-sheet discharge during the last deglaciation. *Nature,* 510(7503):134–138. **https://doi.org/10.1038/nature13397**

Weber, M.E., Clark, P.U., Ricken, W., Mitrovica, J.X., Hostetler, S.W., and Kuhn, G., 2011. Interhemispheric ice-sheet synchronicity during the Last Glacial Maximum. *Science,* 334(6060):1265–1269. **https://doi.org/10.1126/science.1209299**

Weber, M.E., Kuhn, G., Sprenk, D., Rolf, C., Ohlwein, C., and Ricken, W., 2012. Dust transport from Patagonia to Antarctica–a new stratigraphic approach from the Scotia Sea and its implications for the last glacial cycle. *Quaternary Science Reviews,* 36:177–188. **https://doi.org/10.1016/j.quascirev.2012.01.016**

Wei, W., Lohmann, G., and Dima, M., 2012. Distinct modes of internal variability in the global meridional overturning circulation associated with the Southern Hemisphere westerly winds. *Journal of Physical Oceanography,* 42(5):785–801. **https://doi.org/10.1175/JPO-D-11-038.1**

Whitehouse, P.L., Bentley, M.J., and Le Brocq, A.M., 2012. A deglacial model for Antarctica: geological constraints and glaciological modelling as a basis for a new model of Antarctic glacial isostatic adjustment. *Quaternary Science Reviews,* 32:1–24. **https://doi.org/10.1016/j.quascirev.2011.11.016**

Williams, T., van de Flierdt, T., Hemming, S.R., Chung, E., Roy, M., and Goldstein, S.L., 2010. Evidence for iceberg armadas from East Antarctica in the Southern Ocean during the late Miocene and early Pliocene. *Earth and Planetary Science Letters,* 290(3–4):351–361. **https://doi.org/10.1016/j.epsl.2009.12.031**

Winkelmann, R., Levermann, A., Martin, M.A., and Frieler, K., 2012. Increased future ice discharge from Antarctica owing to higher snowfall. *Nature,* 492(7428):239–242. **https://doi.org/10.1038/nature11616**

Wolff, E.W., Fischer, H., Fundel, F., Ruth, U., Twarloh, B., Littot, G.C., Mulvaney, R., et al., 2006. Southern Ocean sea-ice extent, productivity and iron flux over the past eight glacial cycles. *Nature,* 440(7083):491–496. **https://doi.org/10.1038/nature04614**

Yamazaki, T., and Oda, H., 2005. A geomagnetic paleointensity stack between 0.8 and 3.0 Ma from equatorial Pacific sediment cores. *Geochemistry, Geophysics, Geosystems,* 6(11):Q11H20. **https://doi.org/10.1029/2005GC001001**

Zachos, J., Pagani, M., Sloan, L., Thomas, E., and Billups, K., 2001. Trends, rhythms, and aberrations in global climate 65 Ma to present. *Science,* 292(5517):686–693. **https://doi.org/10.1126/science.1059412**

Zhang, X., Lohmann, G., Knorr, G., and Xu, X., 2013. Different ocean states and transient characteristics in Last Glacial Maximum simulations and implications for deglaciation. *Climate of the Past,* 9(5):2319–2333. **https://doi.org/10.5194/cp-9-2319-2013**

Ziegler, L.B., Constable, C.G., Johnson, C.L., and Tauxe, L., 2011. PADM2M: a penalized maximum likelihood model of the 0–2 Ma paleomagnetic axial dipole moment. *Geophysical Journal International,* 184(3):1069–1089. **https://doi.org/10.1111/j.1365-246X.2010.04905.x**

Table T1. Expedition 382 site summary. Two sites are located on the South Falkland Slope, four sites in Dove Basin, six sites in Pirie Basin, and one site in Jane Basin as a contingency. Planned drilling depths, where deeper than current Environmental Protection and Safety Panel (EPSP) depths, are pending review at the September 2018 EPSP meeting.

Site	Primary/ Alternate	Area	Latitude	Longitude	Water depth (m)	Planned drilling depth (mbsf)	Current EPSP depth limit (mbsf)
SFSD–03A	Primary	South Falkland Slope	53.1896°S	58.7608°W	780	300	350
SFSD–02A	Primary	South Falkland Slope	53.1915°S	58.6434°W	830	120	120
SCO–11A	Primary	Pirie Basin	57.4421°S	43.3578°W	3140	620	620
SCO–13A	Primary	Dove Basin	59.4410°S	41.0610°W	3255	806	556
SCO–14A	Primary	Dove Basin	59.8000°S	41.7600°W	3833	592	592
SCO–17A	Primary	Pirie Basin	57.7055°S	43.3620°W	3253	732	732
SCO–15A	Alternate	Dove Basin	59.8520°S	41.4530°W	3486	488	488
SCO–18A	Alternate	Dove Basin	59.1108°S	40.9062°W	3734	612	673
SCO–01A	Alternate	Pirie Basin	57.4333°S	43.4500°W	3101	590	590
SCO–12A	Alternate	Pirie Basin	57.6466°S	43.5000°W	3092	556	556
SCO–16A	Alternate	Pirie Basin	57.7055°S	43.5001°W	3134	810	810
SCO–19A	Alternate	Pirie Basin	57.4285°S	43.5000°W	3131	444	444
SCO–21B	Alternate	Jane Basin	61.7709°S	40.2749°W	3480	468	468

Table T2. Detailed Scotia Sea drilling plan, Expedition 382. Two primary sites will be drilled in Dove Basin (Sites SCO-13 and SCO-14) and Pirie Basin (Sites SCO-11 and SCO-17). The site in Jane Basin (Site SCO-21B) serves as a contingency site. Replication within each area should help retrieve complete composite sediment records for the region. Blue numbers give thickness of individual Units 1–5 (see Site summaries). Total depth to Reflector c and total depth to basement are calculated at a seismic velocity of 1600 m/s. Italic numbers give shot point (SP) and SP range to allow for drilling flexibility. TWTT = two-way traveltime.

Site/ Priority	Basin	Seismic Line	Shot point	SP range	Water Depth (m)	Sea Floor (ms TWTT)	Reflector a' green (ms TWTT)	Reflector a blue (ms TWTT)	Reflector b purple (ms TWTT)	Reflector c yellow (ms TWTT)	Reflector d brown (ms TWTT)	Basement black (ms TWTT)	Total depth to reflector c (m)	Total depth to basement (m)
				from to			Thickness a' (Unit 1a) (m)	Thickness a (Unit 1) (m)	Thickness b (Unit 2) (m)	Thickness c (Unit 3) (m)	Thickness d (Unit 4) (m)	Thick. to basement (Unit 5) (m)		
SCO-14	Dove	03/04	3500	*65*	3833	5120	5305	5520	5655	5860	6300	6390		
Primary				*3449-3501*			148	172	108	164	352	72	592	1016
SCO-13	Dove	10/04	1709	*22*	3255	4390	4650	4870	4945	5085	5320	5415		
Primary				*1722-1700*			208	176	60	112	188	76	556	820
SCO-15	Dove	10/04	2699	*26*	3486	4685	4855	4925	5095	5295	5700	5900		
Alternate				*2708-2682*			136	56	136	160	324	160	488	972
SCO-15	Dove	03/04	3851	*65*	3486	4700	4885	4990	5100	5310	5720	5920		
Alternate				*3851-3916*			148	84	88	168	328	160	488	976
SCO-18	Dove	07/04	4900	*66*	3734	5000	5130	5230	5465	5715	5830	6120		
Alternate				*4854-4920*			104	80	188	200	92	232	572	896
SCO-17	Pirie	11/08	2752	*24*	3253	4250	4570	4730	5000	5165	5385	5510		
Primary				*2740-2764*			256	128	216	132	176	100	732	1008
SCO-11	Pirie	13/13	745	*20*	3140	4220	4340	4715	4890	4960	5380	5440		
Primary				*730-760*			96	304	136	56	336	48	592	976
SCO-01	Pirie	13/13	565	*30*	3101	4210	4335	4430	4830	4920	5395	5480		
Alternate				*540-570*			100	76	320	72	380	68	568	1016
SCO-12	Pirie	11/13	192	*50*	3092	4190	4310	4495	4625	4885	4345	5525		
Alternate				*167-217*			96	148	104	208	368	144	556	1068
SCO-16	Pirie	11/08	2585	*24*	3134	4155	4380	4645	4900	5145	5325	5500		
Alternate				*2573-2597*			180	212	204	196	144	140	792	1076
SCO-16	Pirie	11/13	1		3134	4215	4440	4725	4925	5145	5400	5530		
Alternate							180	228	160	176	204	104	744	1052
SCO-19	Pirie	11/13	972	*26*	3131	4220	4315	4370	4615	4790	5050	5120		
Alternate				*959-985*			76	44	196	140	208	56	456	720
SCO-19	Pirie	13/13	470	*30*	3131	4225	4275	4330	4605	4780	5075	5120		
Alternate				*455-480*			40	44	220	140	236	36	444	716
SCO-21B	Jane	BRAN	*40*		3480	4720	4791	4810	5035	5305	5429	5850		
Contingency		790					57	15	180	216	100	337	468	905

Table T3. Expedition 382 operations summary. The expedition will begin and end in Punta Arenas. Two sites (SFSD-03A and SFSD-02A) will first be drilled on the South Falkland Slope, and then one site (SCO-11) will be drilled in Pirie Basin. Drilling will continue in Dove Basin with two sites (SCO-14 and SCO-14) before drilling the remaining site in Pirie Basin (SCO-17). Total operation time = ~54.6 days; total expedition time = 59.6 days. LWD/MWD = logging while drilling/measurement while drilling. EPSP = Environmental Protection and Safety Panel, APC = advanced piston corer, HLAPC = half-length advanced piston corer, XCB = extended core barrel, triple combo = triple combination, FMS = Formation MicroScanner.

Exp-382 Iceberg Alley (P902-Full-ADD2)
Operations Plan Summary

Grigar, 09 February 2018

Site No.	Location (Latitude Longitude)	Seafloor Depth (mbrf)	Operations Description	Transit (days)	Drilling Coring (days)	LWD/MWD Log (days)
Punta Arenas			Begin Expedition 5.0	port call days		
			Transit ~466 nmi to SFSD-03A@ 10.5	1.8		
SFSD-03A	53°11.3760' S	791	Hole A - APC to 250 mbsf, HLAPC to 300 mbsf	0.0	1.5	0.0
EPSP	58°45.6480' W		Hole B - APC to 250 mbsf, HLAPC to 300 mbsf	0.0	0.9	0.0
to 350 mbsf			Hole C - APC to 250 mbsf, HLAPC to 300 mbsf	0.0	0.9	0.0
			Sub-Total Days On-Site: 3.3			
			Transit ~4 nmi to SFSD-02A@ 1.5	0.1		
SFSD-02A	53°11.4900' S	841	Hole A - APC to 120 mbsf, w/orientation	0.0	0.4	0.0
EPSP	58°38.6040' W		Hole B - APC to 120 mbsf	0.0	0.3	0.0
to 150 mbsf			Hole C - APC to 120 mbsf	0.0	0.5	0.0
			Sub-Total Days On-Site: 1.3			
			Transit ~579 nmi to SCO-11@ 10.5	2.3		
SCO-11	57°26.5260' S	3151	Hole A - APC to 250 mbsf, XCB to 300 w/orientation and temp	0.0	2.3	0.0
EPSP	43°21.4680' W		Hole B - APC to 250 mbsf, XCB to 300 mbsf	0.0	1.8	0.0
to 620 mbsf			Hole C - APC to 250 mbsf, XCB to 300 mbsf, XCB to 620 mbsf log with triple combo and FMS sonic	0.0	4.1	1.1
			Sub-Total Days On-Site: 9.3			
			Transit ~140 nmi to SCO-13@ 10.5	0.6		
SCO-13	59°26.4600' S	3266	Hole A - APC 250 to mbsf, XCB to 300 mbsf w/orientation and temp	0.0	2.3	0.0
EPSP	41°3.6600' W		Hole B - APC to 250 mbsf, XCB to 300 mbsf	0.0	1.8	0.0
to 556 mbsf			Hole C - APC to 250 mbsf, XCB to Basement (~806 mbsf) log with triple combo and FMS sonic	0.0	5.8	1.2
			Sub-Total Days On-Site: 11.1			
			Transit ~30 nmi to SCO-14@ 10.5	0.1		
SCO-14	59°48.0000' S	3844	Hole A - APC to 250 mbsf, XCB to 300 mbsf w/orientation and temp	0.0	2.5	0.0
EPSP	41°45.6000' W		Hole B - APC to 250 mbsf, XCB to 300 mbsf	0.0	2.0	0.0
to 592 mbsf			Hole C - APC to 250 mbsf, XCB to 592 mbsf log with triple combo and FMS sonic	0.0	4.3	1.1
			Sub-Total Days On-Site: 9.9			
			Transit ~135 nmi to SCO-17@ 10.5	0.5		
SCO-17	57°42.3300' S	3264	Hole A - APC to 250 mbsf, XCB to 300 mbsf w/orientation and temp	0.0	2.3	0.0
EPSP	43°21.7200' W		Hole B - APC to 250 mbsf, XCB to 300 mbsf	0.0	1.8	0.0
to 732 mbsf			Hole C - APC to 250 mbsf, XCB to 732 mbsf log with triple combo and FMS sonic	0.0	4.9	1.1
			Sub-Total Days On-Site: 10.2			
			Transit ~1020 nmi to Punta Arenas@ 10.5	4.0		
Punta Arenas			End Expedition	9.5	40.7	4.4

Port Call:	5.0	Total Operating Days:	54.6
Sub-Total On-Site:	45.1	Total Expedition:	59.6

Figure F1. A. Location of Expedition 382 primary sites and contingency site (yellow). Open turquoise arrows = Iceberg Alley of Anderson and Andrews (1999). Large gray arrow = main wind direction of the Southern Hemisphere westerlies (SHW). Yellow dotted line = core profile used for flow-speed reconstructions of the Antarctic Circumpolar Current (ACC) (McCave et al., 2014). Purple dashed line = coast of Patagonia at the Last Glacial Maximum (LGM) (Iriondo, 2000). White dotted line = limit of Patagonian Ice Sheet (PIS) during the LGM (Hein et al., 2010). Blue dashed line = polar front. Gray dashed line = southern boundary (SB) of ACC (Diekmann et al., 2000). Solid turquoise arrows = direction of the ACC. Solid purple arrows = exit route of Weddell Sea Bottom Water (WSBW) (Maldonado et al., 2003). Light blue dashed lines = extent of winter and summer sea ice (Gersonde et al., 2005). PS cores = ice sheet retreat studies in the southeast Weddell Sea (Weber et al., 2011). NPI = northern Patagonian ice fields, SPI = southern Patagonian ice fields; NSR = North Scotia Ridge, SSR = South Scotia Ridge. EDML = EPICA Dronning Maud Land ice core (EPICA Community Members, 2006). Gray rectangle indicates location of the map in B on the next page. Insert shows circum-Antarctic drift of icebergs (turquoise shading; ≥5 km in length) calving off the Antarctic ice shelves (1999–2009) (Stuart and Long, 2011). Black arrows = general counterclockwise flow in the ACC. Figure modified from Weber et al. (2014). (Continued on next page.)

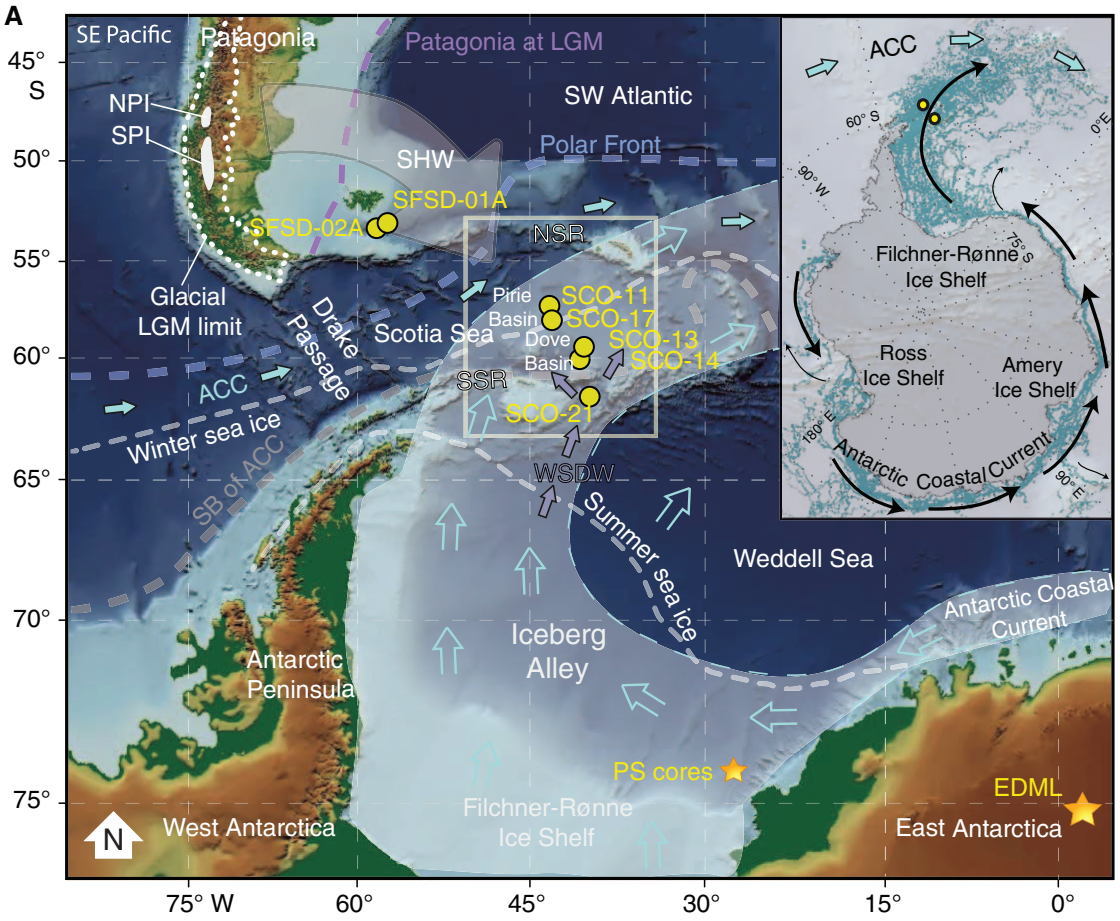

Figure F1 (continued). B. Map of the central Scotia Sea with proposed sites, presite survey cruises SCAN 2001 (Maldonado et al., 2006), SCAN 2004 (Maldonado et al., 2004), SCAN 2008 (Maldonado et al., 2008), and SCAN 2013 (Maldonado et al., 2013), as well as previous, north–south oriented core transect work (Allen et al., 2011; Collins et al., 2013; McCave et al., 2014)

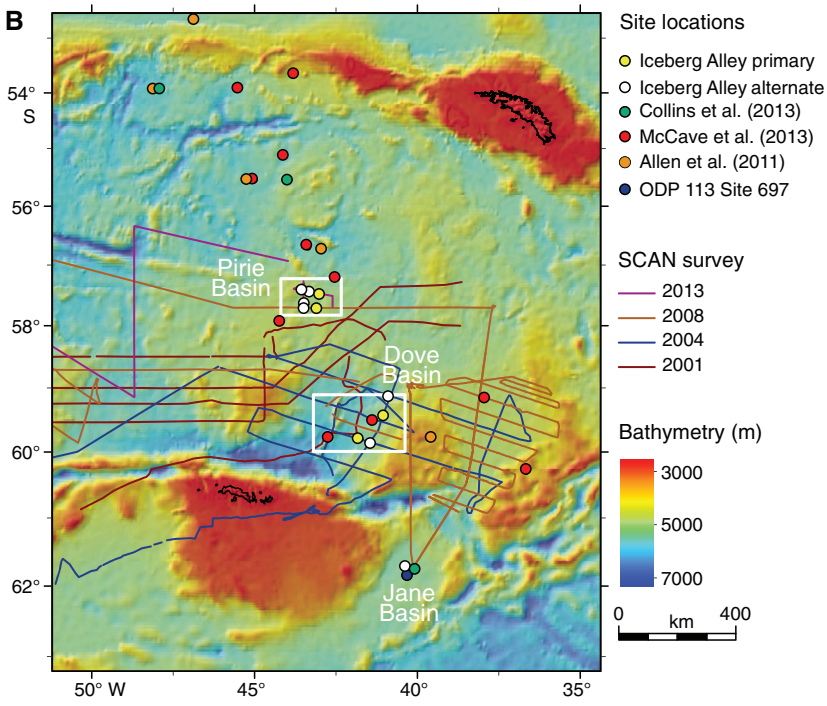

Figure F2. Seismic stratigraphy and associated ice sheet and climate events. Left panel shows geological time table with deep-sea benthic foraminifer oxygen isotope ($\delta^{18}O$) compilation of Zachos et al. (2001) and DeConto et al. (2012). Center panels indicate late Neogene seismic units and reflectors for Dove Basin (Pérez et al., 2015) and Pirie Basin (Pérez et al., 2014) with associated climate and ice sheet events for the Weddell Sea (Lindeque et al., 2013). Right panel gives benthic $\delta^{18}O$ stack of Lisiecki and Raymo (2005) with paleoclimate development for the Plio–Pleistocene. NADW = North Atlantic Deep Water, WSDW = Weddell Sea Deep Water, WAIS = West Antarctic Ice Sheet, EAIS = East Antarctic Ice Sheet, MPT = Mid-Pleistocene Transition.

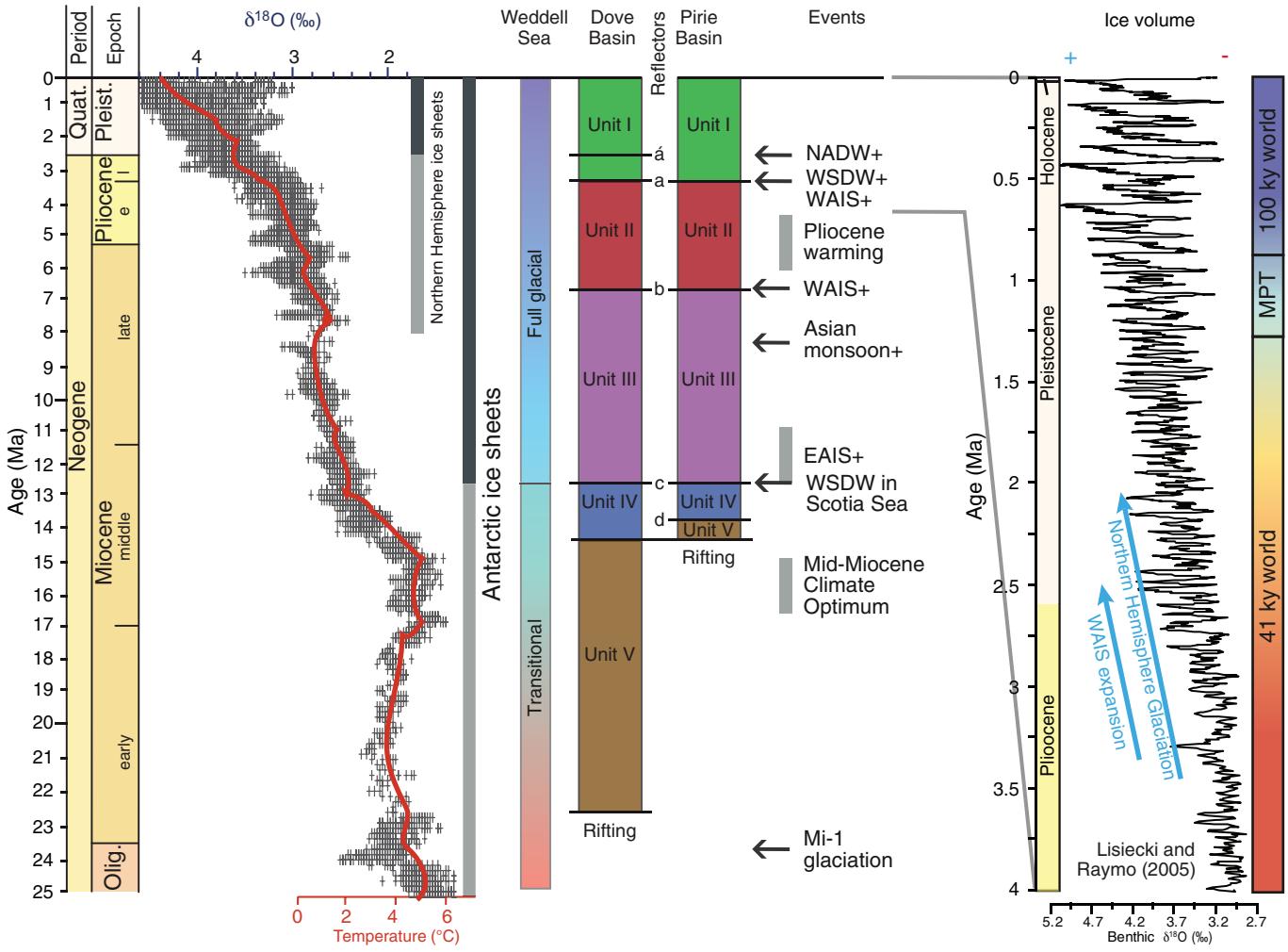

Figure F3. Bathymetry map for Dove Basin with proposed site locations. Map shows satellite (Smith and Sandwell, 1997) and multibeam bathymetry (SCAN team) for the southern study area of Dove Basin and locations of primary Sites SCO-13 and SCO-14 and alternate Sites SCO-15 and SCO-18. For location of Dove Basin, see Figure F1.

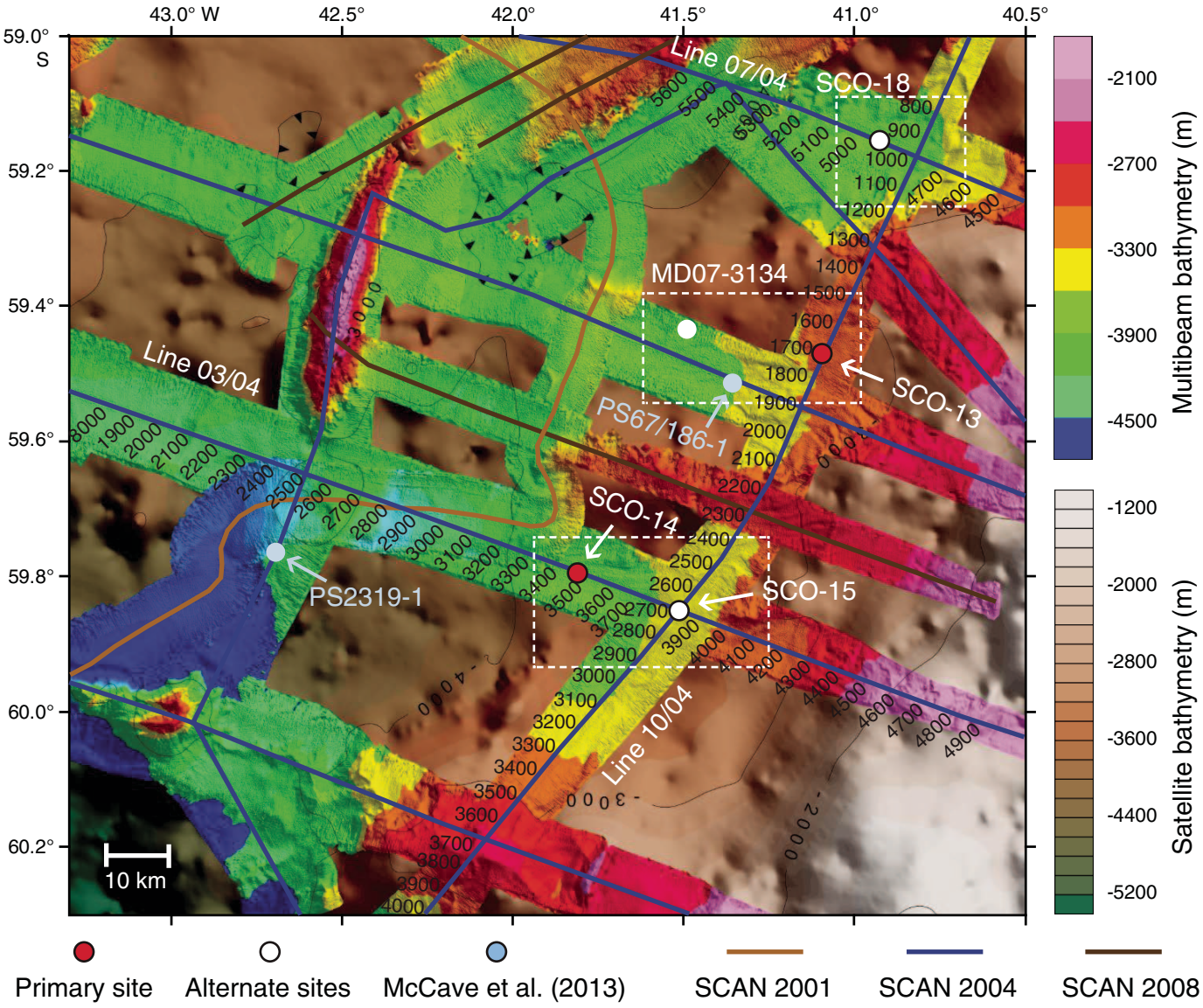

Figure F4. Seismic overview profiles for Dove Basin with proposed drill site locations. Seismic Lines 03/04, 07/04, and 10/04 (Maldonado et al., 2004) were used to determine the best drill locations. SP = shot point, CDP = common depth point, TRC = trace sequence number. A. Seismic Line 10/04 with locations of primary Site SCO-13 and alternate Site SCO-15 (at the crossing with seismic Line 03/04) and Site SCO-18 (projected from the crossing with seismic Line 07/04). B. Seismic line 07/04 with location of alternate Site SCO-18 near the crossing with seismic Line 10/04. C. Seismic Line 03/04 with locations of primary Site SCO-14 and alternate Site SCO-15 (at the crossing with seismic Line 10/04). Brown vertical bars indicate an estimated drilling depth of ~600 m. Colored horizons in seismic lines indicate the six seismic reflectors bounding Units I–V (see Figure F2). Unit thicknesses are detailed in Table T3 and Site summaries.

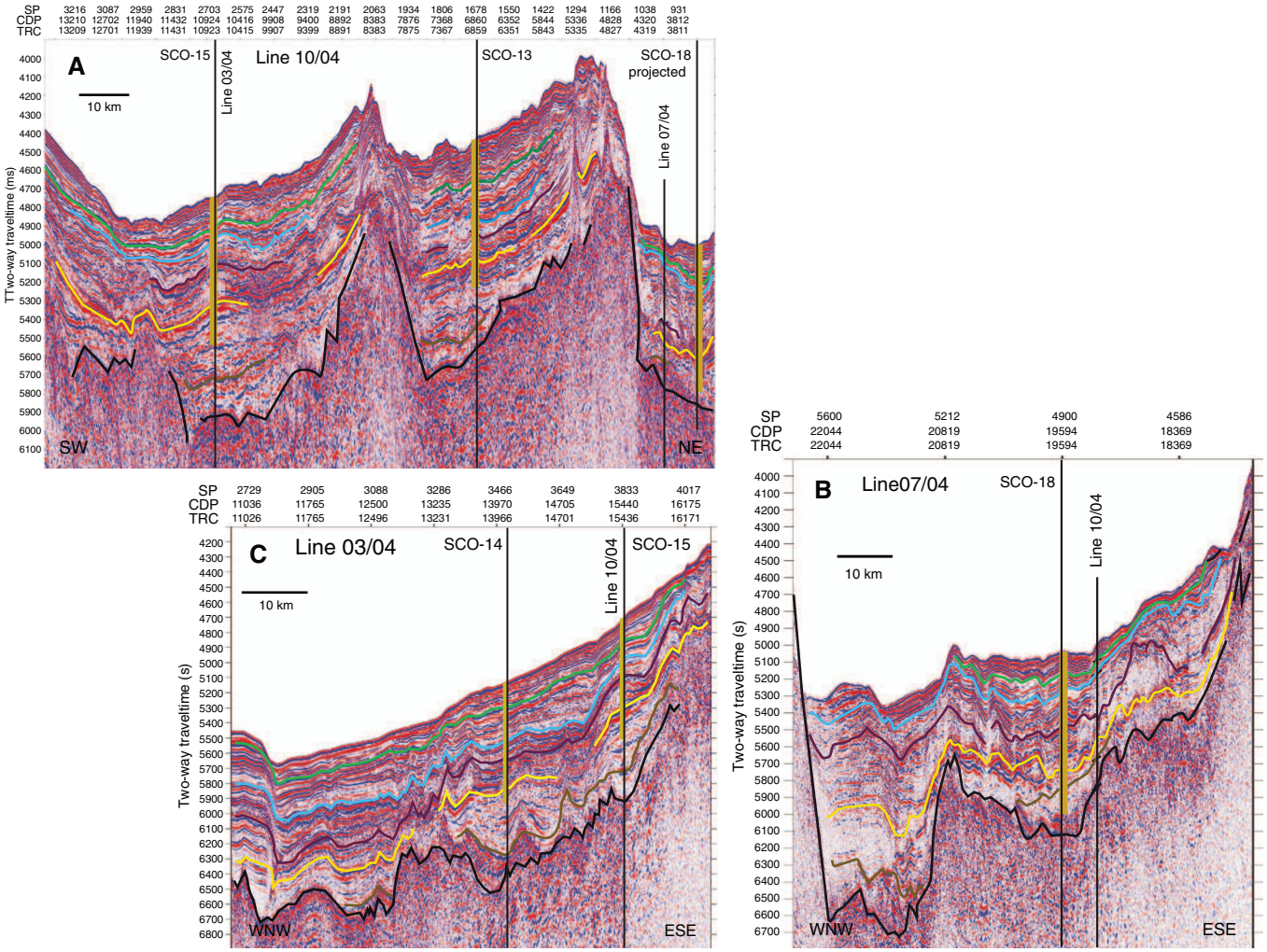

Figure F5. Bathymetry for Pirie Basin with proposed site locations. Map shows satellite (Smith and Sandwell, 1997) and multibeam bathymetry (SCAN team) for the northern study area of Pirie Basin and locations of primary Sites SCO-11 and SCO-17 and alternate Sites SCO-01 (MD07-3133), SCO-12, SCO-16, and SCO-19. For location of Pirie Basin, see Figure F1B.

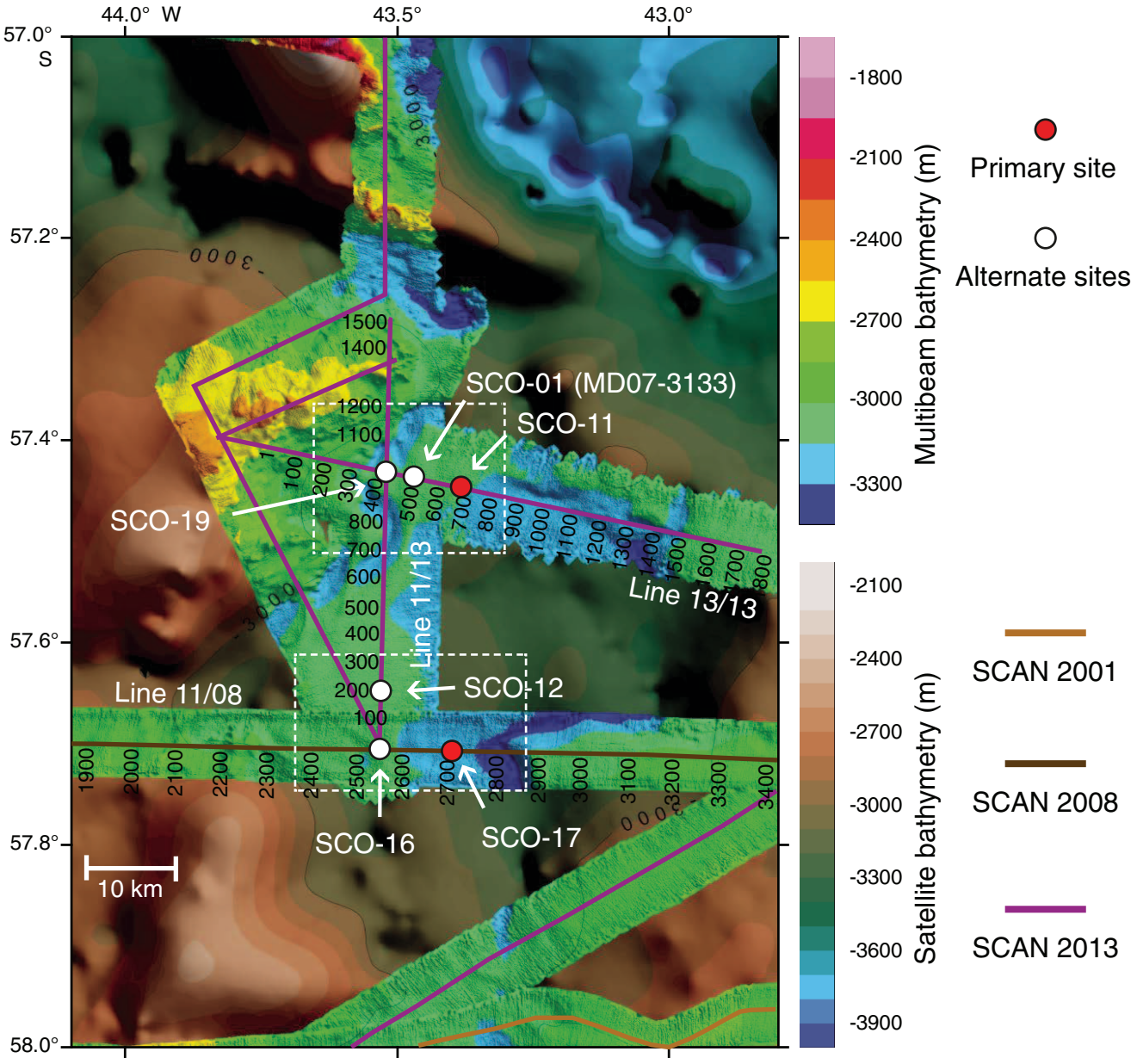

Figure F6. Seismic overview profiles for Pirie Basin with proposed site locations. Seismic Lines 11/08 (Maldonado et al., 2008), 11/13, and 13/13 (Maldonado et al., 2013) were used to determine the best drill locations. SP = shot point, CDP = common depth point, TRC = trace sequence number. A. Seismic Line 13/13 with locations of primary Site SCO-SCO-11 and alternate Sites SCO-01 (MD07-3133) and SCO-19 (at the crossing with seismic Line 11/13). B. Seismic line 11/13 with locations of alternate Sites SCO-01 (projected from seismic Line 13/13), SCO-19 (on the crossing with seismic Line 13/13), and SCO-12 and the position of crossing seismic Line 11/08 (projected). C. Seismic Line 11/08 with location of primary Site SCO-17 in a central basin position and alternate Sites SCO-12 (projected to the crossing with seismic Line 11/13) and SCO-16 (at the crossing with seismic Line 11/13). Brown vertical bars indicate an estimated drilling depth of ~600 m. Colored horizons in seismic lines indicate the six seismic reflectors bounding Units I–V (see Figure F2). Unit thicknesses are detailed in Table T3 and Site summaries.

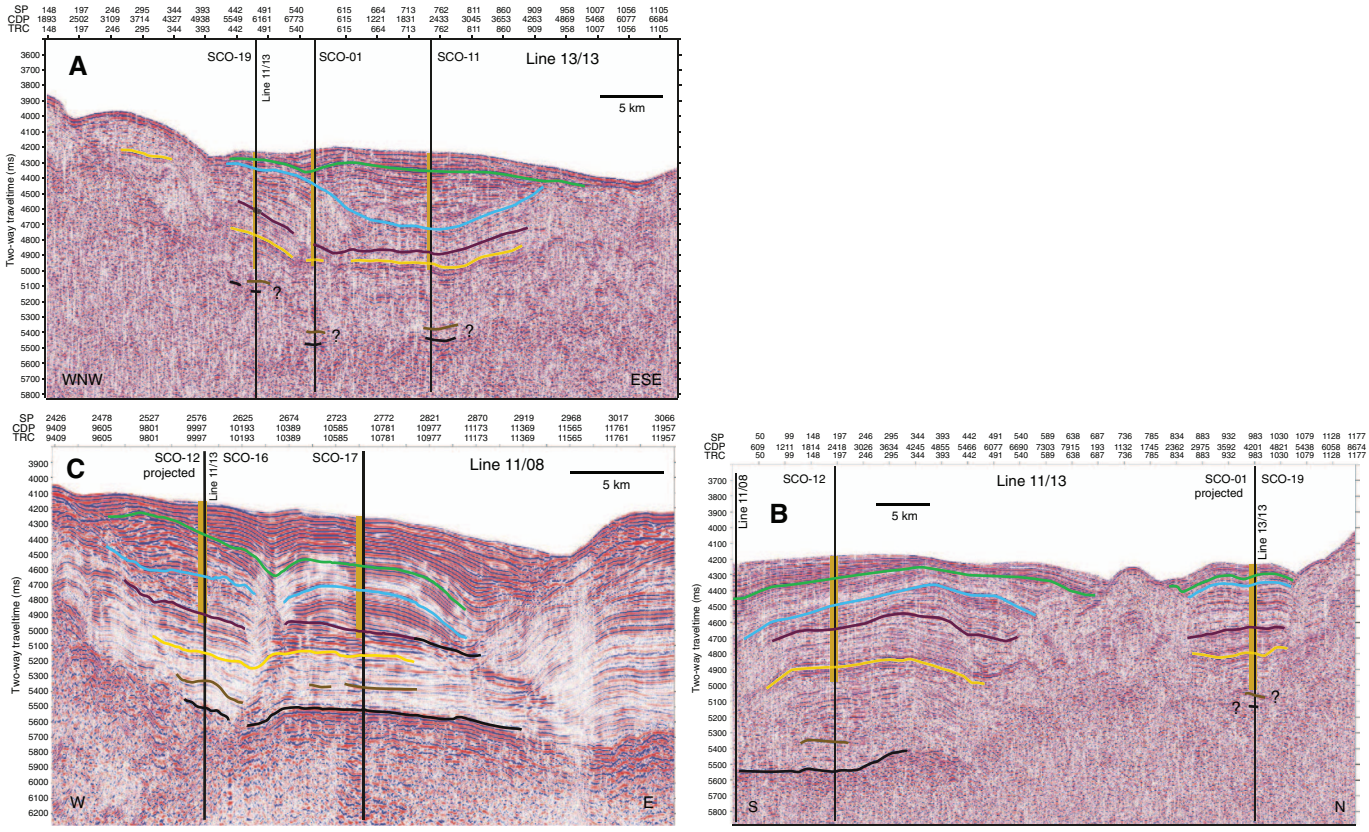

Figure F7. 3-D illustrations of seismic data.

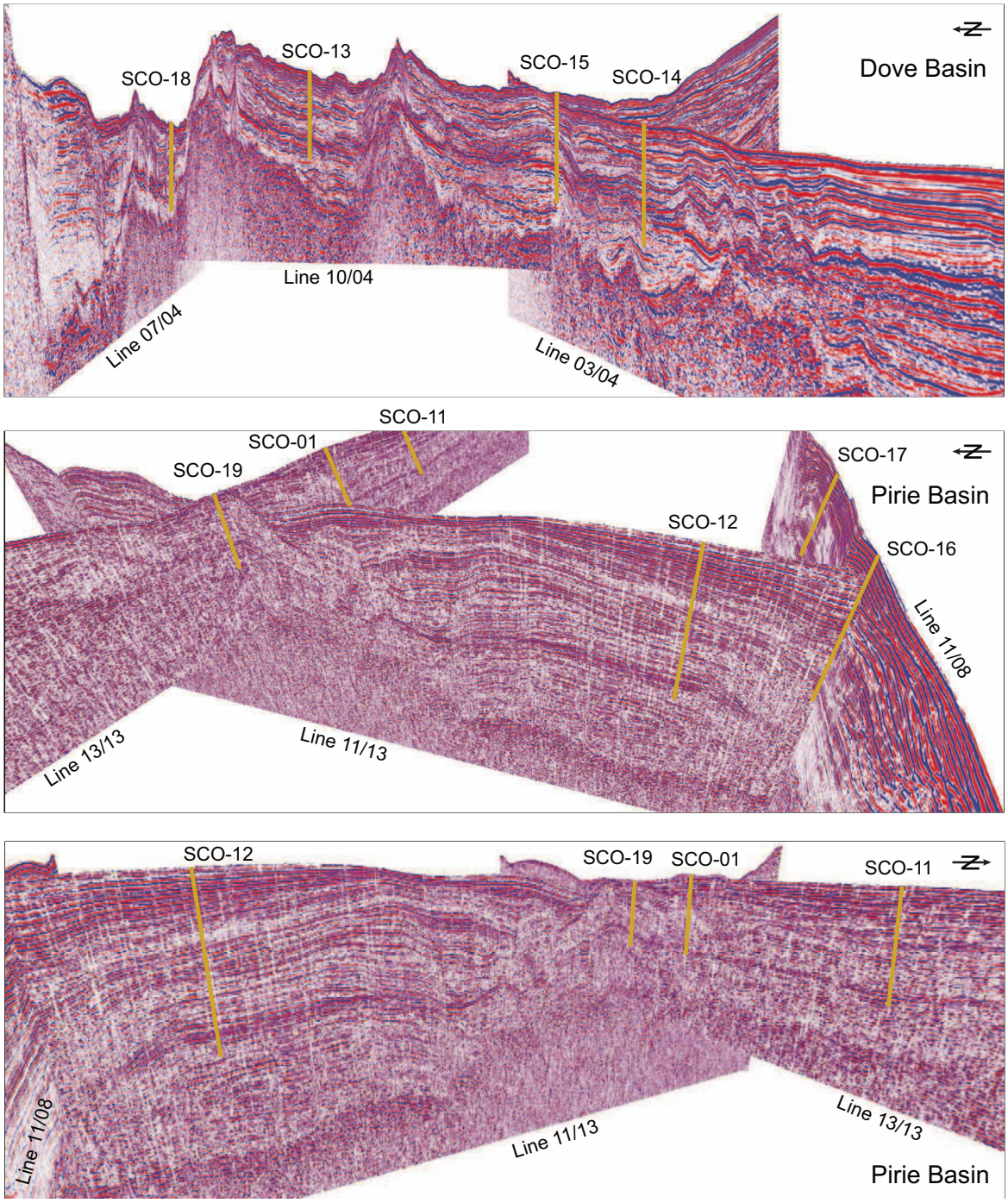

Figure F8. Oceanographic position, sediment thickness, and seismic profiles of the South Falkland Slope Drift. A. The Subantarctic Front (SAF; red) and Polar Front (PF; black). The Magellan Strait freshwater outflow, which became active during the last deglacial, and the Last Glacial Maximum (LGM) extent of the Patagonian (Pat.) Ice Sheet (McCulloch et al., 2000). LGM shoreline (white dotted line) follows Rostami et al. (2000). B. Vertical water temperature profile along North Scotia Ridge transect (black dotted line in A). Neutral density defines water masses (Arhan et al., 1999). SAMW= Subantarctic Mode Water, AAIW = Antarctic Intermediate Water, UCDW = Upper Circumpolar Deep Water, LCDW = Lower Circumpolar Deep Water. C. South Falkland Slope Drift sites (yellow star) relative to seismic profiles. Red star = existing gravity and piston cores and the Toroa F61/5-1 exploratory well (found to be "dry"). Contour: white dashed line = 500 m, gray dashed line = 1000 m. D. Isopachs of sediment thickness (Koenitz et al., 2008).

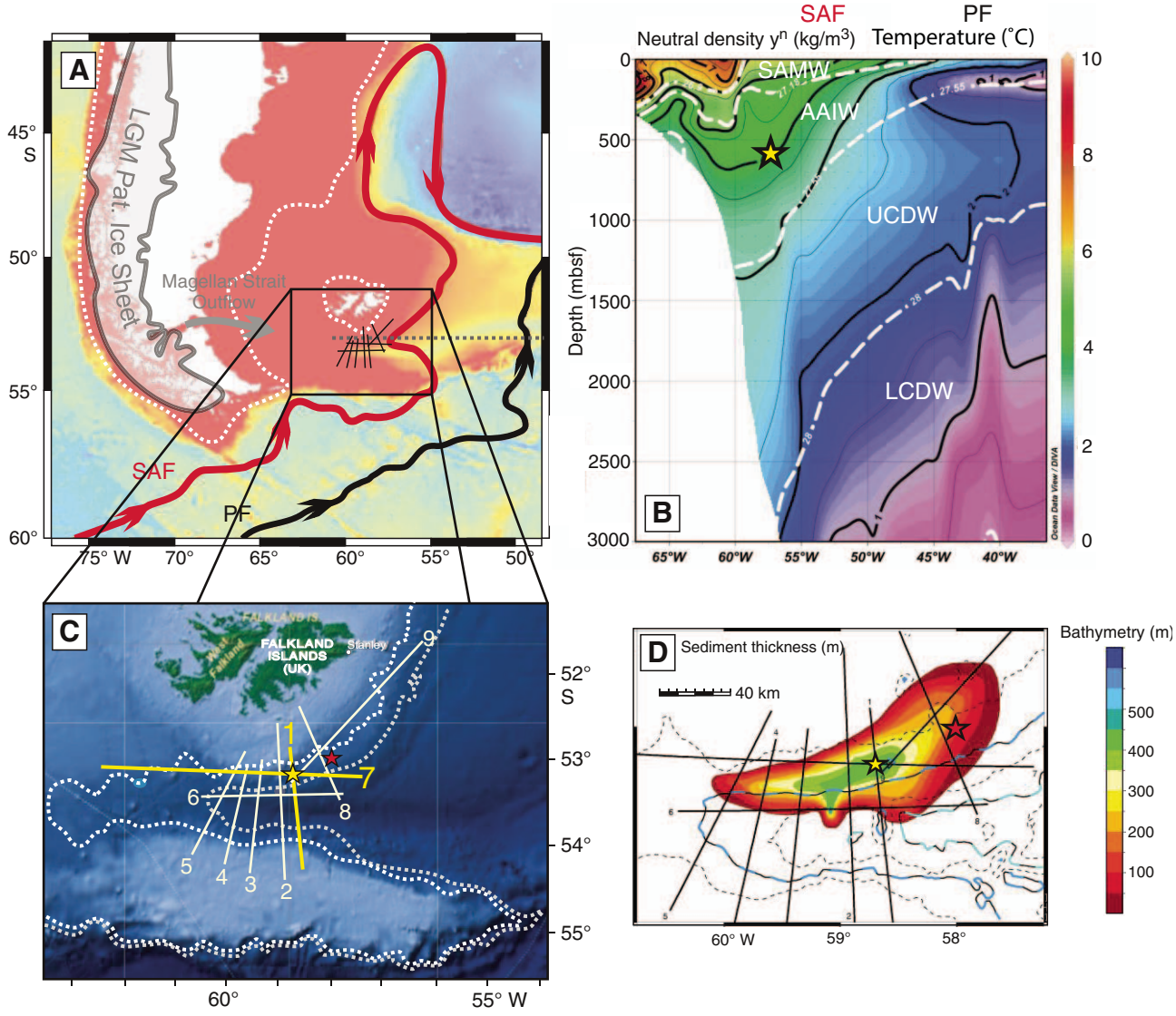

Figure F9. Internal seismic structure of the South Falkland Slope sites on seismic Profile SGF193_107 (Line 7 in Figure F8). Proposed Site SFSD-02 targets optimal recovery of Unit 2A and will be cored to ~120 m. Proposed Site SFSD-03 targets optimal recovery of Units 2B and 1B. Coring to refusal at Site SFSD-03 is anticipated to recover 300–350 m of sediment. Units labelled following Koenitz et al. (2008).

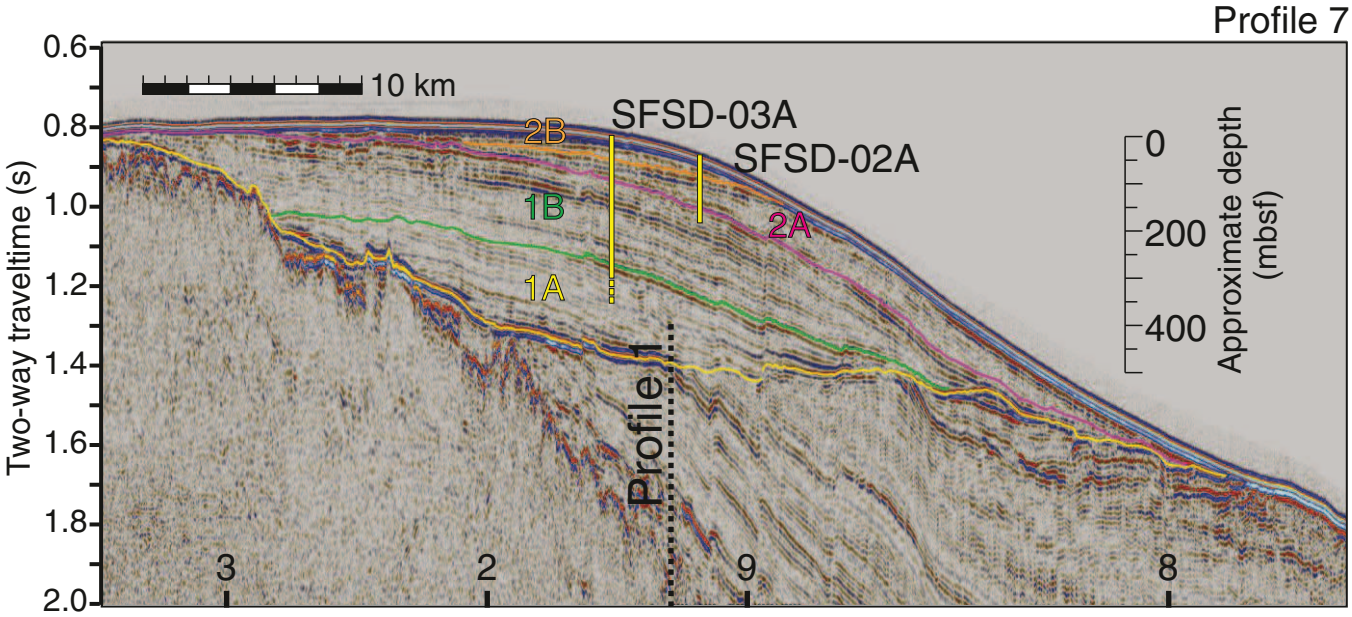

Figure F10. Deglacial AIS discharges (AIDs) in the Scotia Sea. A. Stacked iceberg-rafted debris (IBRD) flux record. B. 500 y averages of stacked IBRD flux relative to Holocene average. C. Antarctic deglacial $\delta^{13}C_{atm}$ stack (Schmitt et al., 2012) as indicator of changes in ventilation of the Southern Ocean. D. Biogenic opal flux records from southeast Atlantic (dashed line) (Anderson et al., 2009) and Scotia Sea Sites MD07-3133 (black) and MD07-3134 (gray) (Sprenk et al., 2013). E, F. EPICA Dronning Maud Land (EDML) $ssNa^+$-flux (Fischer et al., 2007) and $\delta^{18}O$ (EPICA Community Members, 2006). G. $\delta^{18}O$ of North Greenland Ice Core Project (NGRIP) (NGRIP Members, 2004). Vertical brown bars show extent of the eight phases of enhanced iceberg flow through Iceberg Alley AID1–AID8. AIDs respond to Northern Hemisphere (NH) climate signals a meltwater pulse (MWP) at 19 ka, Heinrich 1 (H1), MWP-1A, Bølling-Allerød (B-A), Younger Dryas (YD), and MWP-1B, as well as Southern Hemisphere (SH) Antarctic isotopic maxima (AIM) 1 and Antarctic Cold Reversal (ACR). Antarctic deglaciation commenced during H1, with temperature rise and sea ice reduction, followed by AIS disintegration, increasing CO_2, and enhanced ocean productivity at ~17 ka. The peak deglaciation occurred during MWP-1A (gray arrow). Figure modified from Weber et al. (2014).

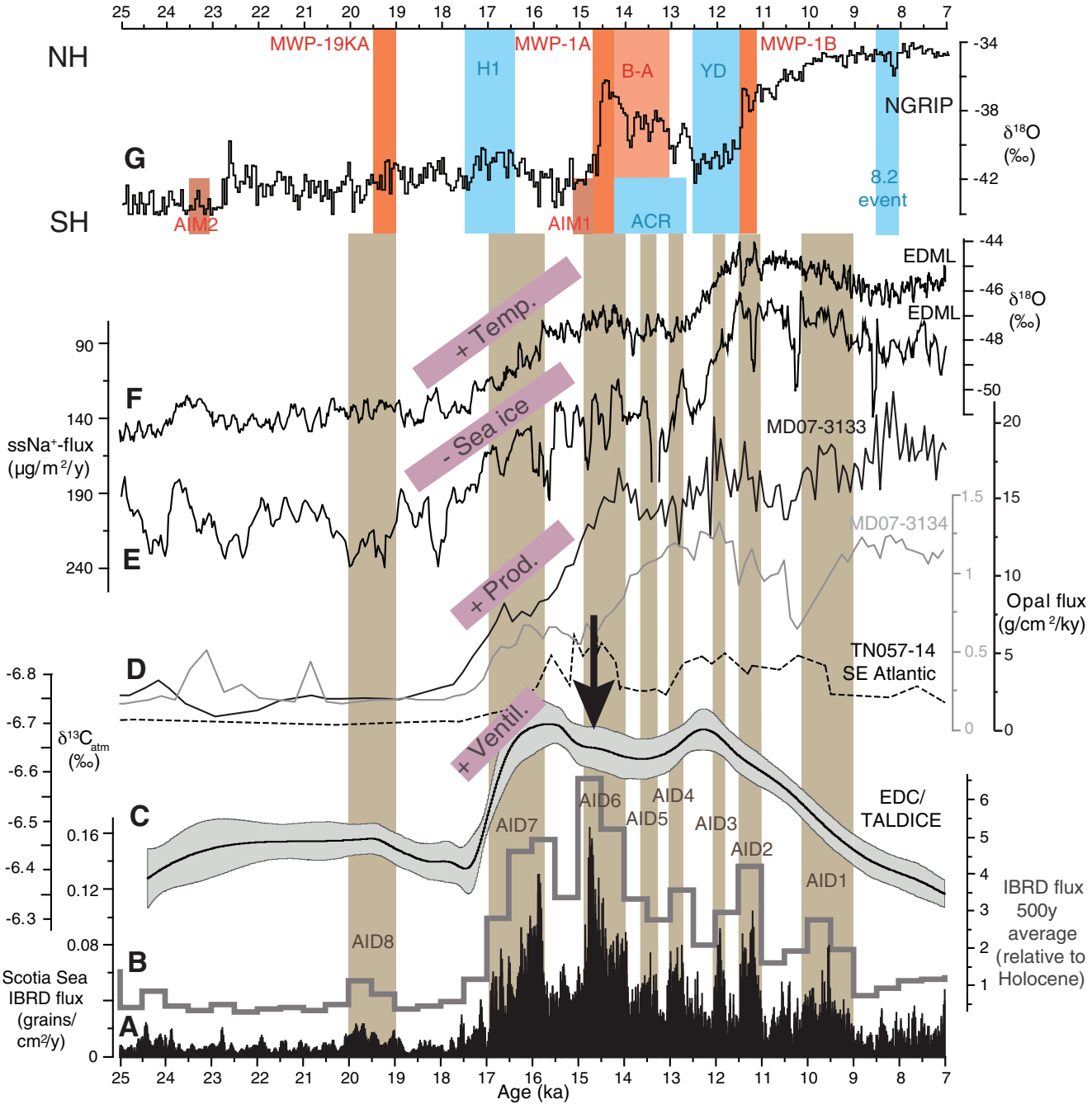

Figure F11. Southern Hemisphere dust and climate couplings during the Pliocene and Quaternary. A. Correlation of the dust proxies magnetic susceptibility (MS; green), Ca (blue), and Fe (red) from Site MD07-3134 (SCO-2) to non–sea salt Ca flux (blue) from the EPICA Dronning Maud Land (EDML) ice core for the last glacial cycle (Weber et al., 2012). MIS = marine isotope stage, AIM = Antarctic isotopic maxima. B. ODP Site 1090 Fe flux rates (red) correlated to dust particle and nssCa flux (blue) of EPICA Dome C (EDC) ice core according to Martínez-Garcia et al. (2011). C. Site 1090 Fe flux rates (red) correlated to isotopic LR04 stack (black) (Lisiecki and Raymo, 2005). Note the one-to-one coupling of marine and ice-core dust signals for the last glacial cycle and the late Quaternary and the changes in amplitude and frequency during the Mid-Pleistocene Transition (MPT). MAR = mass accumulation rate.

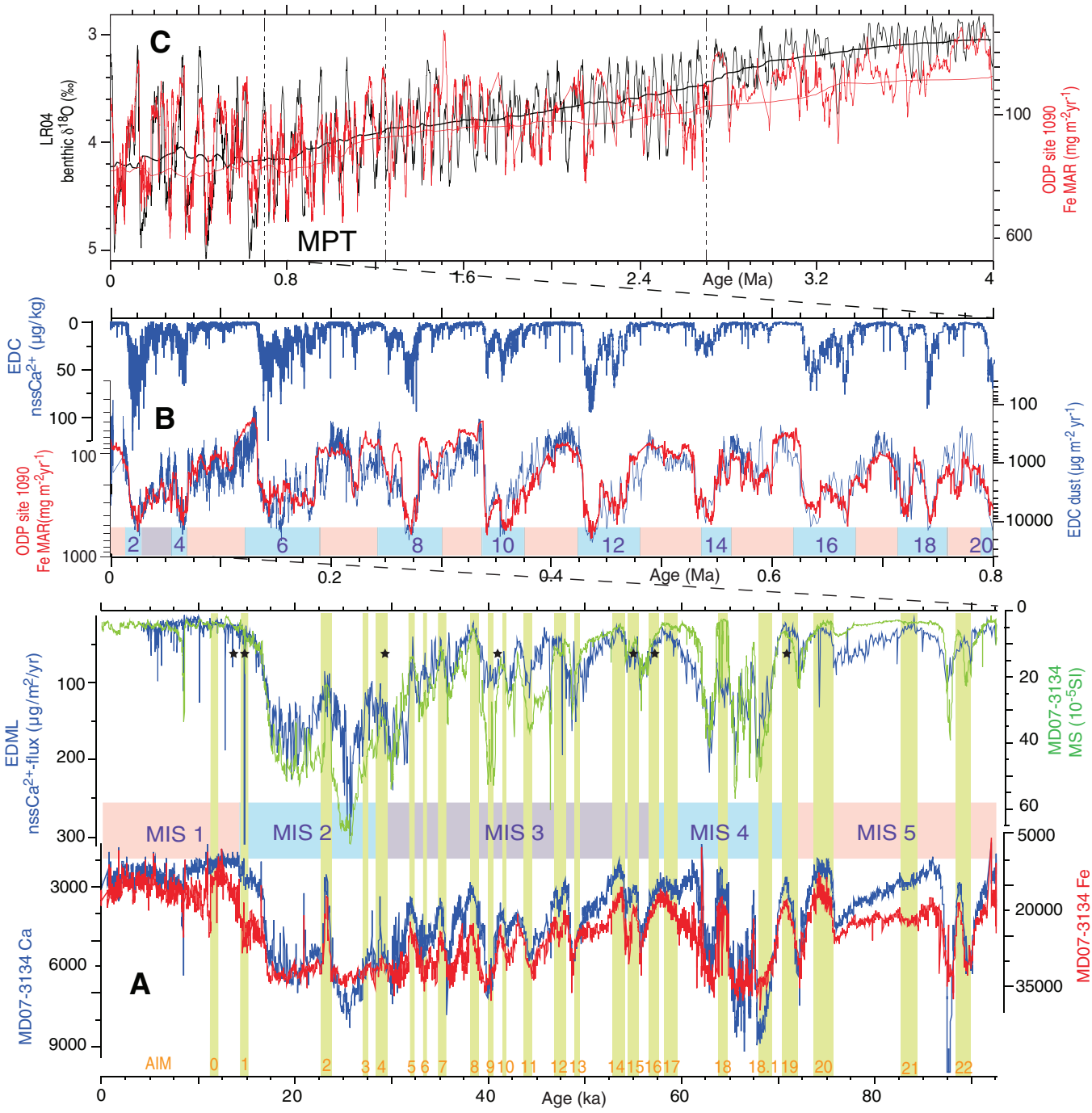

Figure F12. 3-D pattern of temperature anomalies at 14.8–14 ka and associated changes in freshwater flux, sea ice extent, and subsurface temperature for AID6 (meltwater pulse [MWP]-1A). Map shows mean surface-air temperature anomaly; vertical profile indicates zonally averaged ocean temperature anomaly in response to a ~0.22 Sv Antarctic MWP (~50% of the total amplitude of MWP-1A) at ~14.6 ka. The multimodel mean is calculated by averaging the respective anomalies obtained from the Bern3D, LOVECLIM, and COSMOS models. White-purple dashed and purple solid lines show the annual mean extent of 20 cm thick sea ice for 14.8 and 14.6 ka, respectively, simulated by LOVECLIM. Freshwater forcing causes (A) surface cooling, (B) an increase in zonally averaged sea ice extent, and (C) averaged subsurface warming between 800 and 1200 m and 63° and 70°S. For details of the model simulations, see Weber et al. (2014). NADW = North Atlantic Deep Water, CDW = Circumpolar Deep Water.

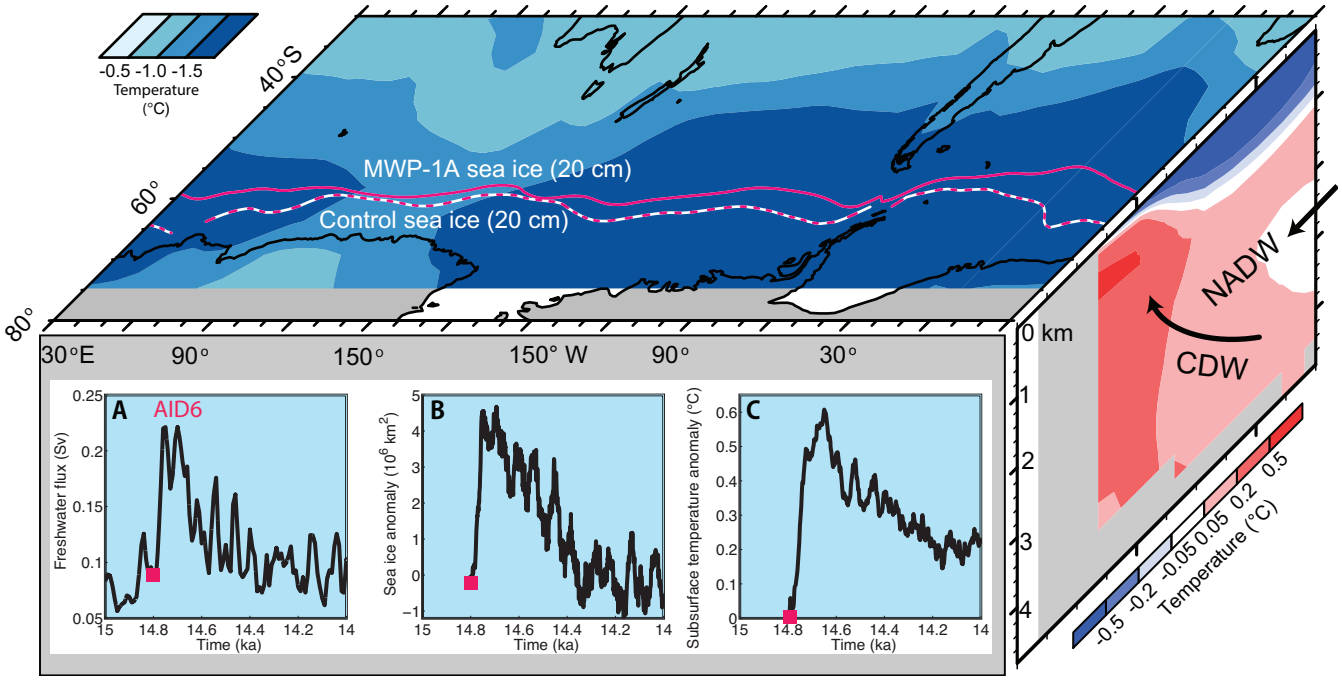

Figure F13. North–south reconstructions of current speed and sea ice environments. A. Sortable silt (SS) averaged for the Last Glacial Maximum (LGM) and Holocene. *X*-axis is distance along a north–south oriented profile. Larger core numbers indicate significant LGM–Holocene differences. South of 56°S, LGM flow was significantly slower than Holocene flow (Cores 6–9), whereas Cores 10–12 show no significant change. North of 56°S (Cores 2–5), flow during the LGM was faster than farther south, with an insignificant decrease in the Holocene (after McCave et al., 2014). Note the locations of Expedition 382 sites on the South Falkland Slope Drift (SFSD) and in Pirie and Dove Basins. B. Subdivision of sea ice environments in the Antarctic Zone. APFZ = Antarctic Polar Front Zone, HNLC = high nutrient/low chlorophyll, SAF = Subantarctic Front, WSIE = winter sea ice extent, SSIE = summer sea ice extent. Modified after Collins et al. (2013), who investigated three sediment cores that also align north–south in the central Scotia Sea. For locations of all sites, see Figure F1.

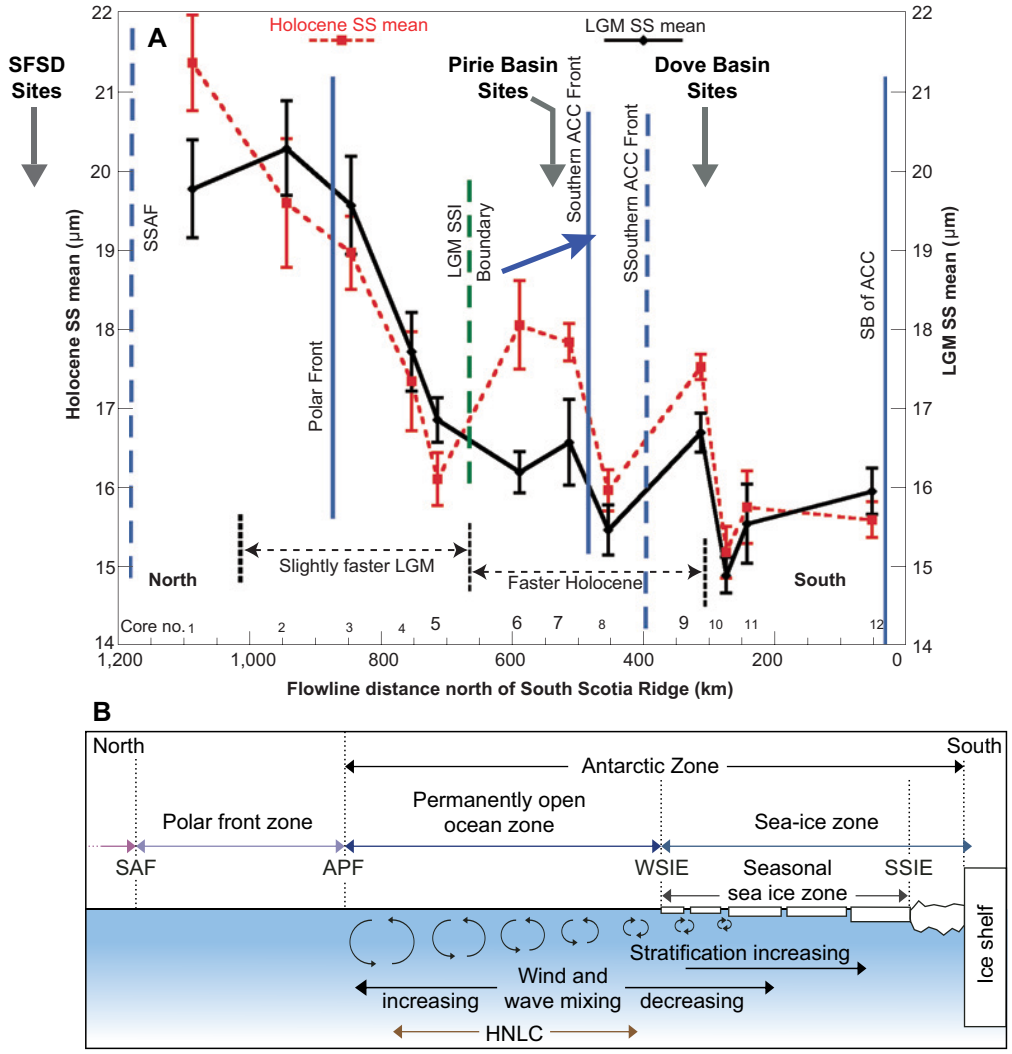

Figure 14. Location of the South Falkland Slope Drift with respect to the Subantarctic Front and Antarctic Intermediate Water. Top: Vertically integrated chlorofluorocarbon (CFC)-12 for the present day (1990s), demonstrating the sequestration of anthropogenic gases by intermediate water formation in the Subantarctic (Global Ocean Data Analysis Project climatology). Arrows indicate zonal transport of the Antarctic Circumpolar Current (ACC): red = Subantarctic Front, orange = Polar Front, yellow = southern ACC front (Orsi et al., 1995). Yellow star = South Falkland Slope Drift. Bottom: Atlantic meridional vertical salinity profile (white line, above). Yellow star = relative hydrographic position of the South Falkland Slope. SAMW = Subantarctic Mode Water, STMW = Subtropical Mode Water, AAIW = Antarctic Intermediate Water, UCDW = Upper Circumpolar Deep Water, NADW = North Atlantic Deep Water, AABW = Antarctic Bottom Water.

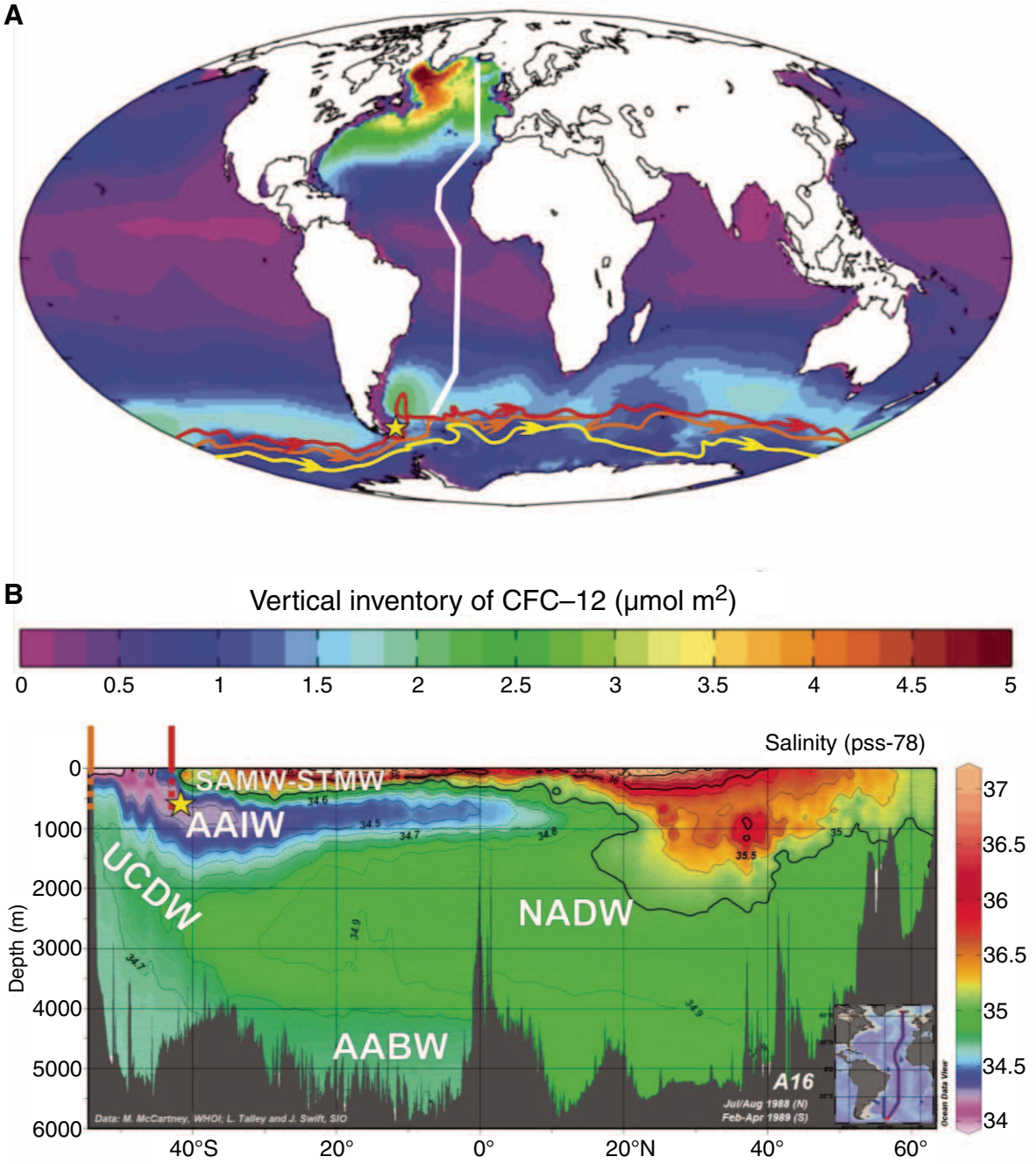

Figure F15. Benthic and planktonic stable isotopes, ice-rafted debris (IRD) concentration, X-ray fluoroscopy (XRF), and benthic foraminifer assemblages from gravity cores collected from the South Falklands Slope deposit (SFSD). A. Sediment rate and IRD concentration both increase during the Last Glacial Maximum (LGM). B. Ln(Ca/Ti) XRF data showing increase concentrations of carbonate during interglacials. C. Planktonic $\delta^{18}O$ (*Neogloboquadrina pachyderma* sinistral). D. EPICA Dome C (EDC) δD (EPICA Community Members, 2004) to illustrate phasing of proxy records from the SFSD with Antarctic temperature. E. Benthic $\delta^{18}O$ (Uvigerina spp.). F. Ln(Ba/Al) XRF data, interpreted as a proxy for productivity, suggested enhanced biological pump is active at the SFSD during interglacials. G, H. Benthic and planktonic $\delta^{13}C$, respectively. Divergent trends between benthic and planktonic $\delta^{13}C$ during interglacials may be suggestive of enhanced productivity. I. Benthic foraminifer assemblage change is also observed in glacial–interglacials cycles, possibly in response to productivity changes in surface water. These proxy records illustrate the potential of SFSD sediments to yield foraminifer-based proxy records (J. Roberts, unpubl. data; Roberts et al., 2016).

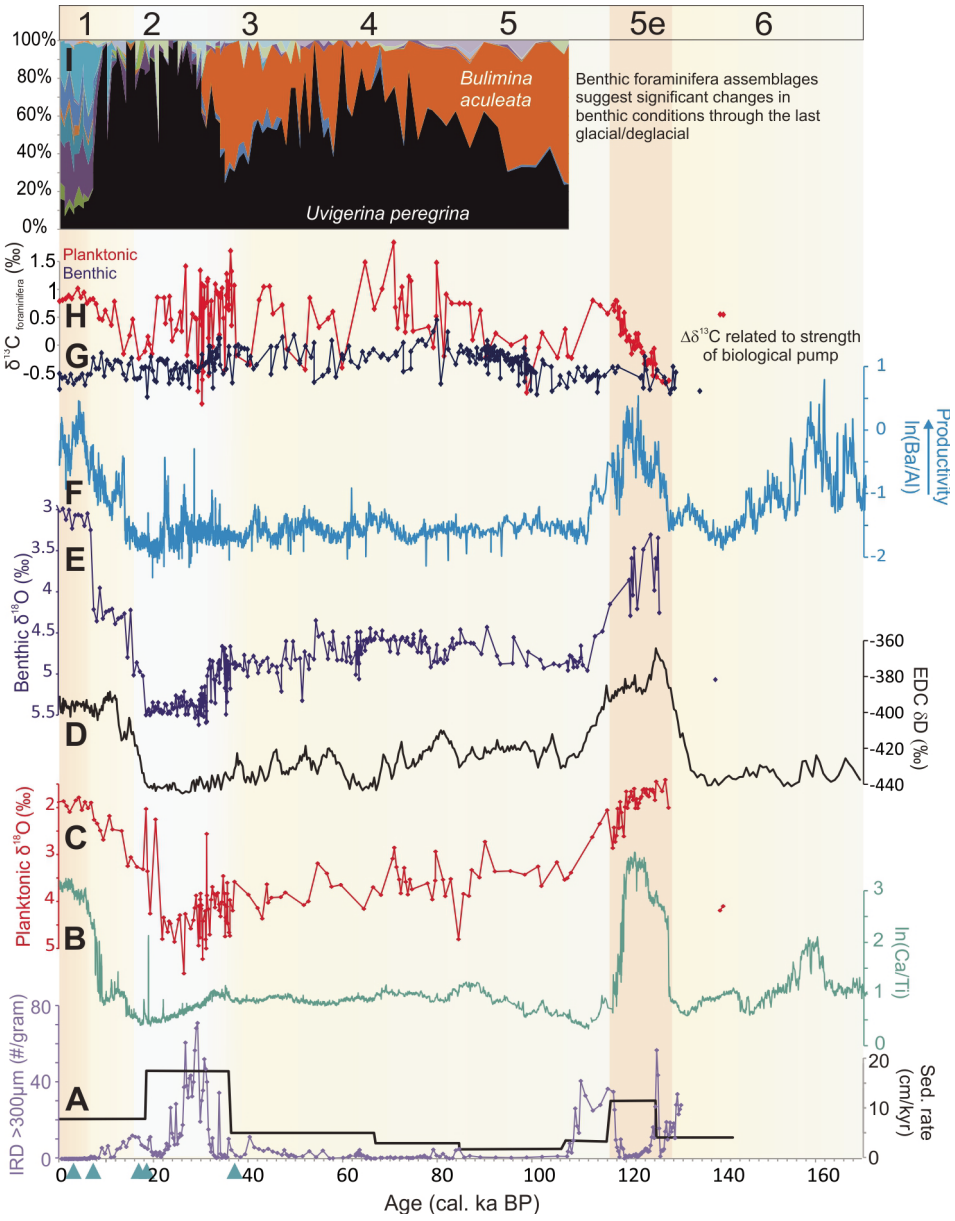

Figure F16. Expedition 382 drilling plan. Two primary sites each will be drilled at South Falkland Slope, Dove Basin, and Pirie Basin. Replication in each area should help retrieve complete composite sediment records. All sites will be triple-cored to refusal using the advanced piston corer (APC) system. The Scotia Sea sites will be extended to Reflector c with one hole using the extended core barrel (XCB) system. Relative positions of the five reflectors (a′ to d) are according to Pérez et al. (2015) for Dove Basin and Pérez et al. (2014) for Pirie Basin, with inferred ages according to Maldonado et al. (2006). The depth to each reflector is based on an assumed seismic velocity of 1600 m/s. When velocity is assumed to increase with depth, Reflectors c and d and the basement are deeper than indicated in the figure.

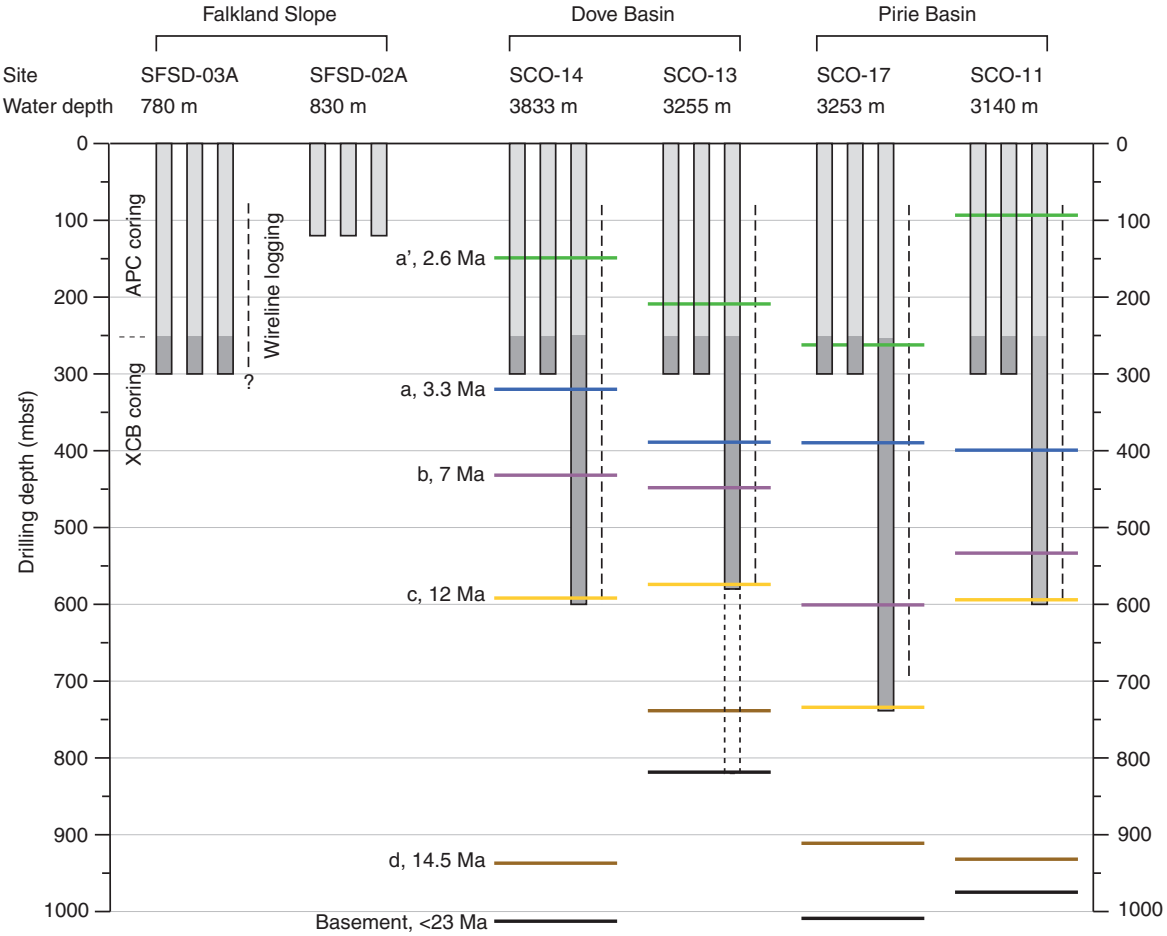

Figure F17. Sea ice maps. Biweekly snapshots of AMSR-E data (see also **http://iup.physik.uni-bremen.de:8084/amsr**) illustrate the annual Antarctic sea ice cycle for the austral summer to fall seasons of the last five years (2013–2017). The data collection method is explained in Spreen et al. (2008). Black dots in upper left corner mark position of the Expedition 382 proposed drill sites. Note the sea ice expansion from March to May during the seasonal cycle and the interannual variability.

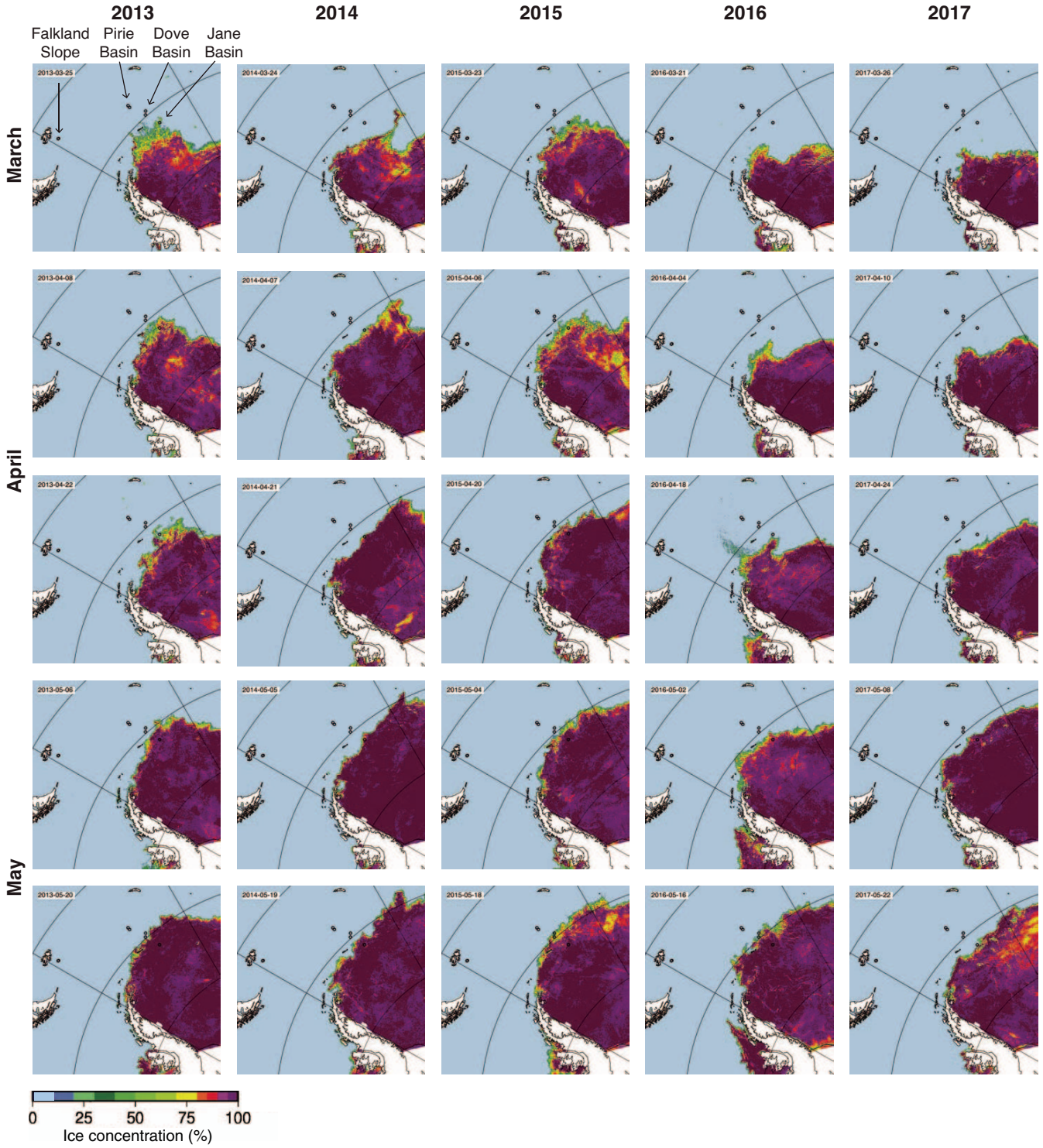

Site summaries

Site SCO-01

Priority:	Alternate
Position:	57.4333°S, 43.45°W
Water depth (mbsl):	3101
Target drilling depth (mbsf):	568
Approved maximum penetration (mbsf):	590
Survey coverage:	Line 11/13, SP 972, SP range 26 (959–985); crossing Line 13/13, SP 565, SP range 30 (540–570) (Figure **AF1**). Site SCO-01 is immediately east of Line 11/13 at the position of existing Core MD-07-3133 near the edge of a basin. The Pleistocene section (Unit I) is likely expanded in thickness. The Pliocene section might be reduced in thickness. Assignation of Reflector d and acoustic basement is questionable.
Objective(s):	Alternate site for Site SCO-11 in Pirie Basin. Objectives are as follows: • Reconstruct past variability in AIS mass loss and the related sea level history in a northerly region of the Scotia Sea closer to Patagonia; • Capture the northern, more CDW-dominated part of the Drake Passage throughflow and associated shifts of frontal systems, water mass properties, ocean temperature, and sea ice extent in the ACC; and • Reconstruct changes in atmospheric circulation and dust-climate couplings between Patagonia and Antarctica and related atmospheric circulation throughout the Plio–Pleistocene in a more proximal location relative to the source.
Drilling, coring, and downhole measurements program:	• Hole A: APC to 250 mbsf with orientation and temperature measurement; XCB to 300 mbsf • Hole B: APC to 250 mbsf; XCB to 300 mbsf • Hole C: APC to 250 mbsf; XCB to 568 mbsf and log with triple combo and FMS-sonic
Nature of rock anticipated:	Diatomaceous ooze to hemipelagic clay to silt

Site SCO-11

Priority:	Primary
Position:	57.4421°S, 43.3578°W
Water depth (mbsl):	3140
Target drilling depth (mbsf):	620
Approved maximum penetration (mbsf):	620
Survey coverage:	Line 13/13, SP 745, SP range 30 (730–760) (Figure **AF2**). Site SCO-11 is in the center of a small basin along Line 13/13 to the east, providing the most undisturbed drilling in this region with probably an extended Pliocene section (Unit II). Assignation of Reflector d and acoustic basement is questionable.
Objective(s):	Site SCO-11 is a primary site (Priority 4) for Pirie Basin. Objectives are as follows: • Reconstruct past variability in AIS mass loss and the related sea level history in a northerly region of the Scotia Sea closer to Patagonia; • Capture the northern, more CDW-dominated part of the Drake Passage throughflow and associated shifts of frontal systems, water mass properties, ocean temperature, and sea ice extent in the ACC; and • Reconstruct changes in atmospheric circulation and dust-climate couplings between Patagonia and Antarctica and related atmospheric circulation throughout the Plio–Pleistocene in a more proximal location relative to the source.
Drilling, coring, and downhole measurements program:	• Hole A: APC to 250 mbsf with orientation and temperature measurement; XCB to 300 mbsf • Hole B: APC to 250 mbsf; XCB to 300 mbsf • Hole C: APC to 250 mbsf; XCB to 620 mbsf and log with triple combo and FMS-sonic
Nature of rock anticipated:	Diatomaceous ooze to hemipelagic clay to silt

Site SCO-12

Priority:	Alternate
Position:	57.6466°S, 43.5°W
Water depth (mbsl):	3092
Target drilling depth (mbsf):	556
Approved maximum penetration (mbsf):	556
Survey coverage:	Line 11/13, SP 192, SP range 50 (167–217); crossing Line 11/08, SP 2585 (projected) (Figure **AF3**). Site SCO-12 is along Line 11/13 between Lines 13/13 and 11/08 at a relatively undisturbed position in the small basin with a potentially good and long recovery.
Objective(s):	• Site SCO-12 is an alternate for Site SCO-17 in the northern study area of Pirie Basin. Objectives are as follows: • Reconstruct past variability in AIS mass loss and related sea level history in a northerly region of the Scotia Sea closer to Patagonia; • Capture the northern, more CDW-dominated part of the Drake Passage throughflow and associated shifts of frontal systems, water mass properties, ocean temperature, and sea ice extent in the ACC; and • Reconstruct changes in atmospheric circulation and dust-climate couplings between Patagonia and Antarctica and related atmospheric circulation throughout the Plio–Pleistocene in a more proximal location relative to the source.
Drilling, coring, and downhole measurements program:	• Hole A: APC to 250 mbsf with orientation and temperature measurement; XCB to 300 mbsf • Hole B: APC to 250 mbsf; XCB to 300 mbsf • Hole C: APC to 250 mbsf; XCB to 556 mbsf and log with triple combo and FMS-sonic
Nature of rock anticipated:	Diatomaceous ooze to hemipelagic clay to silt

Site SCO-13

Priority:	Primary
Position:	59.441°S, 41.061°W
Water depth (mbsl):	3255
Target drilling depth (mbsf):	806 (pending approval from EPSP)
Approved maximum penetration (mbsf):	556
Survey coverage:	Line 10/04, SP 1709, SP range 22 (1722–1700); Site SCO-13 is along Line 10/04 between Lines 03/04 and 07/04 (Figure **AF4**).
Objective(s):	• Site SCO-13 is a primary site (Priority 2) in the southern study area of Dove Basin. Objectives are as follows: • Reconstruct past variability in AIS mass loss and the related sea level history in a southerly region of the Scotia Sea closer to Antarctica; • Capture the Drake Passage throughflow and WSBW inflow and associated shifts in frontal systems, water mass properties, ocean temperature, and sea ice extent in the ACC; and • Reconstruct changes in atmospheric circulation and dust-climate couplings between Patagonia and Antarctica and related atmospheric circulation throughout the Plio–Pleistocene in a more distal location relative to the source.
Drilling, coring, and downhole measurements program:	• Hole A: APC to 250 mbsf with orientation and temperature measurements; XCB to 300 mbsf • Hole B: APC to 250 mbsf; XCB to 300 mbsf • Hole C: APC to 250 mbsf; XCB to basement (~806 mbsf) and log with triple combo and FMS-sonic
Nature of rock anticipated:	Diatomaceous ooze to hemipelagic clay to silt

Site SCO-14

Priority:	Primary
Position:	59.8°S, 41.76°W
Water depth (mbsl):	3833
Target drilling depth (mbsf):	592
Approved maximum penetration (mbsf):	592
Survey coverage:	Line 03/04, SP 3500, SP range 67 (3449–3514) (Figure **AF5**); Site SCO-14 is along Line 03/04 into the center of the basin and should obtain a similar record as neighboring Site SCO-15 to the east.
Objective(s):	Site SCO-14 is a primary site (Priority 1) in the southern study area of Dove Basin. Objectives are as follows: • Reconstruct past variability in AIS mass loss and the related sea level history in a southerly region of the Scotia Sea closer to Antarctica; • Capture the Drake Passage throughflow and WSBW inflow and associated shifts in frontal systems, water mass properties, ocean temperature, and sea ice extent in the ACC; and • Reconstruct changes in atmospheric circulation and dust-climate couplings between Patagonia and Antarctica and related atmospheric circulation throughout the Plio–Pleistocene in a more distal location relative to the source.
Drilling, coring, and downhole measurements program:	• Hole A: APC to 250 mbsf with orientation and temperature measurements; XCB to 300 mbsf • Hole B: APC to 250 mbsf, XCB to 300 mbsf • Hole C: APC to 250 mbsf; XCB to 592 mbsf and log with triple combo and FMS-sonic
Nature of rock anticipated:	Diatomaceous ooze to hemipelagic clay to silt

Site SCO-15

Priority:	Alternate
Position:	59.852°S, 41.453°W
Water depth (mbsl):	3486
Target drilling depth (mbsf):	488
Approved maximum penetration (mbsf):	488
Survey coverage:	Line 03/04, SP 3851, SP range 65 (3851–3916); crossing Line 10/04, SP 2699, SP range 26 (2699–2665) (Figure **AF6**); primary Site SCO-15 is toward the margin of the basin at the crossing point of Lines 10/08 and 10/04, providing complete and relatively undisturbed drilling of all units in this region.
Objective(s):	Site SCO-15 is an alternate site for the southern study area of Dove Basin. Objectives are as follows: • Reconstruct past variability in AIS mass loss and the related sea level history in a southerly region of the Scotia Sea closer to Antarctica; • Capture the Drake Passage throughflow and WSBW inflow and associated shifts in frontal systems, water mass properties, ocean temperature, and sea ice extent in the ACC; and • Reconstruct changes in atmospheric circulation and dust-climate-dust couplings between Patagonia and Antarctica and related atmospheric circulation throughout the Plio–Pleistocene in a more distal location relative to the source.
Drilling, coring, and downhole measurements program:	• Hole A: APC to 250 mbsf with orientation and temperature measurements; XCB to 300 mbsf. • Hole B: APC to 250 mbsf, XCB to 300 mbsf • Hole C: APC to 250 mbsf; XCB to 488 mbsf and log with triple combo and FMS-sonic
Nature of rock anticipated:	Diatomaceous ooze to hemipelagic clay to silt

Site SCO-16

Priority:	Alternate
Position:	57.7055°S, 43.5001°W
Water depth (mbsl):	3134
Target drilling depth (mbsf):	792
Approved maximum penetration (mbsf):	810
Survey coverage:	Line 11/13, SP 1; crossing Line 11/08, SP 2585, SP range 24 (2573–2597) (Figure **AF7**). Site SCO-16 is 640 m south of SP 1 of Line 11/13, where the southern extension would meet Line 11/08, and located at the western perimeter of a small basin with probably thin Units I and II and a thicker Unit III.
Objective(s):	Site SCO-16 is an alternate for Site SCO-17 in the northern study area of Pirie Basin. Objectives are as follows: • Reconstruct past variability in AIS mass loss and related sea level history in a northerly region of the Scotia Sea closer to Patagonia; • Capture the northern, more CDW-dominated part of the Drake Passage throughflow and associated shifts of frontal systems, water mass properties, ocean temperature, and sea ice extent in the ACC; and • Reconstruct changes in atmospheric circulation and dust-climate couplings between Patagonia and Antarctica and related atmospheric circulation throughout the Plio–Pleistocene in a more proximal location relative to the source.
Drilling, coring, and downhole measurements program:	• Hole A: APC to 250 mbsf with orientation and temperature measurements; XCB to 300 mbsf • Hole B: APC to 250 mbsf, XCB to 300 mbsf • Hole C: APC to 250 mbsf; XCB to 792 mbsf and log with triple combo and FMS-sonic
Nature of rock anticipated:	Diatomaceous ooze to hemipelagic clay to silt

Site SCO-17

Priority:	Primary
Position:	57.7055°S, 43.362°W
Water depth (mbsl):	3253
Target drilling depth (mbsf):	732
Approved maximum penetration (mbsf):	732
Survey coverage:	Line 11/08, SP 2752, SP range 24 (2740–2764) (Figure **AF8**); best position for complete and parallel reflectors along Line 11/08 east of Site SCO-16 in the center of a basin; Line 11/08 had acquisition problems. [match punctuation in all tables; survey coverage has ended with a period above]
Objective(s):	Site SCO-17 is a primary site (Priority 3) for Pirie Basin. Objectives are as follows: • Reconstruct past variability in AIS mass loss and related sea level history in a northerly region of the Scotia Sea closer to Patagonia; • Capture the northern, more CDW-dominated part of the Drake Passage throughflow and associated shifts of frontal systems, water mass properties, ocean temperature, and sea ice extent in the ACC; and • Reconstruct changes in atmospheric circulation and dust-climate couplings between Patagonia and Antarctica and related atmospheric circulation throughout the Plio–Pleistocene in a more proximal location relative to the source.
Drilling, coring, and downhole measurements program:	• Hole A: APC to 250 mbsf with orientation and temperature measurements; XCB to 300 mbsf • Hole B: APC to 250 mbsf; XCB to 300 mbsf • Hole C: APC to 250 mbsf; XCB to 732 mbsf and log with triple combo and FMS-sonic
Nature of rock anticipated:	Diatomaceous ooze to hemipelagic clay to silt

Site SCO-18

Priority:	Alternate
Position:	59.1108°S, 40.9062°W
Water depth (mbsl):	3734
Target drilling depth (mbsf):	572
Approved maximum penetration (mbsf):	673
Survey coverage:	Line 07/04, SP 4900, SP range (4854–4920); crossing Line 10/04, SP 990 (projected) (Figure **AF9**); Site SCO-18 was moved 4.99 km northwest along Line 07/04 away from the crossing with Line 10/04 and into a more stable basinal position to achieve a better and more complete record than on the crossing point.
Objective(s):	Site SCO-18 is an alternate site in the southern study area of Dove Basin. Objectives are as follows: • Reconstruct past variability in AIS mass loss and the related sea level history in a southerly region of the Scotia Sea closer to Antarctica; • Capture the Drake Passage throughflow and WSBW inflow and associated shifts in frontal systems, water mass properties, ocean temperature, and sea ice extent in the ACC; and • Reconstruct changes in atmospheric circulation and dust-climate couplings between Patagonia and Antarctica and related atmospheric circulation throughout the Plio–Pleistocene in a more distal location relative to the source.
Drilling, coring, and downhole measurements program:	• Hole A: APC to 250 mbsf with orientation and temperature measurements; XCB to 300 mbsf • Hole B: APC to 250 mbsf, XCB to 300 mbsf • Hole C: APC to 250 mbsf; XCB to 572 mbsf and log with triple combo and FMS-sonic
Nature of rock anticipated:	Diatomaceous ooze to hemipelagic clay to silt

Site SCO-19

Priority:	Alternate
Position:	57.4285°S, 43.5°W
Water depth (mbsl):	3131
Target drilling depth (mbsf):	444
Approved maximum penetration (mbsf):	444
Survey coverage:	Line 11/13, SP 972; crossing Line 13/13, SP 470, SP range 30 (455–485) (Figure **AF10**); Site SCO-19 is exactly at the crossing of Lines 11/13 and 13/13 at the eastern perimeter of a small basin. The lower two units below Reflector c are reduced in thickness. Assignation of Reflector d and acoustic basement is questionable.
Objective(s):	Site SCO-19 is an alternate for Site SCO-11 in the northern study area of Pirie Basin. Objectives are as follows: • Reconstruct past variability in AIS mass loss and the related sea level history in a southerly region of the Scotia Sea closer to Antarctica; • Capture the Drake Passage throughflow and WSBW inflow and associated shifts in frontal systems, water mass properties, ocean temperature, and sea ice extent in the ACC; and • Reconstruct changes in atmospheric circulation and dust-climate couplings between Patagonia and Antarctica and related atmospheric circulation throughout the Plio–Pleistocene in a more distal location relative to the source.
Drilling, coring, and downhole measurements program:	• Hole A: APC to 250 mbsf with orientation and temperature measurements; XCB to 300 mbsf • Hole B: APC to 250 mbsf, XCB to 300 mbsf • Hole C: APC to 250 mbsf; XCB to 444 mbsf and log with triple combo and FMS-sonic
Nature of rock anticipated:	Diatomaceous ooze to hemipelagic clay to silt

Site SCO-21B

Priority:	Alternate
Position:	61.7709°S, 40.2749°W
Water depth (mbsl):	3480
Target drilling depth (mbsf):	468
Approved maximum penetration (mbsf):	468
Survey coverage:	Line BRA790, SP 40; crossing Line SM06, SP 2500 (Figure **AF11**); Site SCO-21 (Jane Basin; former ODP Site 697) is our contingency plan in case drilling is not or is only partially possible in the central Scotia Sea.
Objective(s):	Site SCO-21B is an alternate site as contingency in Jane Basin if no drilling is possible in the Scotia Sea. This site is not far to the north of ODP Site 697 in similar water depth and with good magnetostratigraphy and Pliocene material at APC-coreable depths (Pudsey, 1990). Sedimentation rates are lower (~4 cm/ky for the Quaternary, ~7 cm/ky for the upper Pliocene, and ~15 cm/ky for the lower Pliocene) and would allow us to address the paleoceanographic topics in our proposal. The site was single-cored in 1987 with moderate recovery, which can be improved now with APC/HLAPC technology, triple coring, and deeper drilling.
Drilling, coring, and downhole measurements program:	• Hole A: APC to 250 mbsf with orientation and temperature measurements; XCB to 300 mbsf • Hole B: APC to 250 mbsf, XCB to 300 mbsf • Hole C: APC to 250 mbsf; XCB to 468 mbsf and log with triple combo and FMS-sonic
Nature of rock anticipated:	Diatomaceous ooze to hemipelagic clay to silt

Site SFSD-02A

Priority:	Primary
Position:	53.1915° S, 58.6434° W
Water depth (mbsl):	830
Target drilling depth (mbsf):	120
Approved maximum penetration (mbsf):	150
Survey coverage:	MCS Profile SGFI93 107, CDP 9220; track map and seismic profile (Figure **AF12**).
Objective(s):	Recover an intact sedimentary record to generate the first multiproxy paleoceanographic record that integrates evidence for millennial- to orbital-scale variability in the ocean, atmosphere, nutrients, productivity, and ice sheet dynamics in the southwest Atlantic through at least the last 1 My. This site will recover a complete and expanded core from Units 1B and 2B.
Drilling, coring, and downhole measurements program:	• Hole A: APC to 120 mbsf • Hole B: APC to 120 mbsf • Hole C: APC to 120 mbsf with Icefield MI-5 core orientation tool and formation temperature (APCT-3) measurements
Nature of rock anticipated:	Hemipelagic silt

Site SFSD-03A

Priority:	Primary
Position:	53.1896°S, 58.7608°W
Water depth (mbsl):	780
Target drilling depth (mbsf):	300
Approved maximum penetration (mbsf):	350
Survey coverage:	MCS Profile SGFI93 107, CDP 10005; track map and seismic profile (Figure **AF13**)
Objective(s):	Recover an intact sedimentary record to generate the first multiproxy paleoceanographic record that integrates evidence for millennial- to orbital-scale variability in the ocean, atmosphere, nutrients, productivity, and ice sheet dynamics in the southwest Atlantic through at least the last 1 My. This site will recover a complete and expanded core from Units 1B and 2B.
Drilling, coring, and downhole measurements program:	• Hole A: APC to 250 mbsf; HLAPC to 300 mbsf • Hole B: APC to 250 mbsf; HLAPC to 300 mbsf • Hole C: APC to 250 mbsf; HLAPC to 300 mbsf with Icefield MI-5 core orientation tool and formation temperature (APCT-3) measurements
Nature of rock anticipated:	Hemipelagic silt

Figure AF1. Seismic profiles and bathymetry, Site SCO-01.

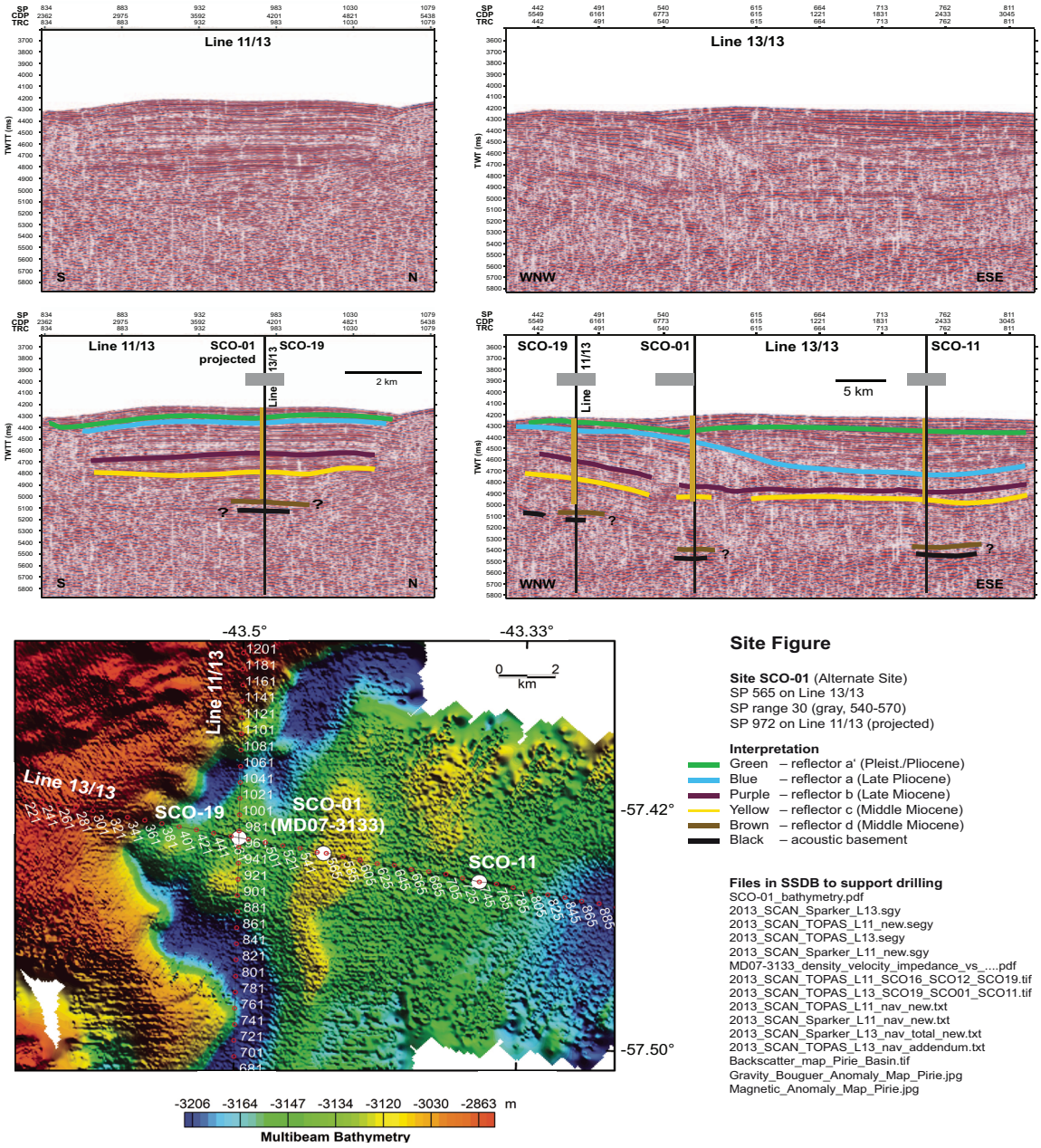

Site Figure

Site SCO-01 (Alternate Site)
SP 565 on Line 13/13
SP range 30 (gray, 540-570)
SP 972 on Line 11/13 (projected)

Interpretation
Green – reflector a' (Pleist./Pliocene)
Blue – reflector a (Late Pliocene)
Purple – reflector b (Late Miocene)
Yellow – reflector c (Middle Miocene)
Brown – reflector d (Middle Miocene)
Black – acoustic basement

Files in SSDB to support drilling
SCO-01_bathymetry.pdf
2013_SCAN_Sparker_L13.sgy
2013_SCAN_TOPAS_L11_new.segy
2013_SCAN_TOPAS_L13.segy
2013_SCAN_Sparker_L11_new.sgy
MD07-3133_density_velocity_impedance_vs_....pdf
2013_SCAN_TOPAS_L11_SCO16_SCO12_SCO19.tif
2013_SCAN_TOPAS_L13_SCO19_SCO01_SCO11.tif
2013_SCAN_TOPAS_L11_nav_new.txt
2013_SCAN_Sparker_L11_nav_new.txt
2013_SCAN_Sparker_L13_nav_total_new.txt
2013_SCAN_TOPAS_L13_nav_addendum.txt
Backscatter_map_Pirie_Basin.tif
Gravity_Bouguer_Anomaly_Map_Pirie.jpg
Magnetic_Anomaly_Map_Pirie.jpg

Figure AF2. Seismic profiles and bathymetry, Site SCO-11.

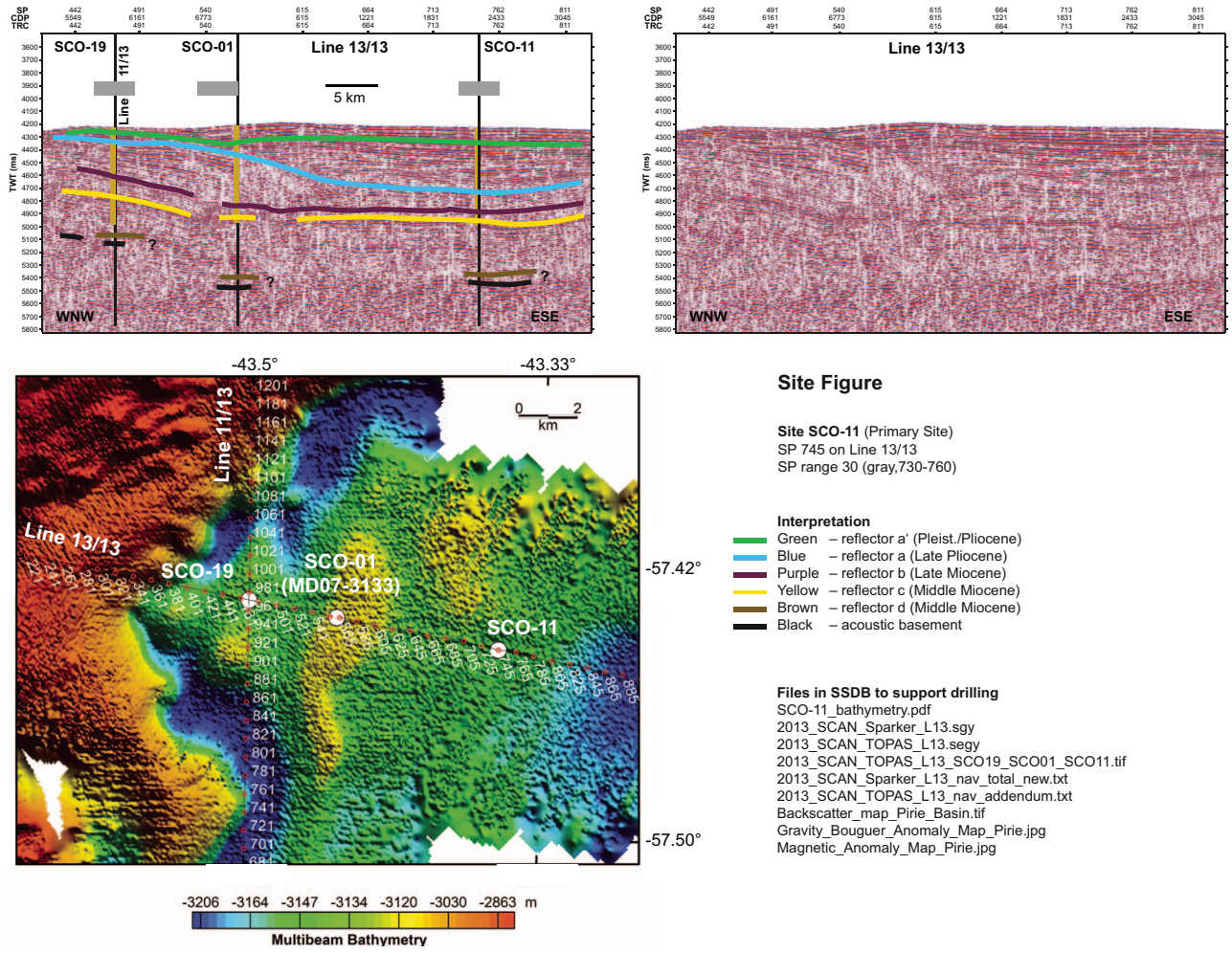

Site Figure

Site SCO-11 (Primary Site)
SP 745 on Line 13/13
SP range 30 (gray,730-760)

Interpretation
Green – reflector a' (Pleist./Pliocene)
Blue – reflector a (Late Pliocene)
Purple – reflector b (Late Miocene)
Yellow – reflector c (Middle Miocene)
Brown – reflector d (Middle Miocene)
Black – acoustic basement

Files in SSDB to support drilling
SCO-11_bathymetry.pdf
2013_SCAN_Sparker_L13.sgy
2013_SCAN_TOPAS_L13.segy
2013_SCAN_TOPAS_L13_SCO19_SCO01_SCO11.tif
2013_SCAN_Sparker_L13_nav_total_new.txt
2013_SCAN_TOPAS_L13_nav_addendum.txt
Backscatter_map_Pirie_Basin.tif
Gravity_Bouguer_Anomaly_Map_Pirie.jpg
Magnetic_Anomaly_Map_Pirie.jpg

Figure AF3. Seismic profiles and bathymetry, Site SCO-12.

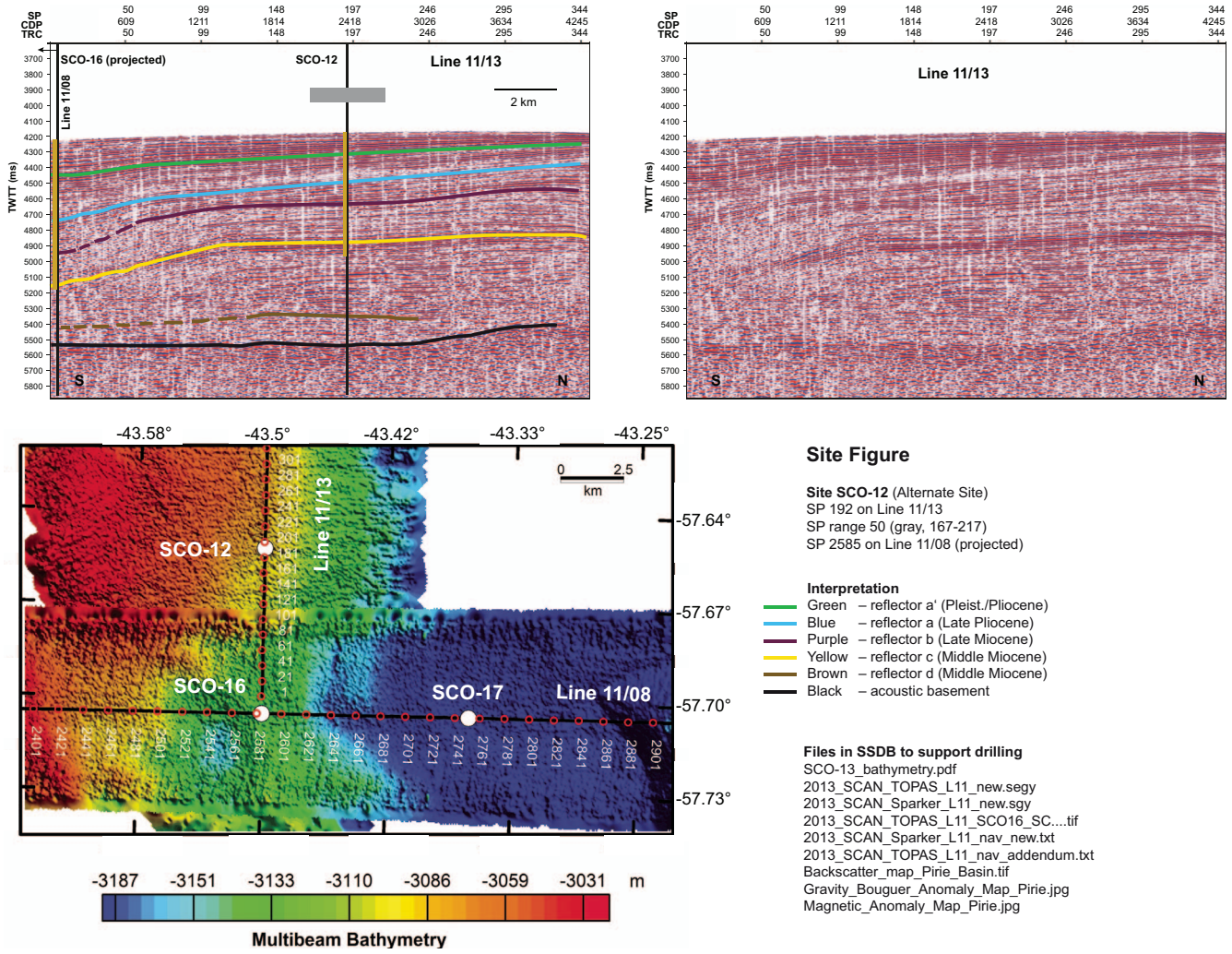

Site Figure

Site SCO-12 (Alternate Site)
SP 192 on Line 11/13
SP range 50 (gray, 167-217)
SP 2585 on Line 11/08 (projected)

Interpretation
Green – reflector a' (Pleist./Pliocene)
Blue – reflector a (Late Pliocene)
Purple – reflector b (Late Miocene)
Yellow – reflector c (Middle Miocene)
Brown – reflector d (Middle Miocene)
Black – acoustic basement

Files in SSDB to support drilling
SCO-13_bathymetry.pdf
2013_SCAN_TOPAS_L11_new.segy
2013_SCAN_Sparker_L11_new.sgy
2013_SCAN_TOPAS_L11_SCO16_SC....tif
2013_SCAN_Sparker_L11_nav_new.txt
2013_SCAN_TOPAS_L11_nav_addendum.txt
Backscatter_map_Pirie_Basin.tif
Gravity_Bouguer_Anomaly_Map_Pirie.jpg
Magnetic_Anomaly_Map_Pirie.jpg

Figure AF4. Seismic profiles and bathymetry, Site SCO-13.

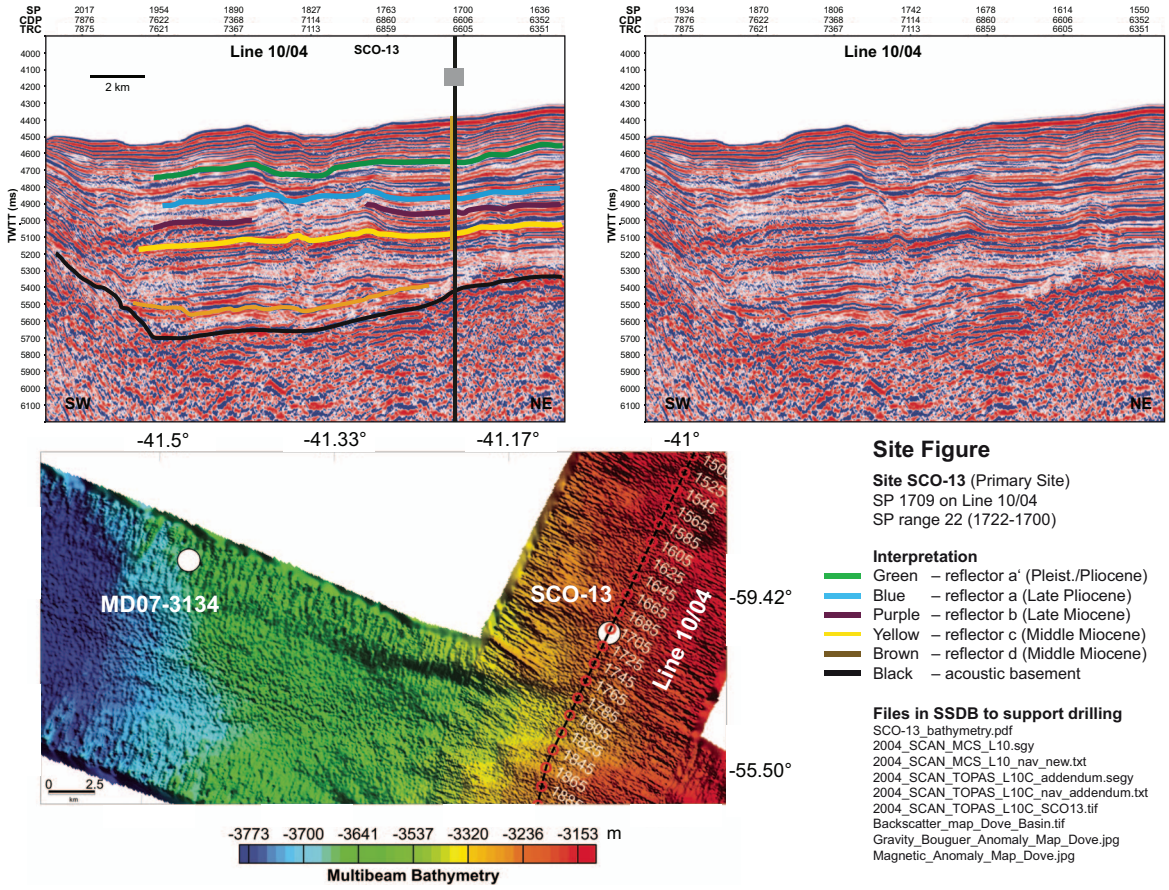

Figure AF5. Seismic profiles and bathymetry, Site SCO-14.

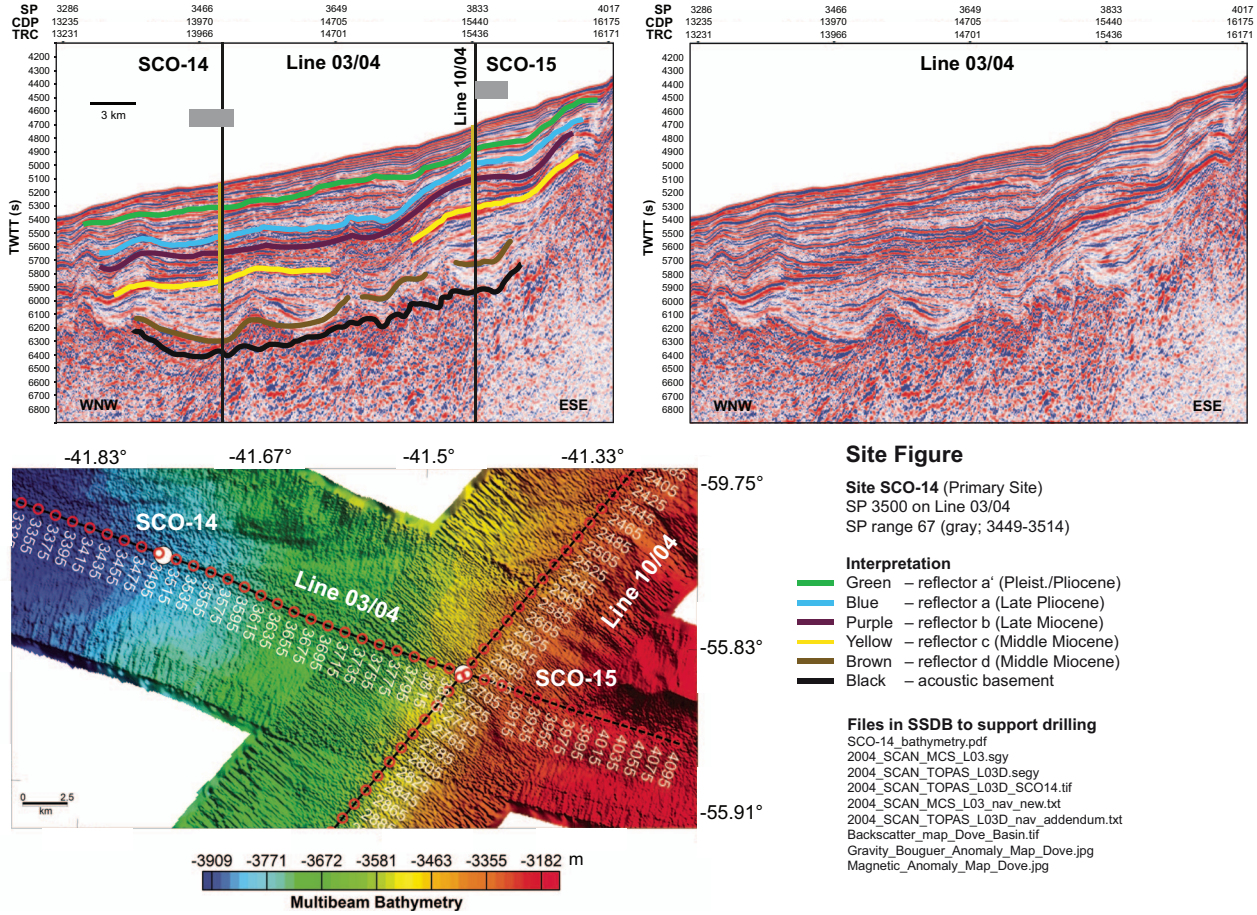

Site Figure

Site SCO-14 (Primary Site)
SP 3500 on Line 03/04
SP range 67 (gray; 3449-3514)

Interpretation

- Green – reflector a‘ (Pleist./Pliocene)
- Blue – reflector a (Late Pliocene)
- Purple – reflector b (Late Miocene)
- Yellow – reflector c (Middle Miocene)
- Brown – reflector d (Middle Miocene)
- Black – acoustic basement

Files in SSDB to support drilling

SCO-14_bathymetry.pdf
2004_SCAN_MCS_L03.sgy
2004_SCAN_TOPAS_L03D.segy
2004_SCAN_TOPAS_L03D_SCO14.tif
2004_SCAN_MCS_L03_nav_new.txt
2004_SCAN_TOPAS_L03D_nav_addendum.txt
Backscatter_map_Dove_Basin.tif
Gravity_Bouguer_Anomaly_Map_Dove.jpg
Magnetic_Anomaly_Map_Dove.jpg

Figure AF6. Seismic profiles and bathymetry, Site SCO-15.

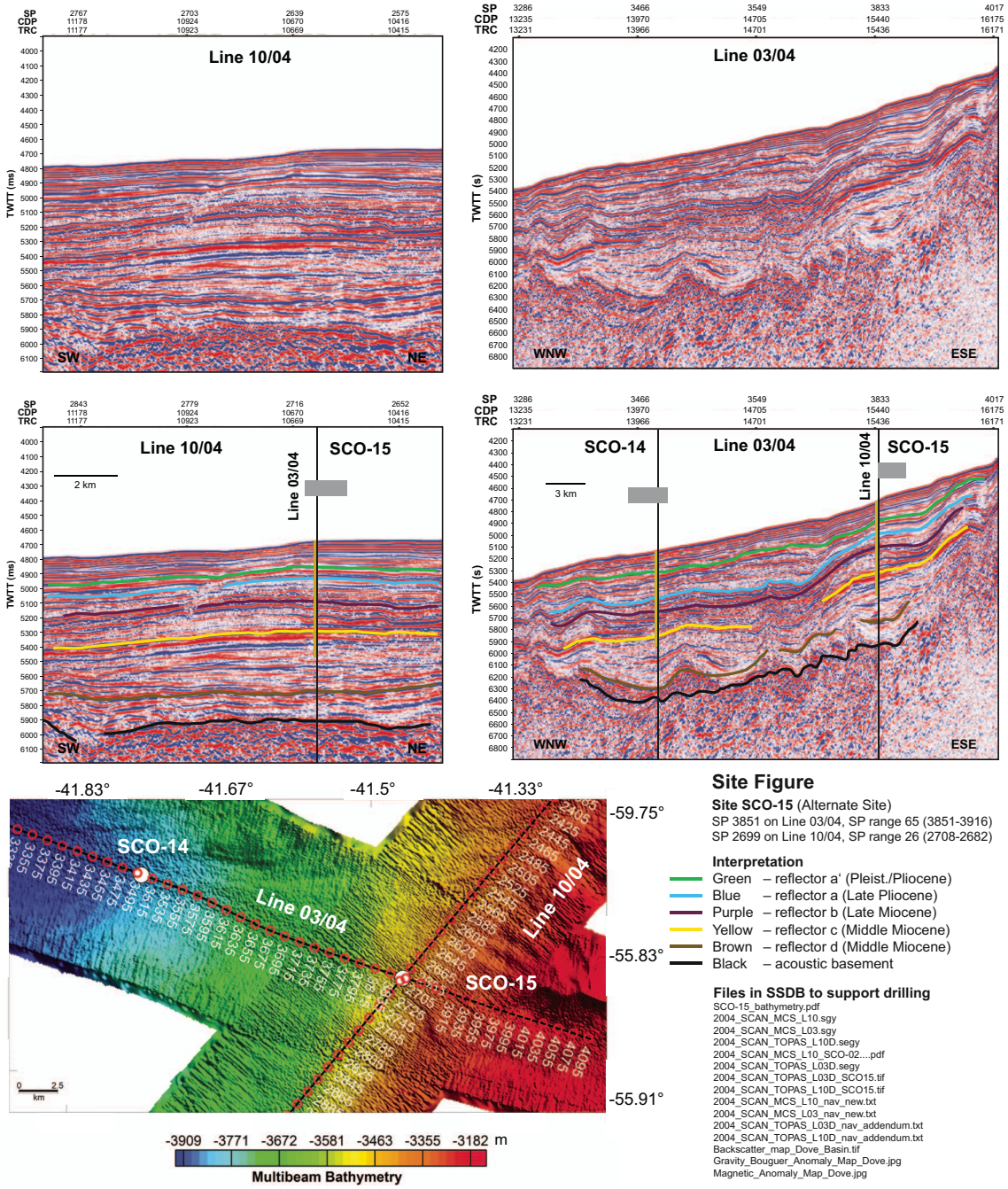

Figure AF7. Seismic profiles and bathymetry, Site SCO-16.

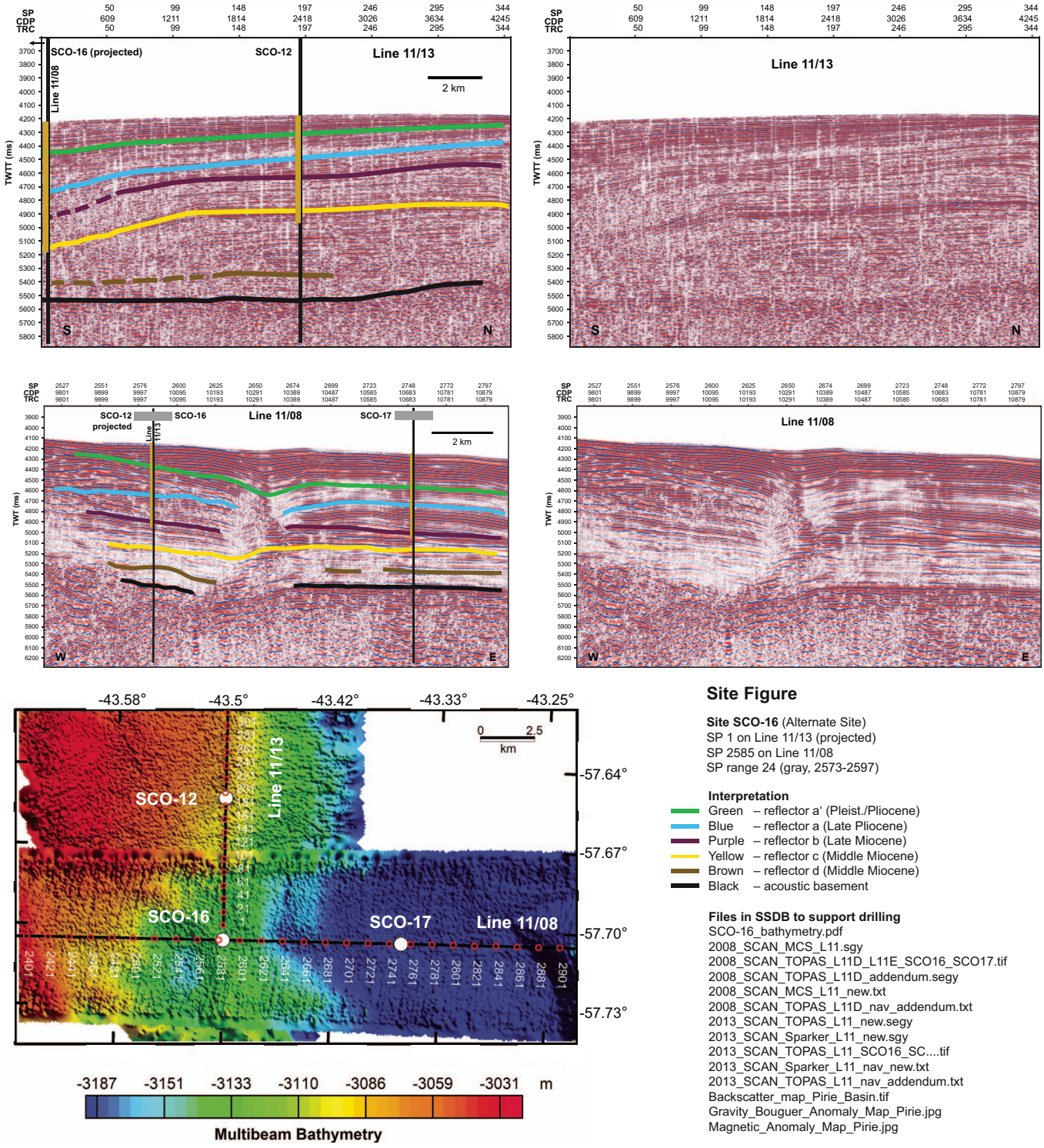

Site Figure

Site SCO-16 (Alternate Site)
SP 1 on Line 11/13 (projected)
SP 2585 on Line 11/08
SP range 24 (gray, 2573-2597)

Interpretation

- Green – reflector a' (Pleist./Pliocene)
- Blue – reflector a (Late Pliocene)
- Purple – reflector b (Late Miocene)
- Yellow – reflector c (Middle Miocene)
- Brown – reflector d (Middle Miocene)
- Black – acoustic basement

Files in SSDB to support drilling

SCO-16_bathymetry.pdf
2008_SCAN_MCS_L11.sgy
2008_SCAN_TOPAS_L11D_L11E_SCO16_SCO17.tif
2008_SCAN_TOPAS_L11D_addendum.segy
2008_SCAN_MCS_L11_new.txt
2008_SCAN_TOPAS_L11D_nav_addendum.txt
2013_SCAN_TOPAS_L11_new.segy
2013_SCAN_Sparker_L11_new.sgy
2013_SCAN_TOPAS_L11_SCO16_SC....tif
2013_SCAN_Sparker_L11_nav_new.txt
2013_SCAN_TOPAS_L11_nav_addendum.txt
Backscatter_map_Pirie_Basin.tif
Gravity_Bouguer_Anomaly_Map_Pirie.jpg
Magnetic_Anomaly_Map_Pirie.jpg

Figure AF8. Seismic profiles and bathymetry, Site SCO-17.

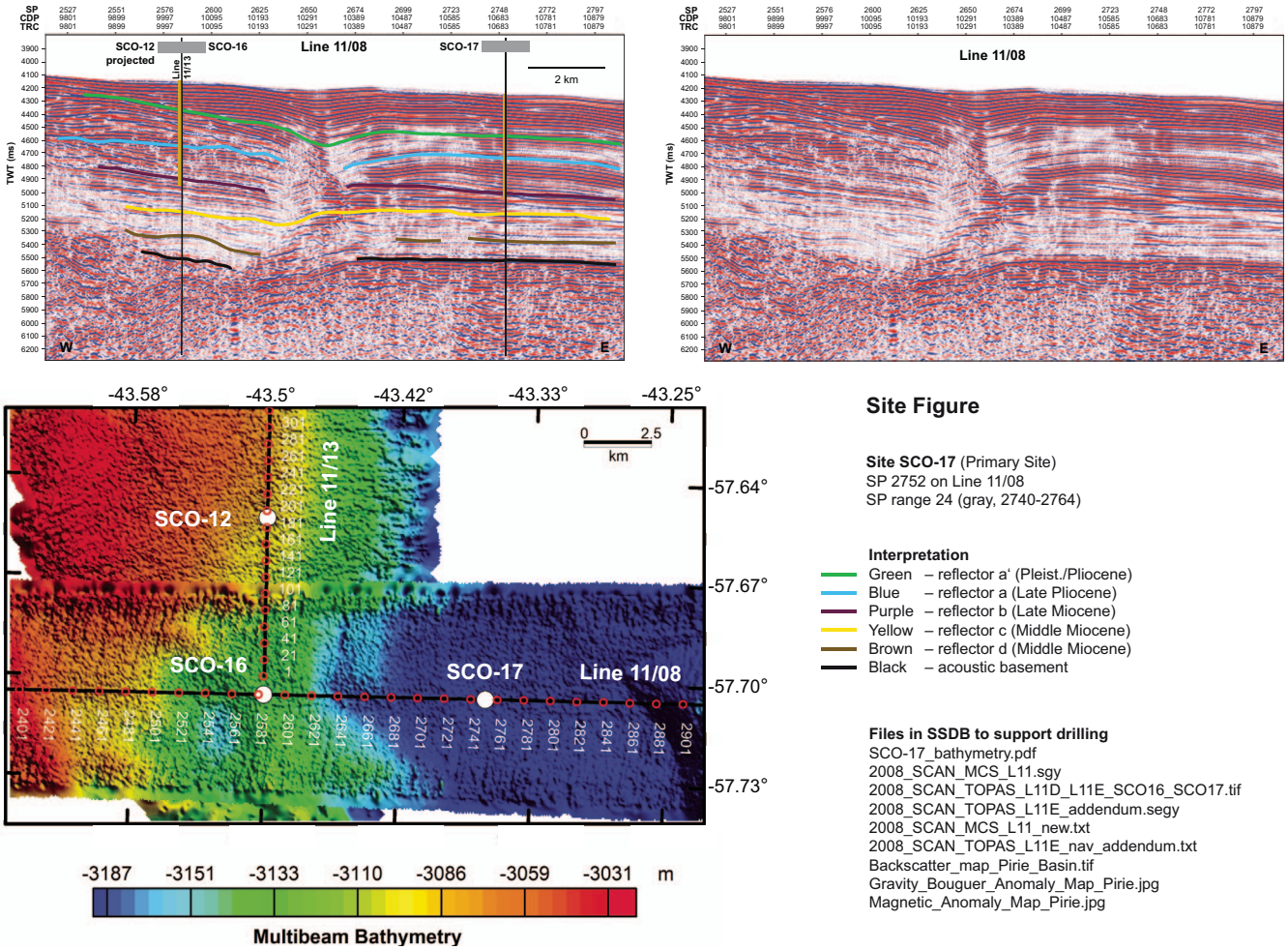

Site Figure

Site SCO-17 (Primary Site)
SP 2752 on Line 11/08
SP range 24 (gray, 2740-2764)

Interpretation

- Green – reflector a' (Pleist./Pliocene)
- Blue – reflector a (Late Pliocene)
- Purple – reflector b (Late Miocene)
- Yellow – reflector c (Middle Miocene)
- Brown – reflector d (Middle Miocene)
- Black – acoustic basement

Files in SSDB to support drilling

SCO-17_bathymetry.pdf
2008_SCAN_MCS_L11.sgy
2008_SCAN_TOPAS_L11D_L11E_SCO16_SCO17.tif
2008_SCAN_TOPAS_L11E_addendum.segy
2008_SCAN_MCS_L11_new.txt
2008_SCAN_TOPAS_L11E_nav_addendum.txt
Backscatter_map_Pirie_Basin.tif
Gravity_Bouguer_Anomaly_Map_Pirie.jpg
Magnetic_Anomaly_Map_Pirie.jpg

Figure AF9. Seismic profiles and bathymetry, Site SCO-18.

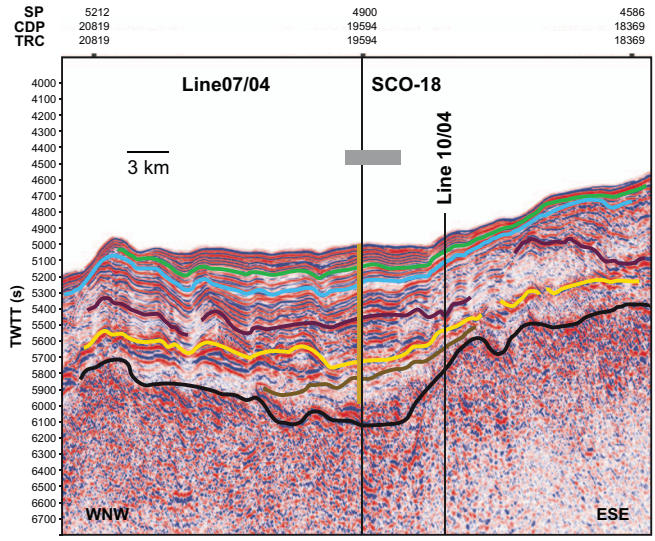

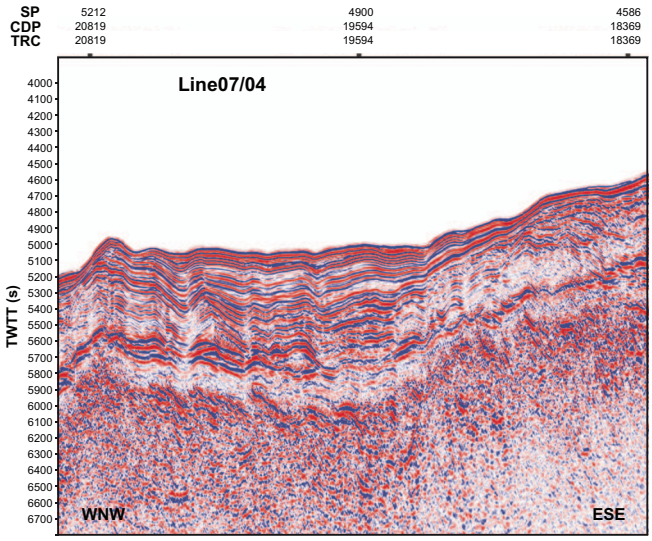

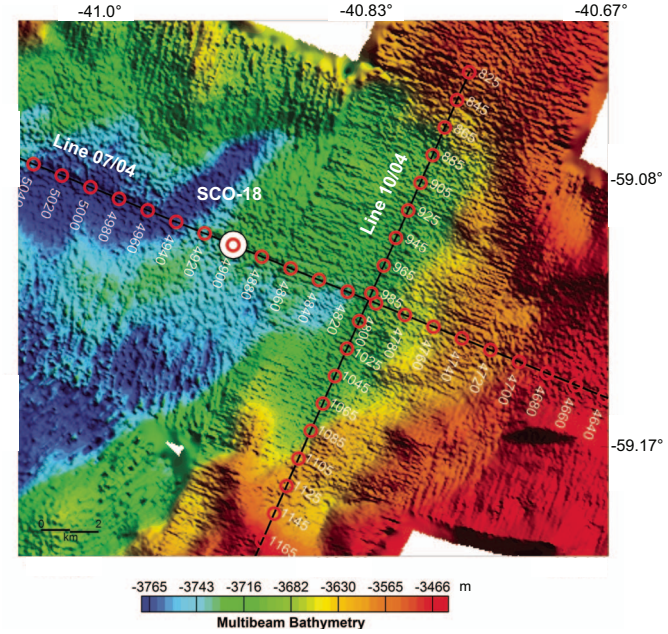

Site Figure

Site SCO-18 (Alternate Site)
SP 4900 on Line 07/04, SP range (gray, 4854-4920)
SP 990 on Line 10/04 (projected)

Interpretation
- Green – reflector a' (Pleist./Pliocene)
- Blue – reflector a (Late Pliocene)
- Purple – reflector b (Late Miocene)
- Yellow – reflector c (Middle Miocene)
- Brown – reflector d (Middle Miocene)
- Black – acoustic basement

Files in SSDB to support drilling
SCO-18_bathymetry.pdf
2004_SCAN_MCS_L10.sgy
2004_SCAN_MCS_L07.sgy
2004_SCAN_TOPAS_L07_F_addendum.seg
2004_SCAN_TOPAS_L10D.segy
2004_SCAN_MCS_L07_nav_new.txt
2004_SCAN_MCS_L10_nav_new.txt
2004_SCAN_TOPAS_L10D_nav_new.txt
2004_SCAN_TOPAS_L07_F_nav_addendum.txt
Backscatter_map_Dove_Basin.tif
Gravity_Bouguer_Anomaly_Map_Dove.jpg
Magnetic_Anomaly_Map_Dove.jpg

Figure AF10. Seismic profiles and bathymetry, Site SCO-19.

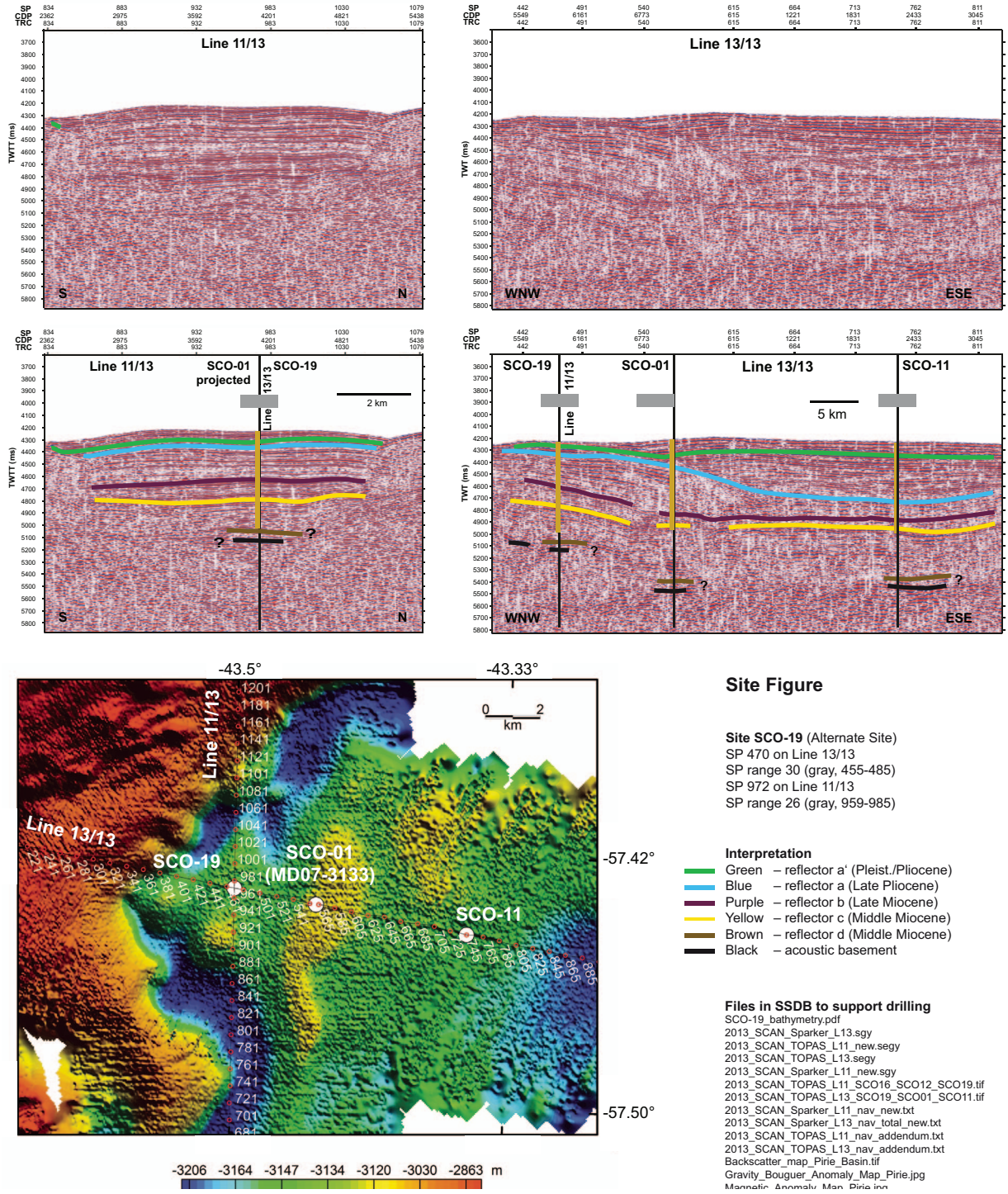

Site Figure

Site SCO-19 (Alternate Site)
SP 470 on Line 13/13
SP range 30 (gray, 455-485)
SP 972 on Line 11/13
SP range 26 (gray, 959-985)

Interpretation
- Green – reflector a' (Pleist./Pliocene)
- Blue – reflector a (Late Pliocene)
- Purple – reflector b (Late Miocene)
- Yellow – reflector c (Middle Miocene)
- Brown – reflector d (Middle Miocene)
- Black – acoustic basement

Files in SSDB to support drilling
SCO-19_bathymetry.pdf
2013_SCAN_Sparker_L13.sgy
2013_SCAN_TOPAS_L11_new.segy
2013_SCAN_TOPAS_L13.segy
2013_SCAN_Sparker_L11_new.sgy
2013_SCAN_TOPAS_L11_SCO16_SCO12_SCO19.tif
2013_SCAN_TOPAS_L13_SCO19_SCO01_SCO11.tif
2013_SCAN_Sparker_L11_nav_new.txt
2013_SCAN_Sparker_L13_nav_total_new.txt
2013_SCAN_TOPAS_L11_nav_addendum.txt
2013_SCAN_TOPAS_L13_nav_addendum.txt
Backscatter_map_Pirie_Basin.tif
Gravity_Bouguer_Anomaly_Map_Pirie.jpg
Magnetic_Anomaly_Map_Pirie.jpg

Figure AF11. Seismic profiles and bathymetry, Site SCO-21B.

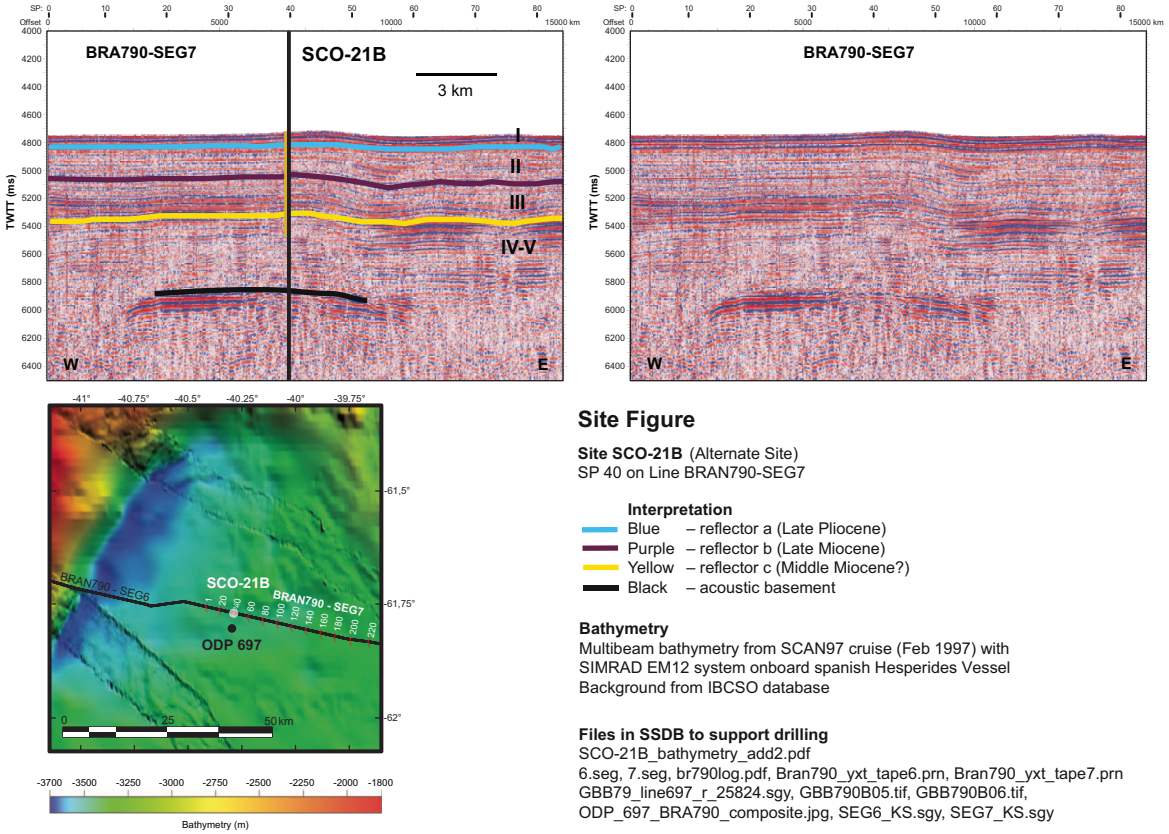

Site Figure

Site SCO-21B (Alternate Site)
SP 40 on Line BRAN790-SEG7

Interpretation
Blue – reflector a (Late Pliocene)
Purple – reflector b (Late Miocene)
Yellow – reflector c (Middle Miocene?)
Black – acoustic basement

Bathymetry
Multibeam bathymetry from SCAN97 cruise (Feb 1997) with SIMRAD EM12 system onboard spanish Hesperides Vessel
Background from IBCSO database

Files in SSDB to support drilling
SCO-21B_bathymetry_add2.pdf
6.seg, 7.seg, br790log.pdf, Bran790_yxt_tape6.prn, Bran790_yxt_tape7.prn
GBB79_line697_r_25824.sgy, GBB790B05.tif, GBB790B06.tif,
ODP_697_BRA790_composite.jpg, SEG6_KS.sgy, SEG7_KS.sgy

Figure AF12. Seismic profiles and bathymetry, Site SFSD-02A.

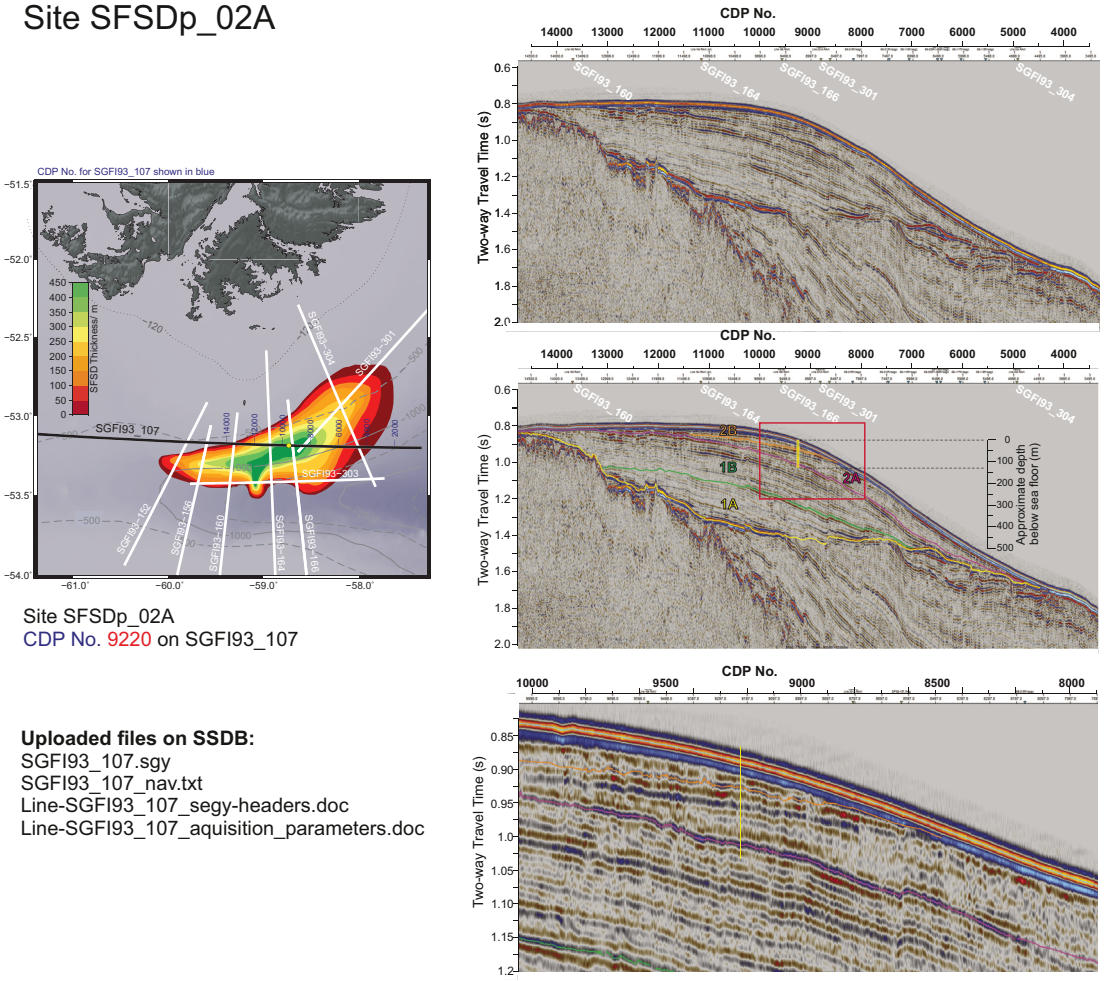

Site SFSDp_02A
CDP No. 9220 on SGFI93_107

Uploaded files on SSDB:
SGFI93_107.sgy
SGFI93_107_nav.txt
Line-SGFI93_107_segy-headers.doc
Line-SGFI93_107_aquisition_parameters.doc

Figure AF13. Seismic profiles and bathymetry, Site SFSD-03A.

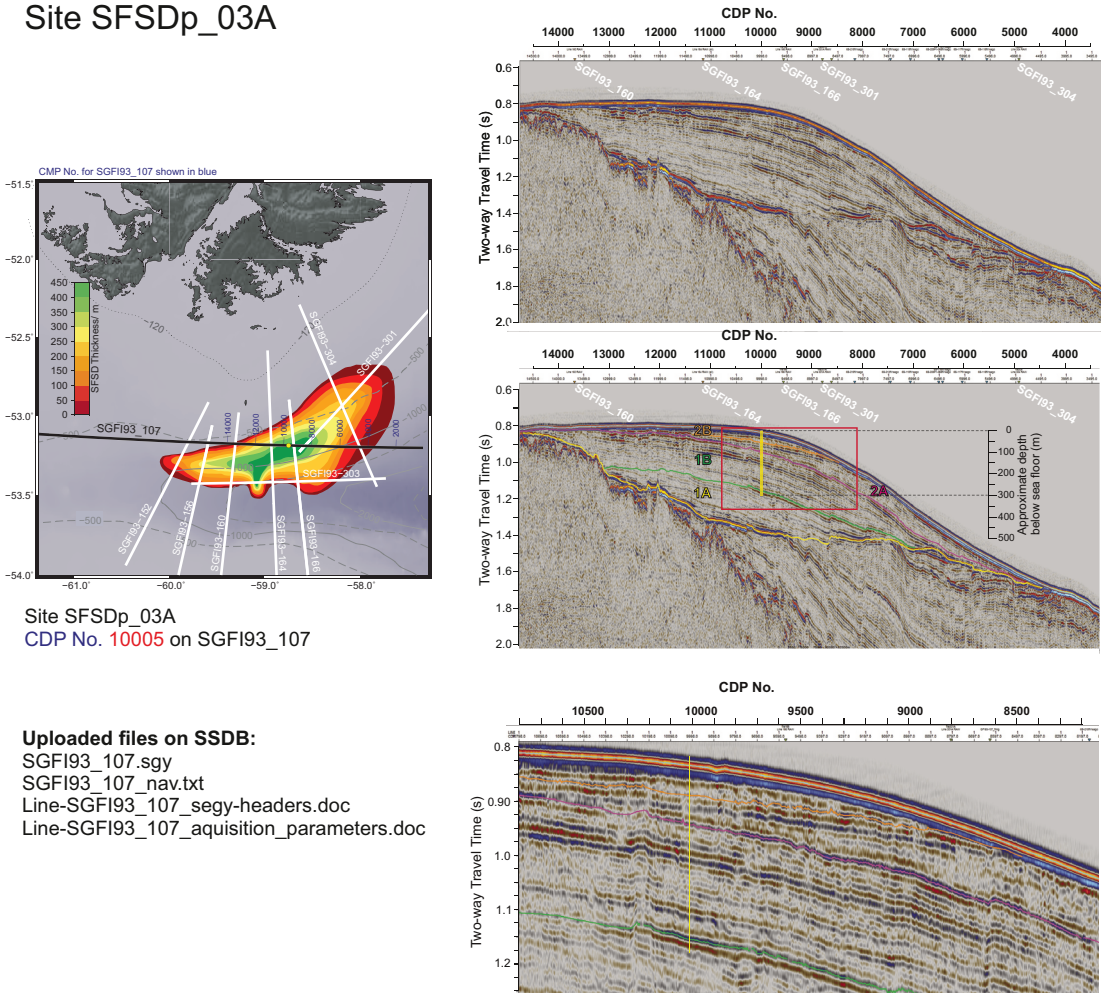

Site SFSDp_03A
CDP No. 10005 on SGFI93_107

Uploaded files on SSDB:
SGFI93_107.sgy
SGFI93_107_nav.txt
Line-SGFI93_107_segy-headers.doc
Line-SGFI93_107_aquisition_parameters.doc